THE UNIVERSITY OF CALGARY

PRESSURE PULSATION CONTROL IN GAS PIPELINE NETWORKS

by

Roman Wojciech Motriuk

A THESIS

SUBMITTED TO THE FACULTY OF GRADUATE STUDIES

IN PARTIAL FULFILLMENT OF THE REQUIREMENTS FOR

THE DEGREE OF MASTER OF SCIENCE

DEPARTMENT OF MECHANICAL ENGINEERING

CALGARY, ALBERTA

SEPTEMBER, 1986

THE UNIVERSITY OF CALGARY

FACULTY OF GRADUATE STUDIES

The undersigned certify that they have read, and recommend to the Faculty of Graduate Studies for acceptance, a thesis entitled, "Pressure Pulsation Control in Gas Pipeline Networks" submitted by Roman Wojciech Motriuk in partial fulfillment of the requirements for the degree of Master of Science.

Chairman, Dr. A.G. Doige

Department of Mechanical Engineering

Dr. E.C. Mikulcik

Department of Mechanical Engineering

Dr. M.A. Hastaoglu

Department of Chemical/Petroleum Engineering

September 30, 1986

ABSTRACT

In almost all natural gas distribution systems and gas metering stations there exists a problem of acoustic pulsation. As a result, excessive vibrations of the piping as well as amplification of the pressure sensed by steady-flow devices may occur.

In this work, a typical, bridge-shaped gas metering station was considered. It was demonstrated how a proper choice of different parameters could influence control of pulsation. These were parameters associated with the arrangement and geometry of the bridge network, flow conditions, medium composition as well as the measuring device's geometry.

A universal mathematical model of a complex piping network was created to predict pressures and volume velocities at any point of a bridge network. The network had an arbitrary number of bridges and orifice plates, any combination of open or closed valves, side branches, and contained a medium whose composition, temperature and pressure could be varied. Two physical models of one- and two-bridge networks, without orifice plates and containing air as a medium, were utilized to verify the mathematical model. The results of this verification were excellent which proved the model to be a useful tool in gas metering station simulation.

A mathematical model of an assembly of a flow measuring device was developed. It was used to assess the behaviour of this coupled acoustic-mechanical system. Three pressure measuring devices: The

Barton, Gould and Rosemount differential gauges have been tested experimentally, and good agreement between theoretical and experimental results was observed. As a result, the model was used to find methods to improve measuring devices' characteristics and to make these devices best suited for a particular gas metering station.

ACKNOWLEDGEMENTS

The author wishes to sincerely thank Dr. A.G. Doige, of the Department of Mechanical Engineering, for his invaluable guidance, suggestions and criticism throughout this entire project.

The help provided in part of this project by Dr. T.K. Groves of the Department of Mechanical Engineering is gratefully appreciated.

Special thanks are due to J. Macleod of the NOVA, An Alberta Corporation for his invaluable practical information.

The cooperation of W.A. Anson and R. Bechtold of the Mechanical Engineering Machine Shop and other technicians has been a vital support to the experimental work of this project.

The financial support received from the Department of Mechanical Engineering at the University of Calgary, the Natural Science and Engineering Research Council of Canada is gratefully acknowledged.

TABLE OF CONTENTS

LIST OF TABLES

LIST OF FIGURES

FIGURE	TITLE	PAGE

FIGURE	TITLE	PAGE

FIGURE	TITLE	PAGE

NOMENCLATURE

A	Element a_{11} of a 2x2 transfer matrix
a	Acceleration
B	Element a_{12} of a 2x2 transfer matrix
b	"Co-volume" of the molecules, Lennard-Jones (6-12) potential model
b_H	"Co-volume" of the molecules, hard sphere model
B'	Second virial coefficient
B^*	Reduced second virial coefficient
B^{n*}	Temperature derivative of order n of the reduced second virial coefficient premultiplied by the reduced temperature to the power n
C	Element a_{21} of a 2x2 transfer matrix
c	Speed of sound
$\bar{c}$	Complex speed of sound
C'	Third virial coefficient
C^*	Reduced third virial coefficient
C^{n*}	Temperature derivative of order n of the reduced third virial coefficient premultiplied by the reduced temperature to the power n

c_c Critical damping

cp_i Specific heat constant at constant pressure for i-th gas

cv_i Specific heat constant at constant volume for i-th gas

$C_{1,2}$ Constants of ordinary differential equation

D Element a_{22} of a 2x2 transfer matrix

D' Fourth virial coefficient

d Pipe diameter

d_b Diameter of a side branch of the orifice plate model

d_{op} Internal diameter of an orifice plate

E' Fifth virial coefficient

F Force

f Frequency

i,j Integer; subscripts i, j

k Wavelength constant

k' Boltzmann's constant

$\bar{k}$ Complex wavelength

k_g Mechanical stiffness of a transmitter membrane

K_c Fluid compliance

K_L Karal correction factor

L Length of the element

l Equivalent length of the orifice plate model

l_b Length of a side branch of the orifice plate model

L_e Corrected length of an element

l_{op} Thickness of an orifice plate

L_p Pressure level

L_V Volume velocity level

M Mach number

m Mass

MW Molecular weight

N Avogadro's number

n Integer; superscript

P Laplace-transformed pressure

P_c Critical pressure

p Pressure; perturbation value

p' Pressure; instantaneous value

p_o Pressure; constant value

P_{ref} Laplace-transformed reference pressure

q Empirical factor

$q(t)$ A random signal

$\bar{q}(t)$ Average value of the $q(t)$ signal

R Universal gas constant

r Separation distance, or ratio of angular frequencies (ω/ω_n)

S Cross-sectional area

s Laplace's operator

S_g Cross-sectional area of a transmitter membrane

T Absolute temperature

t Time

T^* Reduced temperature

T_c Absolute critical temperature

T_p Propagation time

U Laplace-transformed velocity

u Velocity; perturbation value

u' Velocity; instantaneous value

u_o Constant velocity

V Laplace-transformed volume velocity

V' Volume

V_g Transmitter volume space

V_{ref} Laplace-transformed reference volume velocity

W Function as defined by equation (2.27)

x Displacement

X_g Complex amplitude of a transmitter's membrane displacement

x_g Transmitter's membrane displacement

y Mole fraction

Z Acoustic impedance

$\bar{Z}$ Complex acoustic impedance; P/V

Z_n Nondimensional acoustic impedance; $\bar{Z}/(\rho\bar{c}/S)$

Z_o Characteristic impedance; $Z_o = \rho c$

Z' Compressibility factor

α Attenuation factor

γ Complex propagation constant, real part equal zero

$\bar{\gamma}$ Complex propagation constant

ΔL Pollack correction factor

ΔP Fourier-transformed differential pressure

ε Maximum energy of attraction

η Damping factor

θ Potential well depth temperature; $\theta = \varepsilon/k$

θ_M Potential well depth temperature for a hypothetical gas

ρ Density; perturbation value

ρ' Density; instantaneous value

ρ_o Constant density

σ Low velocity collision diameter for the Lennard-Jones (6-12) model

σ_H Low velocity collision diameter for the hard sphere model

σ_M Low velocity collision diameter for a hypothetical gas

$\varphi(f)$ Mean-square spectral density

$\varphi(r)$ Potential energy function

ω Angular frequency

ω' Dimensionless density for the Lennard-Jones (6-12) model

ω_n Natural angular frequency

ω_H Dimensionless density for the hard sphere model

CHAPTER 1

INTRODUCTION

1.1 Problem Description

Pulsation is an inherent phenomenon in almost all natural gas distribution and gas metering stations. The pulsation is due to acoustic energy which is generated by active elements, (as centrifugal or reciprocating compressors) and then, transmitted or reflected by reactive, nonabsorbing elements. The piston-crank-valve mechanism of the reciprocating compressor generates a composite wave which is made up of several components that are multiples of the rotational frequency. The composite wave propagates downstream and upstream in the piping network at the speed of sound, and interacts with the piping. As a result, various undesirable events may be observed:

a) Longitudinal and lateral vibrations of the piping elements which can lead to fatigue failure in the piping network when a piping system is not rigidly clamped (flexible supports).

b) Acoustic resonances in the piping system causing local pressure build-ups.

c) Local acoustic resonances in the meter transmission lines. These resonances amplify the dynamic pressure sensed by the differential recorder. This often results in significant monetary losses due to erroneous readings.

d) Impaired compressor performance which can lead to significant power losses.

Therefore, it is necessary to control the amplitude of pulsation, making it as low as possible [6,23,24,49,84].

In general, there are three approaches in dealing with gas pulsation problems. The first is a conventional technique of building additional supports at critical piping locations to prevent excessive vibration. A second approach is to attenuate the fluid pressure pulsation by using acoustic filters. This can lower the pulsation level but usually is not completely effective. A third and most advanced approach is to reduce the pulsation level by changing the arrangement and geometry of the piping network. Applied properly, this approach is able to counteract most phenomena associated with pulsation. It requires, however, a complete understanding of the acoustic characteristics of the entire piping network.

In general, the complete elimination of pulsations in a complex network (see Figure 1.1 in which a typical bridge-shaped gas metering station is depicted) is impossible, even with careful application of the available attenuation methods described above. Therefore, the following management of systems containing pulsating gas is proposed:

a) Select a system geometry to control pulsation, giving special attention to orifice plate locations.

b) Employ a properly designed differential pressure sensing-recording device [51,93]. Any of its natural frequencies should be out of the region of probable exciting frequencies, otherwise, the readings may be severely affected even if the pulsation at the orifice plate is very low. Williams [92] characterizes the situation as follows:

> "...the orifice plate or nozzle flowmeter does not of necessity follow the steady-flow square law when the flow being metered is pulsating in character, manometer errors can, nevertheless, greatly exceed all errors associated with the primary element".

Kulik affirms this in his paper [42]:

> "The errors contributed by the sensing lines can greatly exaggerate those at the orifice plate. Sensing line length, diameter and symmetry can affect signal resonance and attenuation at the output device".

c) Identify the pulsation magnitudes at orifice plate tappings using control equipment which reads so-called "square root error". This error results from the inexact determination of the average flow from the instantaneous differential pressures across an orifice plate. If the error is 1% or less the pulsations can be treated as moderate [84].

The first two procedures give the possibility to handle the problem of pulsation most effectively because they may be implemented at the design stage where any changes are most easily executable. A designer may therefore choose proper dimensions with confidence that any pulsation in the system will have a minimal level and future structural changes will not be necessary.

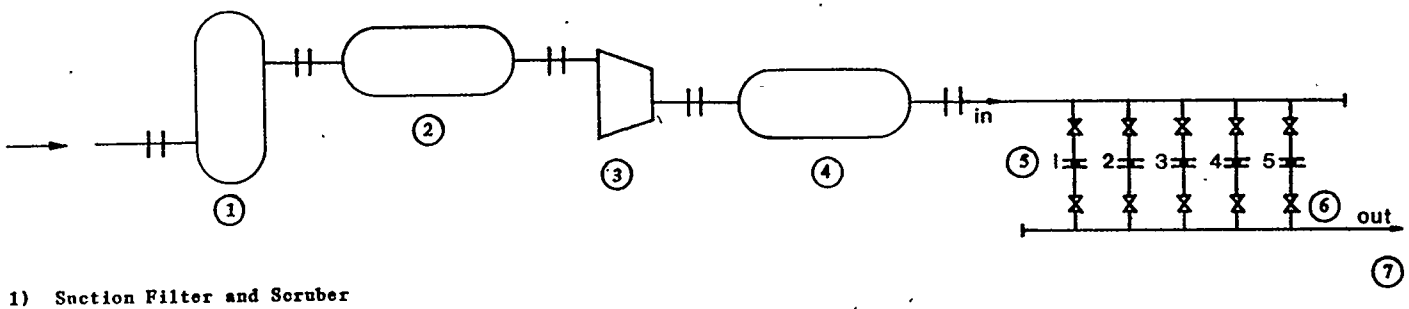

1) Suction Filter and Scruber
2) Suction Surge Drum
3) Compressor
4) Discharge Surge Drum and Pulsation Damper
5) Orifice Plate
6) Ball Valve
7) Non-Reflecting Pipeline

Figure 1.1 Typical Bridge-Shaped Gas Metering Station

1.2 Review of Previous Studies

The basic element of most acoustic systems is a constant-diameter circular pipe. Different connection arrangements and changes in the pipe diameters give more complex but still relatively simple components such as: sudden expansion and contraction chambers, extended outlets and inlets, side-branch resonators etc. These components are usually built into a more complicated system whose role is to fulfill certain functions under imposed restrictions. These functions are for example, efficient removal of exhaust gases from an engine with simultaneous noise control, transportation of gas for long distances with high efficiency of the pipeline and high accuracy pressure transmission to transducers.

The evaluation and understanding of any complex acoustic system requires, as a base, knowledge of the acoustic properties of the system's components. They are reviewed first, in this chapter. Both empirical and analytical methods for their determination are discussed.

Next, the factors influencing pulsating pressure measurement are reviewed. There is a great variety of work related to this subject, and in most cases, the authors are concerned with one or a few specific aspects.

Finally, studies on pulsation in complex piping networks are reviewed. Representative works are presented to outline the most important approaches used in the modelling of this type of network.

1.2.1 Impedance and Reflection Factor

In many practical cases, the acoustic impedance and the reflection factor can not be determined accurately by analytical means [79]. Owing to complex geometry, the presence of mean flow, or for other reasons, experimental techniques must be used. The non-dimensional impedance (Z_n) and reflection factor (R) are directly associated with each other [89] by the following relationship: $Z_n = (1+R)/(1-R)$. Either of them is sufficient to evaluate several other acoustic properties (absorption and transmission coefficients, transmission loss etc.). The standard relationships can be found in numerous works and textbooks [5,11,40,41,55,79,89]. The impedance can be regarded as a linear function that relates the dynamic pressure and volume velocity at any point of an acoustic element. Furthermore, the impedance is dependent on the downstream geometry only.

Several techniques have been used to experimentally determine the normal incidence acoustic impedance. Some of these techniques are described below along with a discussion of their major advantages and disadvantages. The well known Standing-Wave-Ratio (SWR) method [2] requires a travelling microphone to determine the locations and magnitudes of maxima and minima of the standing wave pattern in a tube terminated by the unknown system. Discrete frequency excitation has to be used, and the tube is recommended to be at least one wavelength long. Due to these prerequisites the method is time consuming and requires the use of an additional

correction factor to compensate for losses. Gatley and Cohen [20] considered using pulse or transient excitations of the system with wall-mounted microphones. However, the required long tube and problems with separation in time of the incident and reflected waves convinced them that the method was laborious and inconvenient. Seybert and Ross [79] employed a two-microphone random excitation method to measure impedance of a uniform pipe with no-flow and mean flow conditions. Their equations were derived in terms of auto and cross spectra of microphone signals. No-flow experiments agreed very well with the results obtained from steady-state methods. Kathuriya and Munjal [37] introduced a method for determining the acoustic impedance of a black box at low frequencies. The sound pressures at three different locations were required to evaluate the reflection coefficient. Subsequently, the impedance of the termination could be obtained. The same authors also presented another work [39] in which they evaluated the acoustic impedance of a black box by measuring pressure at fixed positions. In this study the attenuation factor of the tube was required to describe the impedance. Scott [76] proved that the tube attenuation can not be neglected when precise measurements are to be made at lower frequencies.

Singh and Katra [82] developed an acoustic impulse method to determine the acoustic properties of a system. They used a wall-mounted microphone located midway along a tube connecting an acoustic driver to the system being tested. The system was excited by a

short duration rectangular pulse supplied to the driver. This arrangement allowed incident and reflected pulses to be separated. Lambert and Stainbrueck [44] determined experimentally both the magnitude and phase of the acoustic pressure reflection coefficient at a sudden area expansion in a flowduct with the presence of flow (low Mach numbers). They used the impedance tube method with fixed microphone positions as described in [39] by Kathuriya and Munjal. The authors expressed the acoustic reflection coefficient as a ratio of reflected to incident pressure amplitudes. The mean square pressure was sampled at various discrete points by flushed-mounted microphones. Chung and Blaser [11] developed a method employing a random signal as an excitation input. Using two microphones, they measured the pressure at two locations along the tube wall. They determined reflection factors employing a transfer function between the two pressures; they did not account for attenuation between two microphone ports. Their method appeared to be simpler than that of Seybert and Ross [79]. No-flow results presented in the study agreed well with theory. To and Doige [88] presented more practical expressions for determining the acoustic impedance and reflection factor. These expressions worked for both random and deterministic inputs. Both were functions of the pressure ratio measured between two microphone locations and the four-pole matrix parameters (known for the considered system). Tube attenuation was included, no mean flow was present in the tube, but the formulation was adaptable for the mean-flow case.

The reflection of sound waves due to a change in the cross-section of a circular pipe was first described by Miles [52]. Based on the assumption of plane wave propagation in the pipe, he determined the pressure distribution in the neighbourhood of the discontinuity. This was used to calculate the reflection coefficient. Another important work dealing with the same problem appeared in the early fifty's. The author, Karal [35], determined theoretically the discontinuity impedance (called also inductance) as a function of the tube radius ratio. He treated this impedance as a correction term to be added to the acoustical impedance of the tube. Further works, analytically treating the acoustic properties, have appeared in the last decade. Levine and Schwinger [46] determined the reflection factor for the case when the Mach number is zero. The expressions they derived describing the dependence of reflection factor on the wave number were tedious to evaluate, but a close empirical fit to their results can be found in [14]. More recently, Munt [57] predicted the value of the reflection factor for subsonic flow using a theoretical model in which the jet of medium flows out of a pipe. He showed that as the flow velocity increases the magnitude of the reflection factor also increases. He did not use the end correction factors in his calculations. Ronnenberger [71] investigated the behaviour of sudden area expansions with an anechoic downstream termination. He assumed that the flow in the vicinity of discontinuity was quasi-stationary and one-dimensional. Ronnenberger presented both predicted and meas-

ured values of the acoustic pressure reflection coefficient for upstream mean flow Mach numbers up to 0.6. The agreement was poor except for low Mach numbers. Alfredson and Davies [2] showed predictions and measurements of reflection coefficients for upstream low Mach numbers in the inlets and outlets to exhaust silencer chambers. The results were predicted under the same flow assumptions as described in [71]. The predicted and measured values agreed quite well under tested flow conditions up to M = 0.15. However, it is not known if such an agreement exists for higher Mach numbers.

1.2.2 Transmission Lines - Factors Influencing Pressure Measurement

A differential flow-measuring device generally can be divided into two distinct parts: the primary meter such as an orifice plate, nozzle, etc., producing a signal which is a function of the flow rate and other variables of the flow; and the secondary system translating the signal into a reading. The secondary system normally consists of the transmission lines from the primary system to the recording element, and the recording element itself.

Several authors [9,17,27,28,36,50,58,87] have investigated the response of transmission lines to oscillatory inputs. This kind of input was meant to simulate pressure pulsation. Iberall's [27] and Nichols's [58] investigations are probably the best known and their results have been verified theoretically and experimentally [34,36,70].

Iberall described the attenuation and lag of a sinusoidal pressure signal applied to the end of a tube which terminated in a volume. His analysis was based on the assumption of incompressible viscous-fluid flow. The solution was then modified to account for compressible flow, finite amplitudes, end effects, fluid acceleration and heat transfer into the tube. The foregoing modifications appeared to be important factors influencing behaviour of transmission lines. Iberall also pointed out the importance of the line geometry and the sensor volume. He also emphasized the influence of the ratio between the instrument and line volume on frequency response.

Nichols [58] discussed the subject of small signal transmission through pneumatic lines. He derived equations which governed transmission line performance. These equations were written in terms of series impedances and admittances per unit length. The author included in his mathematical description the behaviour of the medium (air) which was assumed to be governed by isothermal conditions at low frequencies and adiabatic conditions at high frequencies. He considered the behaviour of the fluid to be a decisive factor influencing the system response. Therefore, he defined a characteristic frequency separating the transmission problem into low and high frequency cases. His theory was tested by Rohman and Grogan [70] and was found to give accurate results. Brown [7] in a concurrent but independent investigation, described the equations for small signal inputs governing the behaviour of

fluid enclosed in a semi-infinite line. For sinusoidal excitation imposed on the system, the predictions were identical to those of Iberall [27] and Nicols [58]. The factors specified by Iberall [27] were again found to play an important role in the description of the transmission lines.

Karam and Franke [36] used an electro-pneumatic analogy to find gain curves for different tubing lengths. They employed a small periodic input as an excitation to their system. The results obtained agreed very well with results predicted by Nichols's method [58]. Franke et al. [19], and Prasad and Crocker [64] derived a calculation procedure for muffler system that included the effect of a linear temperature gradient. They compared their results with experiments and obtained good agreement. Some researchers [4,81] have developed approximate formulas for viscous flow in manometer tubes connected in series. Generally, the authors' approach assumed an instantly established flow regime. The volume of the entire tubing was taken into account and variable sensor volume was included. Benedict [4] has proved the significance of such an approach, particularly when the time lag must be predicted.

Bell et al. [3] conducted a study of pneumatic pulse transmission in uniform area circular tubes. They provided signal attenuation and distortion information for the design of pneumatic systems. They reported that bends and fittings in a transmission line had no noticeable effect on the pulse shape if there was little

change in the cross-sectional area. The pulse attenuation per unit length depended only on its input level, time history and tube diameter but did not depend on the pulse length.

Hord [26] stated that although some data for estimating pressure losses in fittings, bands etc. is available [62], these irregularities can be considered to have very little effect, particularly for low frequency ranges. This was confirmed by Botros et al. [6] and Lung [47,49]. Further, Hord added that most of the problems associated with pressure transmission lines occur with laminar flow (usually long, small-diameter lines) and not with turbulent flow (short, large-diameter lines). As a result there was little need for including turbulent flow into the analyses.

More recent works assume different flow regimes. Brown [9], and Ohmi and Usui [60] assumed unsteady turbulent flow through the line and proposed to cover the whole frequency domain using low-frequency and high frequency models developed by Nichols [58]. Seimer et al. [77] took an even more complex approach and described transitional flow (large-amplitude pulsating laminar / turbulent / laminar flow) mathematically. However this method is difficult to assess because of the lack of experimental data.

1.2.3 Complex System Analyses

The main purpose of all studies dealing with the pulsation problem in a complex system is to predict pressure and velocity distributions throughout the system for any given input. This has to be done for a particular character of pulsating flow. A wide range of flow regimes have been investigated theoretically and empirically [9,47,48,49,59,72,73,74,77,85,86]. The key to a theoretical solution of the problem was to properly model the system by utilizing adequate assumptions and techniques. The most frequent approach was to linearize the system and assume steady flow conditions [6,47,48,49,85,86]. More recently, some efforts have been made to obtain the solution of the problem when unsteady nonlinear flow conditions are present [31,50].

Sakai and Saeki [72] developed a method to calculate the natural frequency of a complex piping system connected to a reciprocating compressor. They assumed no mean flow in the system, and only very small sinusoidal pressure fluctuations. The fluid in the tubing was compressible with constant density. The authors divided the system into basic elements with prescribed end conditions. For example, when a tubing element incorporated a valve or a piston, they assumed a closed end for this element. On the other hand, when a large volume was connected to its side, an open end was assumed. The authors derived the transmission matrices for each element, solving differential equations for one-dimensional fluid flow. Afterwards, they obtained the overall transfer matrix

by simple cascade multiplication. Using Holtzer's method, and taking into account end conditions, they were able to calculate the natural frequency for the entire system. Their calculated results agreed well with preliminary experimental data. Sakai and Mitsuhashi [73] collected natural frequency data for piping system elements with prescribed boundary conditions. Then they combined these elements together and looked for the natural frequency of the new structure. The authors selected elements and their arrangement to reproduce the complex piping network considered in the work of Sakai and Saeki [72]. They were then able to compare a resonable number of collected empirical data with the data previously predicted. In general, they obtained good agreement between calculated and measured natural frequencies. In their next work, Sakai and Mitsuhashi [74] modified the previous method [73] of natural frequency calculation. The authors did not consider viscous damping, so their predicted pressures did not coincide well with their experimental data in the vicinity of the resonant frequency. Still, they found this result satisfactory, as it gave them the values of the frequencies associated with higher pressures.

To and Doige [88] developed an experimental method which could be used to evaluate matrix parameters of any acoustic component or system. This method can be applied to both known and unknown acoustic elements or complex systems. For an unknown system, one has to collect experimental pressure data to derive the four-pole matrix parameters. The authors derived equations which could be

used in connection with random, transient or steady state excitation. The authors gave a few examples for the evaluation of matrix parameters for some chosen acoustic components. They emphasized the advantages of the transient testing technique: it can be completed in a short time, because few averages are required, there are no leakage errors since a rectangular time window can be used, and it can be employed for any acoustic system, including all complicated wave phenomena in the system (higher order modes). Lung in his work [47] extended this technique to cases with flow for low Mach numbers. He used several models to predict the four-pole matrix parameters. He verified these models with experimental tests. Botros et al. [6] pointed out how selection of the element lengths in a particular complex network affects the pressure pulsation levels at the desired locations. These pulsations can often be attenuated to low enough levels so that the use of acoustic filters becomes unnecessary. Using four-pole parameter matrix principles, the authors employed two different techniques to describe the system: the matrix chain multiplication methods, and the linear equation solver by determinants. They used an overall transfer matrix to calculate instantaneous pressure amplitudes at the characteristic points of a sample network. Then, the authors verified experimentally the calculated values by performing tests on a smaller scale laboratory model. Subsequently, the method was utilized for actual field conditions. Small geometrical changes made for the Monchy meter station of the Alaska pipeline were suf-

ficient to secure relatively low pulsation levels. In section three of their study [49], Lung and Doige addressed briefly the problem of pressure pulsation in a complex piping network. The authors created a computer program to simulate a sample piping network. Meanwhile, in the laboratory, they tested a model of such a system. They predicted acoustic characteristics for this model by using the transient testing technique. The authors obtained excellent agreement between predicted and empirical data.

1.3 Thesis Relevance

The review of previous works reveals that a complete and universal method to analyze complex networks does not exist. A number of questions overlooked or treated superficially have been addressed in this work. They include:

a) The investigation of systems having more than one orifice plate.

b) The simultaneous prediction of volume velocity pulsations and pressure pulsations at orifice plate locations.

c) The influence of complexity of the network on its pulsation behaviour.

d) The influence of any combination of open or closed valves on pressure and volume velocity pulsations at orifice plate locations.

e) The implications of the presence of flanged end pipes which can create a side-branch resonator effect.

f) The treatment of a pressure sensing-recording device as a coupled acoustic-mechanic system instead of purely acoustic system.

g) The investigation of the performance of modern measuring devices like the Gould or Rosemount differential gauges.

h) The inclusion of non-ideal gas for the calculation of density and speed of sound and implications of changes in composition, pressure and temperature of medium.

The purpose of this work was to assess the behaviour of a bridge-shaped gas metering station as a whole that is to include not only the network of transporting pipes but also the medium enclosed in them and the flow measuring devices. The ultimate objective was to suggest the methods to control pulsations in the system.

A universal mathematical model of a complex network was created to predict values of pressure and volume velocities at any point of a bridge network. This model was subsequently implemented in the form of a computer program. The network may have an arbitrary number of bridges and orifice plates, any combination of open or closed valves , side branches, and contains a medium whose composition, temperature and pressure can be varied. Two physical

models of one- and two-bridge networks, without orifice plates and containing air as a medium, were used to verify the mathematical model.

A mathematical model of an assembly of a pressure sensing-recording device and transmission lines was also developed. Its purpose was to predict the behaviour of this coupled acoustic-mechanical system. The Gould, Rosemount and Barton differential gauges have been tested experimentally and the data was used both to evaluate their performance and to verify the mathematical model.

In conclusion, a procedure was proposed to control the performance of a flow measuring device incorporated in a specific bridge network. The control can be realized by means of the network geometry, flow or medium changes as well as by rearranging the measuring device.

CHAPTER 2

DETERMINATION OF DENSITY AND SPEED OF SOUND FOR MIXTURES OF TWO OR MORE GASES IN MODERATE PRESSURE AND TEMPERATURE RANGE

There are two thermodynamic properties, density and speed of sound, which play a decisive role in a prediction of pressure and volume velocity distributions throughout an acoustic system. The speed of sound determines the wave length which enables one to obtain an acoustical length of the system. Consequently, the pressure build-ups and resonances in the system are obtainable. On the other hand, the medium density describes the inertia of the medium, a property which produces wave motion and permits one element of the medium to transfer momentum to adjacent elements, and, consequently, influences magnitudes of the peaks. Therefore, the prediction of these two thermodynamic properties is essential when one wants to analyze piping systems in acoustic terms.

The gas and oil industry deals with an ever increasing number of chemical compounds. Experimental evaluation of accurate pressure-volume-temperature data and related thermodynamic properties, such as density and speed of sound, for these substances is expensive, time consuming and not always convenient. It is therefore desirable to determine such information analytically.

In this study an equation of state for gas mixtures has been developed on the basis of the virial equation of state. The

compressibility factor, which is a function of temperature and pressure and is different for each substance included in the mixture, was evaluated by using the forces of repulsion and attraction between molecules. This work is limited to non-polar gases with sphericalized molecules and to mixtures of such gases. Accordingly, the Lennard-Jones (6-12) potential function model was assumed to describe most accurately the molecular interaction. Mixtures were assumed to be described by a hypothetical pure gas with intermolecular force constants which were average representations of the constants related to the mixture's species. Two types of mixing rules were implemented [22,61] to calculate the force constants' values. Three hybrid virial equations based on the Lennard-Jones (6-12) potential function model and the hard sphere model were developed. Different combinations of the hybrid virial equations and mixing rules resulted in five distinct methods by which PVT relations were immediately determinable. Instead of using two or three virial coefficients, which is generally done [45,61,75], five virial coefficients were used. As a result, the well known virial equation of state gave much better results and could be applied to wider ranges of pressure and temperature.

All the required formulae used to calculate parameters associated with the mixtures were tested for three pure gases: argon, carbon dioxide and nitrogen. The ranges of temperature and pressure considered in this work, are 243.15 to 318.15 ^{o}K and 101.325 to 10132.500 kPa respectively. These are commonly encountered

conditions in gas networks.

2.1 Theoretical Background

An empirical equation of state with a sound theoretical basis is the virial equation of state [22,25,80]. It gives good agreement with experimental data for pure gases at low and moderate densities. Of particular importance to this work is the possibility to extend the virial equation to mixtures. The virial equation of state can be written as a power series in the inverse volume:

$$\frac{pV'}{RT} = 1 + \frac{B'(T)}{V'} + \frac{C'(T)}{V'^2} + \frac{D'(T)}{V'^3} + \frac{E'(T)}{V'^4} + \ldots \qquad (2.1)$$

This equation is valid when the series converges; the condition is satisfied for low and moderate densities. $B'(T)$, $C'(T)$, ... are called the second, third etc. virial coefficients. They are functions of temperature, and represent the deviations from ideal behaviour when collisions involving the molecules become unimportant. For a highly dilute gas, the virial equation reduces to the well known ideal gas law ($pV'/RT = 1$). At low densities the second virial coefficient adequately describes the deviations; at higher densities more coefficients must be used. The virial coefficients can be calculated by the methods of statistical mechanics, using assumed intermolecular potential energy functions.

The simplest potential function, which allows one to obtain the virial coefficients in analytical form, is a function represented by the rigid sphere model[22,25]. The virial coefficients for this model are temperature-independent and all positive. The compressibility factor Z is therefore greater than unity and is a function of the density only. The rigid sphere model gives relatively good results only at very high temperatures, since in this case the attractions between the molecules are unimportant. The virial coefficients are calculated from the following expressions:

$$B' = \frac{2}{3}\pi N\sigma_H^3 = b_H \tag{2.2}$$

$$C' = \frac{5}{8}b_H^2 \tag{2.3}$$

$$D' = 0.2869b_H^3 \tag{2.4}$$

$$E' = 0.115b_H^4 \tag{2.5}$$

where N is the Avogadro's number, and σ_H is the diameter of the hard sphere molecule.

The best known realistic potential function, for nonpolar molecules is the Lennard-Jones (6-12) potential:

$$\phi(r) = 4\varepsilon\left[\left(\frac{\sigma}{r}\right)^{12} - \left(\frac{\sigma}{r}\right)^{6} \right] \tag{2.6}$$

where the parameters σ and ε are the so-called "force constants". They are characteristic constants of the chemical species of the colliding molecules. σ represents the low velocity collision diameter. ε is the maximum energy of attraction or depth of the potential well which occurs at a separation distance given by: $r=2^{1/6}\sigma$. This model provides good estimates of the second and third virial coefficients. The remaining coefficients have not been verified experimentally. The expressions for the second and third coefficients, in their dimensionless form, are as follows:

$$B^*(T^*) = B(T)/\tfrac{2}{3}\pi N\sigma^3 = B(T)/b \tag{2.7}$$

$$C^*(T^*) = C(T)/b^2 \tag{2.8}$$

Their temperature derivatives are:

$$B^{n*}(T^*) = T^{*n}(d^nB^*/dT^{*n}) \tag{2.9}$$

$$C^{n*}(T^*) = T^{*n}(d^nC^*/dT^{*n}) \tag{2.10}$$

where

$T^* = \frac{T}{\frac{\varepsilon}{k}} = \frac{T}{\theta}$ is dimensionless (reduced) temperature,

k is the Boltzmann's constant, and

θ is the potential well depth temperature.

Figure 2.1 shows the potential functions for the hard sphere and

the Lennard-Jones models.

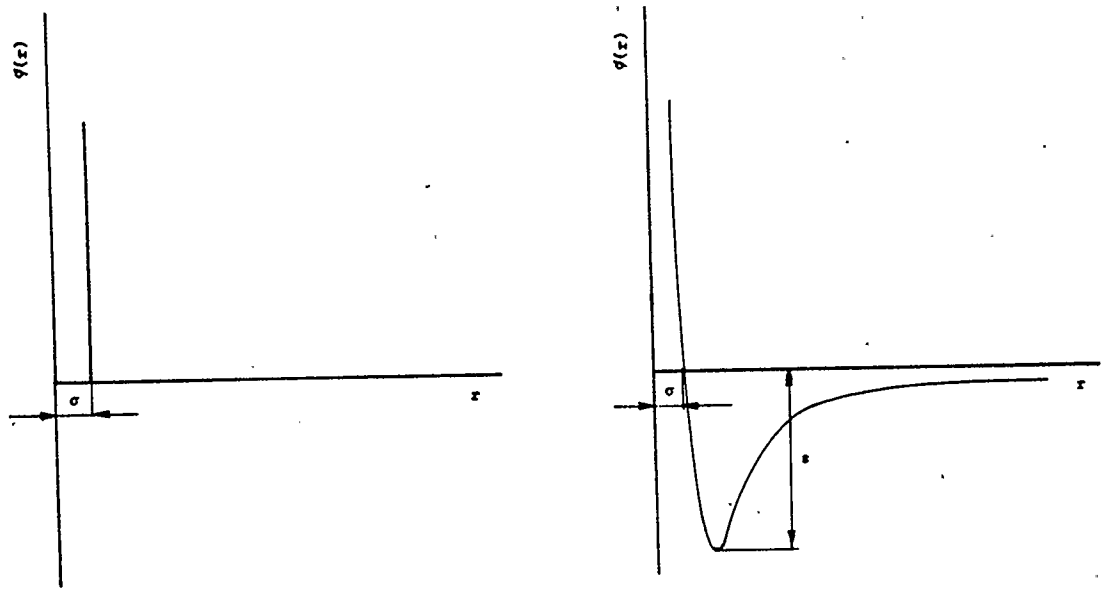

a) Hard Sphere Model

b) Lennard-Jones Model

Figure 2.1 Potential Energy Functions

Groves [22] proposed a hybrid virial equation of state in which the second and third virial coefficients were evaluated using Lennard-Jones (6-12) potential and the fourth and fifth virial coefficients were taken from the hard molecule assumption. This equation has the following form:

$$pV = Z = 1 + B^*(T^*)\frac{b}{V'} + \frac{C^*(T^*)b^2}{V^{2'}} + \frac{0.2869b_H^3}{V^{3'}} + \frac{0.1928b_H^4}{V^{4'}}$$
$$= 1 + B^*(T^*)\omega' + C^*(T^*)\omega'^2 + 0.2869\omega_H^3 + 0.1928\omega_H^4 \tag{2.11}$$

where ω' is dimensionless density for Lennard-Jones potential, and ω_H is a dimensionless density for hard molecules,

$$\omega' = \frac{b}{V'} = b\rho \tag{2.12}$$

$$\omega_H = \frac{b_H}{V'} = b_H\rho \tag{2.13}$$

Hirshfelder [25] proposed a different form of a hybrid virial equation to eliminate dependency on shape introduced by the third virial coefficient. He utilized the Lennard-Jones potential to evaluate only the second virial coefficient. His hybrid virial equation has the following form:

$$\frac{pV'}{RT} = Z = 1 + B^*(T^*)\omega' + 0.625\omega_H^2 + 0.2869\omega_H^3 + 0.1928\omega_H^4 \tag{2.14}$$

A third hybrid virial equation was proposed [22], [25] by substituting 0.115 instead of 0.1928 for the fourth virial coefficient.

$$\frac{pV'}{RT} = 1 + B^*(T^*)\omega' + 0.625\omega_H^2 + 0.2869\omega_H^3 + 0.115\omega_H^4 \tag{2.15}$$

Groves [22] defined the following relationship between parameters associated with Lennard-Jones and the hard sphere model as follows:

$$\omega_H = \left[\frac{2}{1 + (1+T^*)^{1/2}}\right]^{1/2} \omega' \tag{2.16}$$

$$\sigma_H = \left[\frac{2}{1 + (1+T^*)^{1/2}}\right]^{1/6} \sigma \tag{2.17}$$

Since this work dealt with binary and multicomponent mixtures, three hybrid virial equations (2.6), (2.9), and (2.10) were then expanded over a gaseous mixture. It was assumed that the mixture of gases had the same thermodynamic properties as some hypothetical gas of only one component. For example, the force constants of the mixture were the same as the force constants of this hypothetical gas. Hirshfelder, et al.[25] proposed the following expressions for the force constants of the hypothetical gas:

$$\sigma_M = \sum_{i=1}^{i=n} \sum_{j=1}^{j=n} y_i y_j \sigma_{ij} \tag{2.18}$$

$$\theta_M = \sum_{i=1}^{i=n} \sum_{j=1}^{j=n} y_i y_j \theta ij \tag{2.19}$$

where n is the number of species in the mixtures, subscripts i and j denote the components of the mixture,

$$\sigma_{ij} = \frac{\sigma_i + \sigma_j}{2} \tag{2.20}$$

$$\theta_{ij} = (\theta_i \theta_j)^{1/2} \tag{2.21}$$

Othmer and Chen [61] gave a different method to calculate the force constants:

$$\sigma_M = \left[\sum_{i=1}^{i=n} \sum_{j=1}^{j=n} y_i y_j \sigma_{ij}^3 \right]^{1/3} \tag{2.22}$$

$$\theta_M = \left[\frac{\sum_{i=1}^{i=n} \sum_{j=1}^{j=n} y_i y_j \sigma_{ij}^3 \theta_{ij}}{\sigma_M^3} \right]^{1/q} \tag{2.23}$$

where values of the factor q, evaluated empirically are:

$$q = 1.6, \text{if} \quad W \geq 1.64 \tag{2.24}$$

$$q = 0.15, \text{if} \quad W \leq 0.20 \tag{2.25}$$

$$q = 0.15 + 0.025(W-0.2) + 0.563(W-0.2)^2 \; 1-0.089(W-0.2)^3 + 0.124(W-0.2)^4, \tag{2.26}$$

if $0. \leq W \leq 1.64$

where

$$W = \frac{T}{P} \frac{\sum_{i=1}^{i=n} y_i P_{c_i}}{\sum_{i=1}^{i=n} y_i T_{c_i}} \tag{2.27}$$

2.2. Procedure of Calculations

The computation of the desired thermodynamic properties were done using a computer. SI units are used throughout. The stepwise procedure used for computation is outlined below.

1. The force constants (σ_i, θ_i), specific heats at constant pressure (cp_i), critical temperatures (T_{c_i}), and critical pressures (P_{c_i}) for the species under consideration were taken from tables [25,30,78,97].

2. The specific heat constants at constant volume (cv_i) were computed (see Appendix A).

3. The force constants for mixtures (σ_M, θ_M) were evaluated using equations (2.18), (2.19), (2.14) and (2.23).

4. The reduced temperature (T^*) was calculated, and the corresponding second and third virial coefficients as well as their temperature derivatives were taken from the tables [25].

5. The density (ρ) was obtained by solving the three different hybrid virial equations (2.11), (2.14), and (2.15), in the required temperature and pressure range.

6. The compressibility factors Z for a given ρ was readily obtainable from the equations of state.

7. The speed of sound (c) in the mixtures concerned was calculated from the compressibility factors and the thermodynamic formulae given in Appendix A.

2.3. Results and Conclusions

The mixing rule given by (2.18) and (2.19) was applied to the virial equations given by (2.11) and (2.14). The other mixing rule (2.22) and (2.23) was applied to equations (2.11), (2.14) and (2.15). This resulted in five distinct methods to calculate the density, compressibility factor and, consequently, the speed of sound. Before the parameters associated with the mixtures were evaluated, all the required formulae were tested for pure gases (argon, carbon dioxide and nitrogen). More than two hundred and fifty experimental values of the densities, speeds of sound and compressibility factors were collected [45,61,65,66,67,68,80,97]. This data represents twenty-nine binary mixtures, one four com-

ponent mixture and three pure gases. The average deviation of the values calculated with these five methods from the experimental data was taken as a measure of the effectivness of each method. Using this criterion, the method based on the equations (2.14), (2.22) and (2.23) was classified as most accurate. This method gave an average deviation from observed values of the compressibility factors of 2.34%, that of densities for pure gases of 1.5% and that of speeds of sound for air and the pure gases of 1.27% (see Tables 1, 2, 3, 4 and Figures 2.2 to 2.7). The maximum deviations of compressibility factors, densities and speeds of sound were 17.42%, 3.46% and 6.66% respectively (see Tables 1, 2, 3, 4). The deviations may be actually lower, because the accuracy of the experimental data determination varied from source to source.

The hybrid virial equation has a significant advantage over the virial equation because it takes into account five virial coefficients, instead of three. It can handle pressure and temperature data in a very wide range with relatively little error. The error was probably introduced by σ and θ whose values are inconsistent in the literature.

Table 2.1 Calculated Compressibility Factors and Their Absolute Deviations from Experimental Data

System		CH_4 $-CO_2$	CH_4 $-C_2H_6$	CH_4 $-C_3H_8$	CH_4 $-nC_4H_{10}$
No. of Experimental Points		24	16	4	10
Temp. [°K]		310.93	310.93	310.93	310.93
Pressure [kPa]		1379 - 8618	1723 - 6895	3448 - 8247	690 - 8618
Mole Fraction of First Comp.		0.2035 - 0.8469	0.3900 - 0.9200	0.5209 - 0.6779	0.0175 - 0.8473
METHOD 1					
Abs. Dev.[%]	Max	21.71	14.72	19.47	25.71
	Min	2.45	5.43	12.35	13.97
METHOD 2					
Abs. Dev.[%]	Max	12.35	13.21	20.03	17.41
	Min	2.61	5.32	12.53	9.47
METHOD 3					
Abs. Dev.[%]	Max	9.81	9.57	4.94	8.62
	Min	1.65	4.13	2.03	5.47
METHOD 4					
Abs. Dev.[%]	Max	8.11	8.68	3.35	7.06
	Min	1.51	3.99	2.29	2.79
METHOD 5					
Abs. Dev.[%]	Max	7.52	8.63	3.39	7.05
	Min	1.46	3.99	2.24	4.94

Table 2.1 (continued)

System		CH_4 $-nC_5H_{12}$	C_2H_6 $-CO_2$	N_2 $-C_2H_6$	CO_2 $-nC_3H_8$
No. of Experimental Points		2	30	6	1
Temp. [^oK]		310.93	310.93	310.93	277.59
Pressure [kPa]		1379 - 5516	1379 - 7585	2633 - 7719	1379 - 1379
Mole Fraction of First Comp.		0.8940 - 0.9460	0.1777 - 0.8280	0.7318 - 0.7318	0.6036 - 0.6036
METHOD 1					
Abs.	Max	3.30	12.99	2.38	0.83
Dev.[%]	Min	2.10	3.60	1.81	0.83
METHOD 2					
Abs.	Max	3.77	26.65	3.20	0.95
Dev.[%]	Min	2.35	5.82	2.18	0.95
METHOD 3					
Abs.	Max	0.69	16.78	2.83	1.98
Dev.[%]	Min	0.50	3.64	1.36	1.98
METHOD 4					
Abs.	Max	0.67	17.42	3.22	2.12
Dev.[%]	Min	0.57	3.90	1.61	2.12
METHOD 5					
Abs.	Max	0.64	23.97	3.21	2.12
Dev.[%]	Min	0.55	4.80	1.61	2.12

Table 2.2 Calculated Densities and Their Absolute Deviations from Experimental Data

System		Argon	Nitrogen	Carbon Dioxide
No. of Experimental Points		26	24	22
Temp. [°K]		273.15 - 298.15	273.15 - 298.15	273.15 - 298.1
Pressure [kPa]		1080.3 - 9844.6	1137.3 8927.9	1000.3 4590.7
Mole Fraction		1.000	1.000	1.000
METHOD 1				
Abs.	Max	0.56	2.20	2.02
Dev.[%]	Min	0.14	1.19	0.54
METHOD 2				
Abs.	Max	1.11	2.18	1.09
Dev.[%]	Min	0.53	1.35	0.43
METHOD 3				
Abs.	Max	3.09	2.13	2.12
Dev.[%]	Min	2.81	1.29	0.54
METHOD 4				
Abs.	Max	3.46	2.34	1.12
Dev.[%]	Min	2.86	1.39	0.40
METHOD 5				
Abs.	Max	3.45	2.33	1.03
Dev.[%]	Min	2.86	1.39	0.39

Table 2.3 Calculated Speeds of Sound and Their Absolute Deviations from Experimental Data

System		Air*	Ar	N_2	CO_2
No. of Experimental Points		17	26	24	22
Temperature [°K]		245.00 - 315.00	273.15 - 298.15	273.15 - 298.15	273.15 - 298.15
Pressure [kPa]		95.43 - 229.43	1080.3 9844.6	1137.3 8927.9	1000.3 4590.7
METHOD 1					
Abs. Dev.[%]	Max	0.90	1.76	1.14	4.37
	Min	0.68	1.46	0.64	0.74
METHOD 2					
Abs. Dev.[%]	Max	2.78	14.79	8.89	24.00
	Min	2.59	11.99	4.91	16.10
METHOD 3					
Abs. Dev.[%]	Max	3.09	2.99	1.07	5.33
	Min	1.66	1.32	0.61	0.89
METHOD 4					
Abs. Dev.[%]	Max	3.08	3.25	1.34	6.66
	Min	1.66	1.40	0.87	1.13
METHOD 5					
Abs. Dev.[%]	Max	3.08	3.24	1.37	6.54
	Min	1.66	1.40	0.88	1.12

* Mole Fraction: 0.7809 N_2, 0.2095 O_2, 0.0093 Ar, 0.0003 CO_2

Table 2.4 Methods' Efficiency

Total Average Deviation [%]					
Method	1	2	3	4	5
Compressibility Factor	5.32	5.15	2.68	2.34	2.71
Density	0.62	0.77	1.55	1.55	1.55
Speed of Sound	0.88	8.90	1.12	1.27	1.27
Total Average	2.27	4.94	1.78	1.72	1.84

Table 2.5 Gas Constants

Property \ Gas	He	Ar	N_2	CO_2
MW	4.003	39.948	28.016	44.011
$\theta[^oK]$	10.80	121.00	95.48	187.50
$\sigma[A]$	2.560	3.420	3.704	4.550
$P_c[kPa]$	2300.00	4860.00	3390.00	7386.63
$T_c[^oK]$	5.3	151.0	126.2	304.2
$t_{cp}[^oK]$	200.00	200.00	200.00	200.00
$cp_i[J/mol^oK]$	20.78585	20.78585	29.12757	32.38071
$t_{cp}[^oK]$	298.00	298.00	298.00	298.00
$cp_i[J/mol^oK]$	20.78585	20.78585	29.14432	37.15366
$t_{cp}[^oK]$	300.00	300.00	300.00	300.00
$cp_i[J/mol^oK]$	20.78585	20.78585	29.14432	37.24577
$t_{cp}[^oK]$	400.00	400.00	400.00	400.00
$cp_i[J/mol^oK]$	20.78585	20.78585	29.26573	41.35302

Table 2.5 (continued)

Property \ Gas	CH_4	C_2H_6	C_3H_8	C_2H_2
MW	16.043	30.068	44.094	26.038
$\theta[^oK]$	142.50	243.00	242.00	212.00
$\sigma[A]$	3.355	3.954	5.637	4.114
$P_c[kPa]$	4640.73	4880.00	4255.65	6273.01
$T_c[^oK]$	191.1	305.5	369.9	309.2
$t_{cp}[^oK]$	200.00	0.00	0.00	200.00
cp_i $[J/mol^oK]$	33.49859	0.00000	0.00000	35.60873
$t_{cp}[^oK]$	298.00	298.16	298.16	298.00
cp_i $[J/mol^oK]$	35.66316	52.69088	73.56208	44.12469
$t_{cp}[^oK]$	300.00	300.00	300.00	300.00
cp_i $[J/mol^oK]$	35.73434	52.95465	73.93889	44.25866
$t_{cp}[^oK]$	400.00	400.00	400.00	400.00
cp_i $[J/mol^oK]$	40.52822	65.64902	94.37047	50.51374

Table 2.5 (continued)

Property \ Gas	$n-C_4H_{10}$	$i-C_4H_{10}$	$n-C_5H_{12}$	$i-C_5H_{12}$*
MW	58.124	58.124	72.146	72.146
$\theta[^oK]$	297.00	321.55	219.50	293.65*
$\sigma[A]$	4.971	5.309	8.497	6.537*
$P_c[kPa]$	3796.67	3647.74	3374.16	3241.801*
$T_c[^oK]$	425.2	408.1	469.8	450.0*
$t_{cp}[^oK]$	0.00	0.00	0.00	0.00
cp_i $[J/mol^oK]$	0.00000	0.00000	0.00000	0.00000
$t_{cp}[^oK]$	298.16	298.16	298.16	298.16
cp_i $[J/mol^oK]$	98.85035	96.88255	122.67324	120.70544
$t_{cp}[^oK]$	300.00	300.00	300.00	300.00
cp_i $[J/mol^oK]$	99.52024	97.34310	123.55247	121.29160
$t_{cp}[^oK]$	400.00	400.00	400.00	400.00
cp_i $[J/mol^oK]$	124.76664	124.64104	154.53479	155.12094

* - Uncertain data

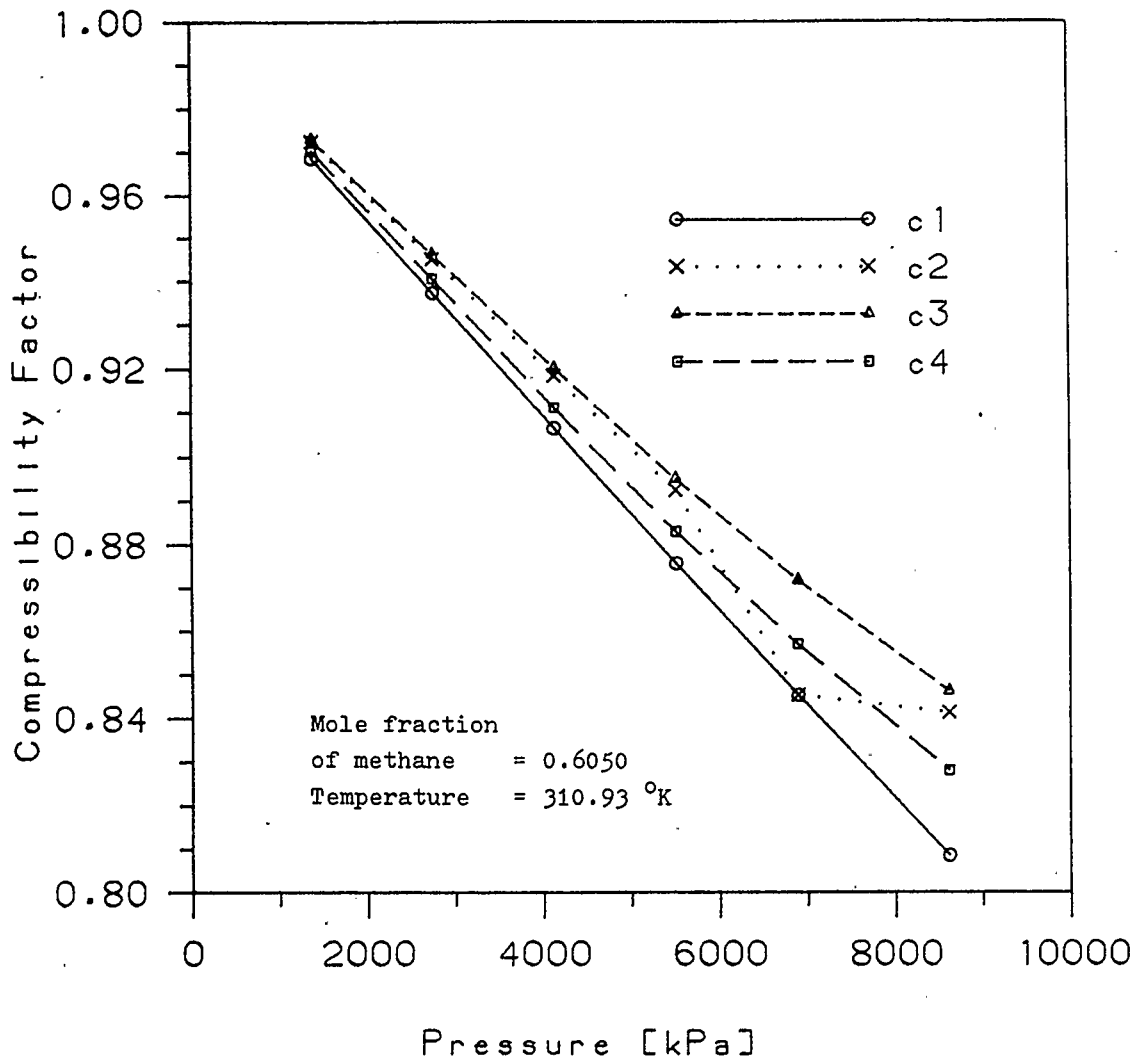

c1 - experimental results
c2 - results obtained from equations (2.11), (2.18), (2.19)
c3 - results obtained from equations (2.14), (2.18), (2.19)
c4 - results obtained from equations (2.14), (2.22), (2.23)

Figure 2.2 Compressibility Factors of a Mixture of Methane and Carbon Dioxide

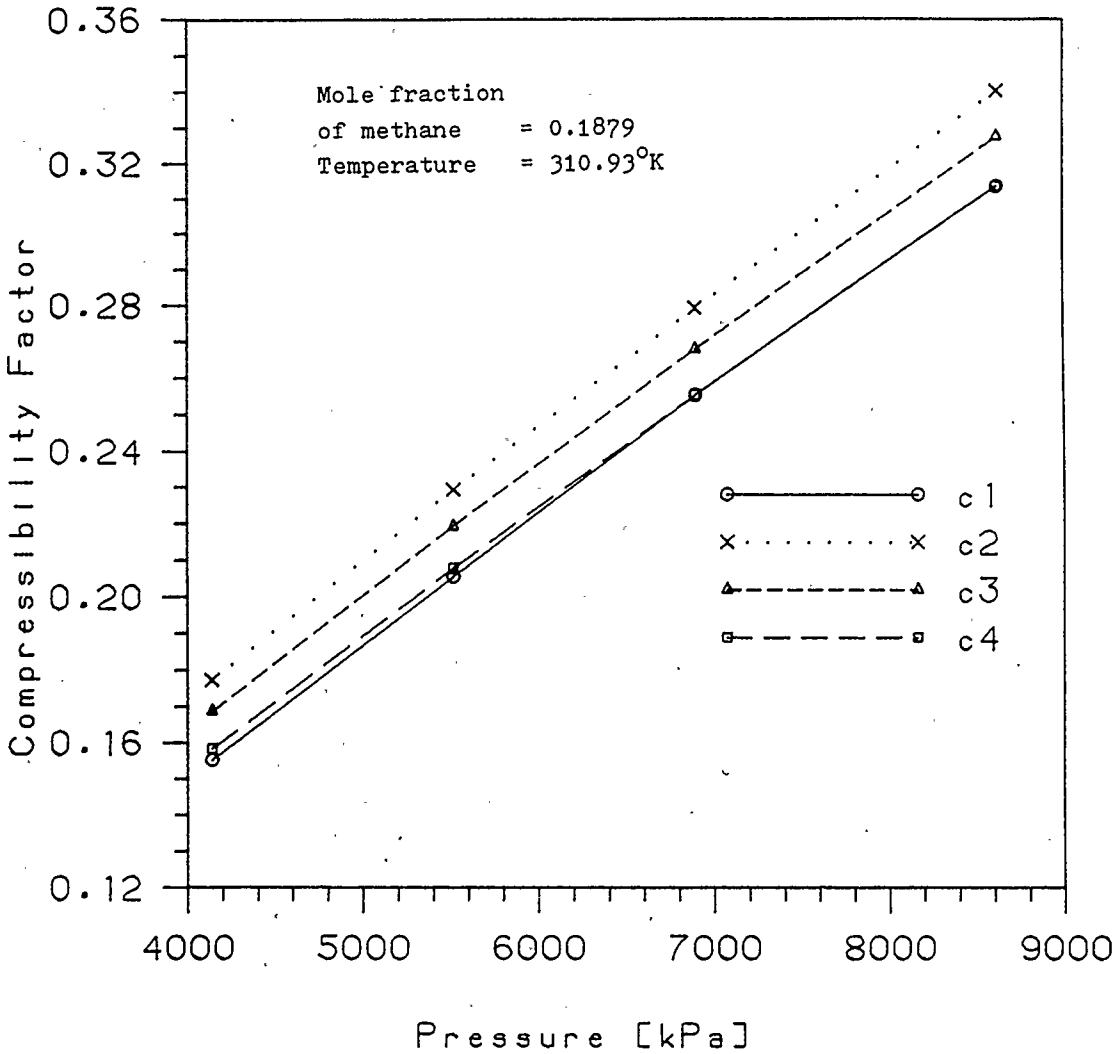

c1 - experimental results
c2 - results obtained from equations (2.11), (2.18), (2.19)
c3 - results obtained from equations (2.14), (2.18), (2.19)
c4 - results obtained from equations (2.14), (2.22), (2.23)

Figure 2.3 Compressibility Factors of a Mixture of Methane and n-Butane

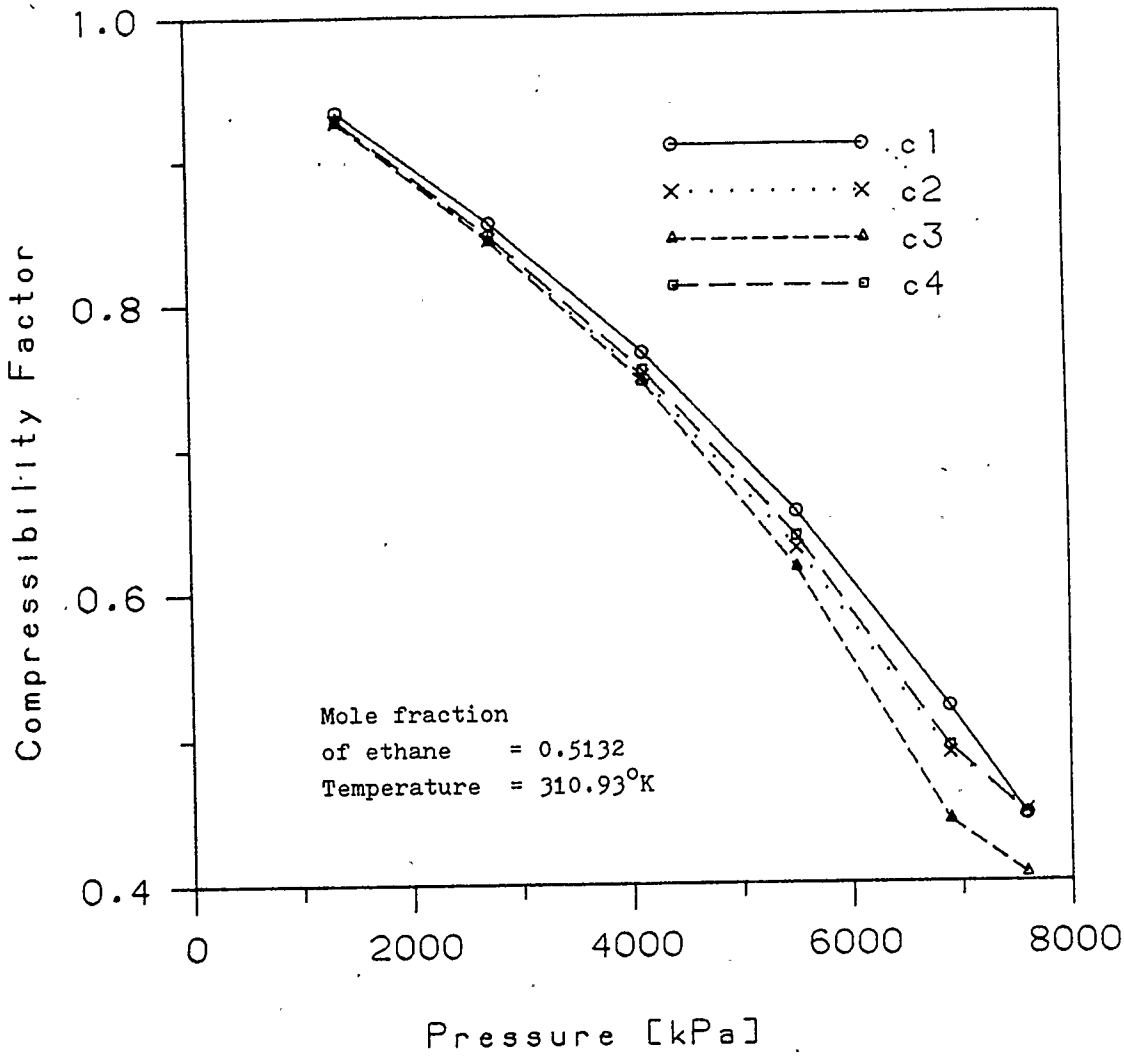

c1 - experimental results
c2 - results obtained from equations (2.11), (2.18), (2.19)
c3 - results obtained from equations (2.14), (2.18), (2.19)
c4 - results obtained from equations (2.14), (2.22), (2.23)

Figure 2.4 Compressibility Factors of a Mixture of Ethane and Carbon Dioxide

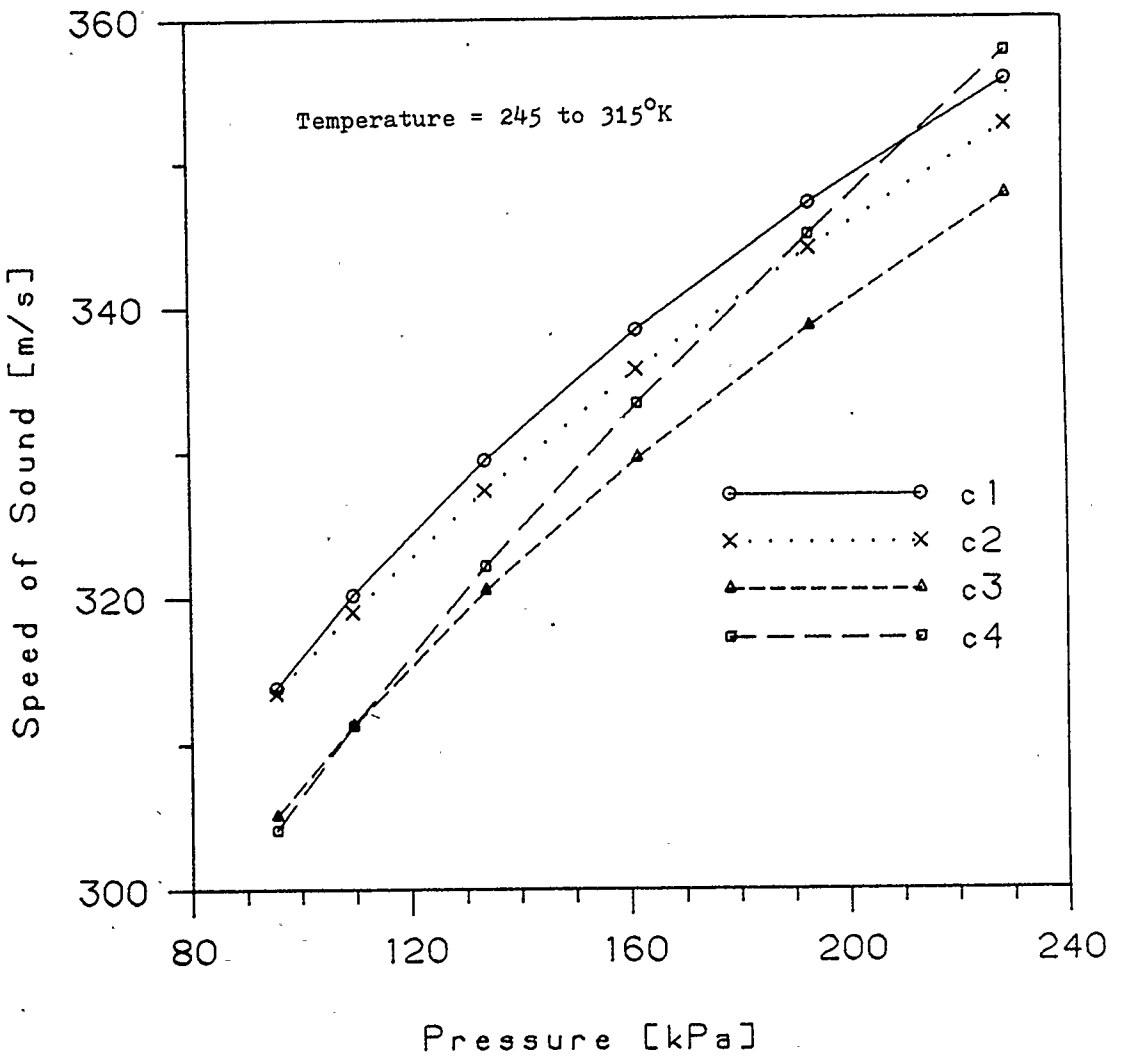

c1 - experimental results
c2 - results obtained from equations (2.11), (2.18), (2.19)
c3 - results obtained from equations (2.14), (2.18), (2.19)
c4 - results obtained from equations (2.14), (2.22), (2.23)

Figure 2.5 Speed of Sound in Air

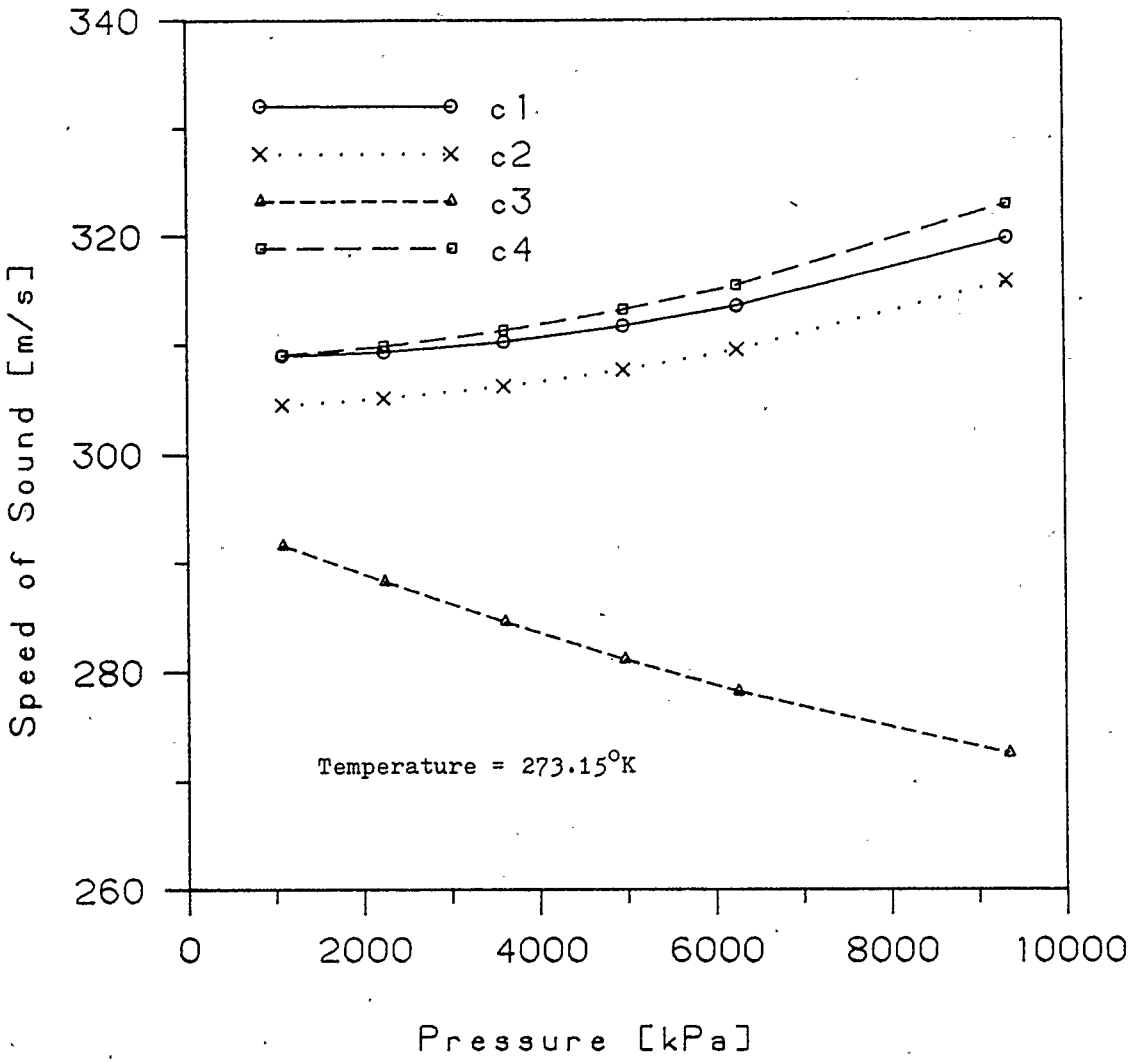

c1 - experimental results
c2 - results obtained from equations (2.11), (2.18), (2.19)
c3 - results obtained from equations (2.14), (2.18), (2.19)
c4 - results obtained from equations (2.14), (2.22), (2.23)

Figure 2.6 Test for Pure Gases: Speed of Sound in Argon

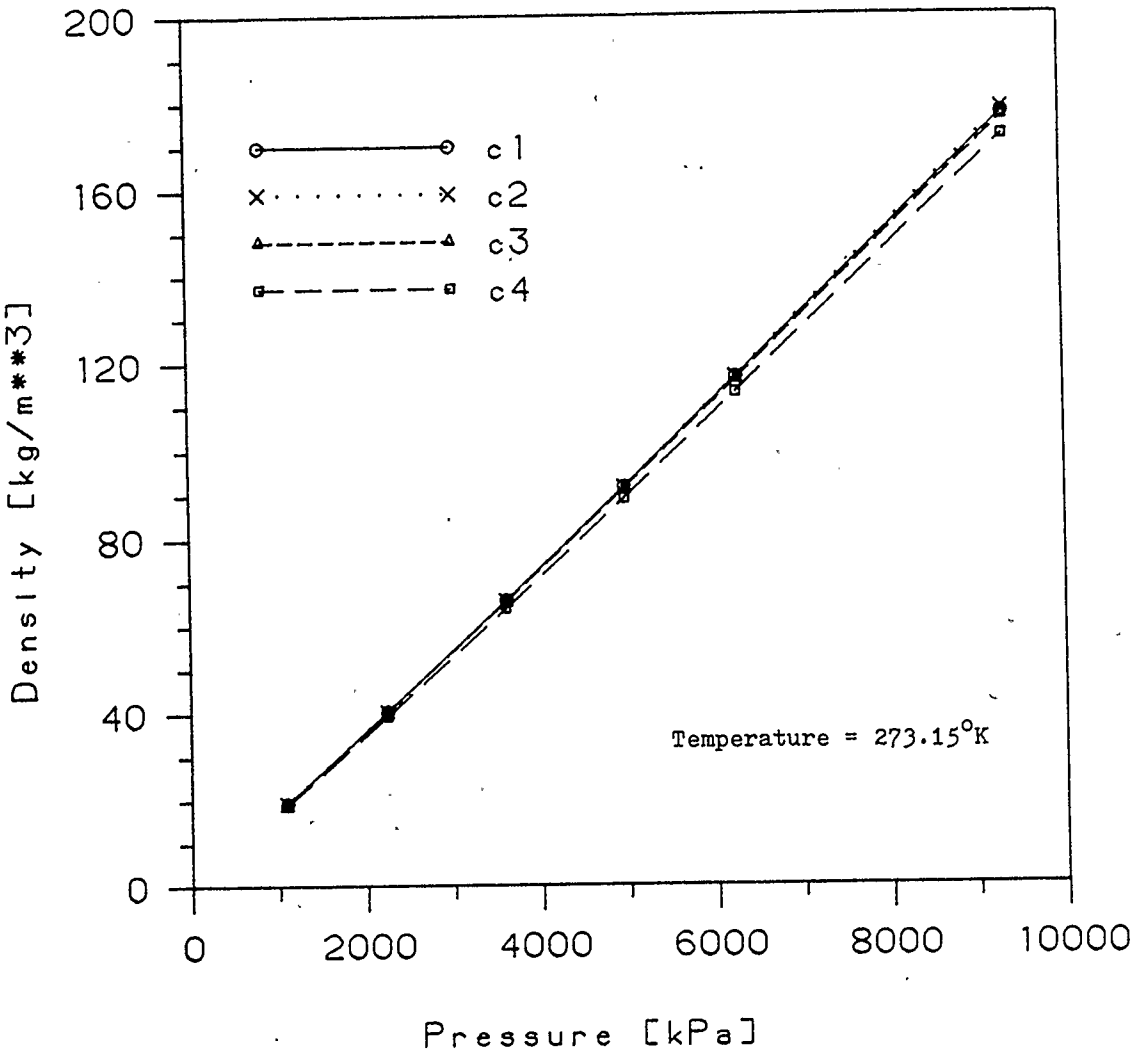

c1 - experimental results
c2 - results obtained from equations (2.11), (2.18), (2.19)
c3 - results obtained from equations (2.14), (2.18), (2.19)
c4 - results obtained from equations (2.14), (2.22), (2.23)

Figure 2.7 Test for Pure Gases: Density of Argon

CHAPTER 3

FUNDAMENTALS OF TRANSFER MATRIX MODELLING

3.1. Introductory Remarks about Modelling Techniques

Modelling is a process of describing the behaviour of a physical system by means of suitably selected mathematical equations. Systems to be modelled are often made up of a large number of components, interconnected in a complex fashion. The system method, used in this work, addresses system complexity not by a detailed physical description of the components, but by the portrayal of a multitude of components, the behaviour of each of which is modelled in a relatively simple fashion. When the dynamic behaviour of a system is considered, generally, the use of linear constant-coefficient ordinary differential equations is sufficient [16,43,32]. The reason is that this approach gives an opportunity to examine systems with many components while still preserving a large measure of qualitative and quantitative understanding.

The system approach emphasizes "modular" methods in dealing with complex processes because they simplify the problem, are efficient and adaptable. That is, if the model components are easily interfaced, at the input and output ports, they can be used in any context. As a result, the transfer function of the whole system can be determined by multiplying the component transfer functions.

In the prediction of systems' responses, three main approaches have been used: the finite element method [10,12,13,33,91], the method of characteristics [8,18,31,34,94], and the transfer matrix method [43,53,54,64,90]. Generally, the transfer matrix method is the simplest, most versatile, and well suited for digital computation. Furthermore, the transfer matrix method has some distinct advantages over the other two methods for the applications considered. These are:

- The method can be applied to a very complex system as well as to any of its parts.
- It requires relatively little computer time.
- It is applicable in a field testing situation.
- It can be used for a variety of acoustic systems with or without mean flow.

3.2 Transfer Matrix Approach

Four pole parameter equations for a uniform circular pipe have been derived in the literature [16,43,53,64]. A summary of these derivations has been included in this work for reasons of clarity and completeness. The description of the physical condition of a sound field in mathematical terms requires the introduction of some assumptions. These are outlined below.

3.2.1 Assumptions

1) Sound propagation is in the form of plane waves.

2) Nonviscous flow through a constant area.

3) A homogenous medium; no temperature gradient or humidity change through the system.

4) Gravitational forces within the medium are neglected.

5) Changes in density of the medium are small.

6) The sound pressures are small in comparison with the average equilibrium pressure in the system.

3.2.2 Momentum and Continuity Equations

In order to derive four pole parameter equations, a two-port model relating Fourier-transformed pressure and velocity at x = 0 to those at x = L (see Figure 3.1) was developed [16,43,53]. For simplicity, damping effects are excluded in the derivation presented below.

The force acting on the element dx in the longitudinal direction is due to the pressure difference across dx,

$$F = \left[p' - (p' + \frac{\partial p'}{\partial x}dx)\right]S = -\frac{\partial p'}{\partial x}Sdx \tag{3.1}$$

The mass of the free body element dx is

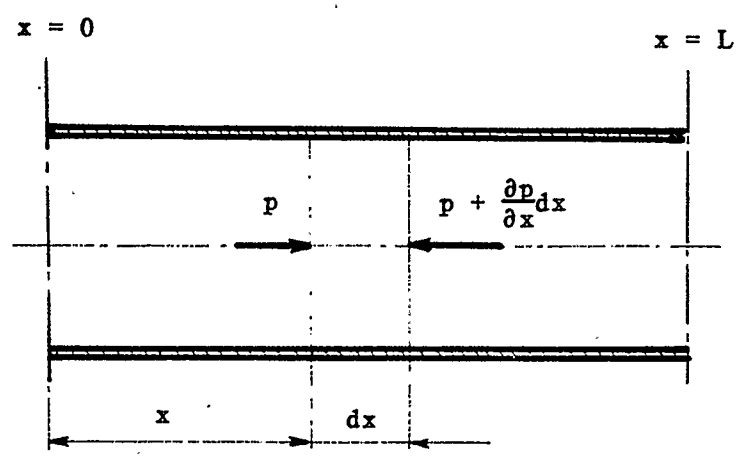

Figure 3.1 Two-Port Model of a Circular Pipe

$$dm = \rho' S dx \tag{3.2}$$

Its velocity is a function of both x and t,

$$du = \frac{\partial u'}{\partial x} dx + \frac{\partial u'}{\partial t} dt \tag{3.3}$$

The acceleration is then

$$a = \frac{\partial u'}{dt} = \frac{\partial u'}{\partial x}\frac{dx}{dt} + \frac{\partial u'}{\partial t} = u'\frac{\partial u'}{\partial x} + \frac{\partial u'}{\partial t} \tag{3.4}$$

Applying Newton's law to the element dx and using equations (3.1), (3.2), and (3.4) yields

$$-\frac{\partial p'}{\partial x} S dx = \rho' S dx\left(u'\frac{\partial u'}{\partial x} + \frac{\partial u'}{\partial t}\right) \tag{3.5}$$

which gives the following form of the momentum equation:

$$\frac{\partial p'}{\partial x} + \rho' u' \frac{\partial u'}{\partial x} + \rho' \frac{\partial u'}{\partial t} = 0 \tag{3.6}$$

From the conservation of mass for the space dx, the following must hold: The mass influx rate minus the mass efflux rate equals the mass storage rate,

$$\rho' \frac{Sdx}{dt} - \left[\frac{\rho' Sdx}{dt} + \frac{\partial}{\partial x}\left(\frac{\rho' Sdx}{dt}\right) dx \right] = \frac{\partial}{\partial t}(\rho' Sdx) \tag{3.7}$$

The continuity equation for constant area S, reduces to

$$S\frac{\partial \rho'}{\partial t} + \rho' S\frac{\partial u'}{\partial x} + u' S\frac{\partial \rho'}{\partial x} = 0 \tag{3.8}$$

3.2.3 Linearization

Steady-state operating-point values (subscript 0) and small perturbation values (with no subscripts) are introduced for the purpose of linearization. Assuming an initial steady state characterized by constant velocity u_o, pressure p_o, and density ρ_o, the instantaneous values can be written:

$$u' = u_o + u \tag{3.9}$$

$$p' = p_o + p \tag{3.10}$$

$$\rho' = \rho_o + \rho \tag{3.11}$$

Equation (3.11) can be rewritten in another form, thus eliminating the unknown ρ. The density change is accomplished by compressing a fixed mass into a smaller volume by applying a pressure change:

$$\rho' = \rho_o (1 + K_c p) \tag{3.12}$$

where K_c is called the fluid compliance. The momentum and continuity equations can now be written in terms of perturbations. For that purpose equations (3.9) and (3.12) are substituted into (3.6) and (3.8). When simplifying, the products of the perturbation quantities are assumed to be very small and are neglected. Furthermore, $\frac{\partial p_o}{\partial x}$ is zero since there is no pressure gradient in steady, frictionless, constant-area flow. Finally, $\frac{\partial u_o}{\partial t}$, $\frac{\partial u_o}{\partial x}$, $\frac{\partial \rho_o}{\partial t}$, and $\frac{\partial \rho_o}{\partial x}$ are all zero as there are no variations in velocity and density for the initial steady flow. Hence, equations (3.6) and (3.8) take the form:

$$\frac{1}{\rho_o}\frac{\partial p}{\partial x} + u_o\frac{\partial u}{\partial x} + \frac{\partial u}{\partial t} = 0 \tag{3.13}$$

$$\frac{1}{K_c}\frac{\partial u}{\partial x} + u_o\frac{\partial p}{\partial x} + \frac{\partial p}{\partial t} = 0 \tag{3.14}$$

3.2.4 Analytical Solutions of the Equations for a Stationary Medium

For the case when there is no flow, $u_o = 0$, the linearized momentum and continuity equations (3.13) and (3.14) reduce to

$$\frac{1}{\rho_o}\frac{\partial p}{\partial x} + \frac{\partial u}{\partial t} = 0 \tag{3.15}$$

$$\frac{1}{K_c}\frac{\partial u}{\partial x} + \frac{\partial p}{\partial t} = 0 \tag{3.16}$$

Using the Laplace transform for time and taking the initial conditions $u(x,0)$ and $p(x,0)$ as zero (there are no disturbances initially) yields:

$$\frac{1}{\rho_o}\frac{\partial P(x,s)}{\partial x} + sU(x,s) = 0 \tag{3.17}$$

$$\frac{1}{K_c}\frac{dU(x,s)}{dx} + sP(x,s) = 0 \tag{3.18}$$

This pair of simultaneous ordinary differential equations can be solved by using the classical method. Eliminating first P, then U leads to

$$\frac{d^2U(x,s)}{dx^2} - s^2K_c\rho_oU(x,s) = 0 \tag{3.19}$$

$$\frac{d^2P(x,s)}{dx^2} - s^2K_c\rho_oP(x,s) = 0 \tag{3.20}$$

Since equations (3.19) and (3.20) are analogous, only one of them is solved as an example. Solution of 3.19 yields:

$$U = C_1 e^{s(K_c\rho_o)^{1/2}x} + C_2 e^{-s(K_c\rho_o)^{1/2}x} \tag{3.21}$$

Applying boundary conditions at x = 0 and x = L:

$$C_1 = \frac{U(L,s) - U(0,s)e^{-s(K_c\rho_o)^{1/2}L}}{2\sinh\,[s(K_c\rho_o)^{1/2}L]} \tag{3.22}$$

$$C_2 = \frac{U(0,s)e^{s(K_c\rho_o)^{1/2}L} - U(L,s)}{2\sinh\,[s(K_c\rho_o)^{1/2}L]} \tag{3.23}$$

Introducing the so called propagation time T_p,

$$T_p = L\,(K_c\rho_o)^{1/2} = \frac{L}{(1/K_c\rho_o)^{1/2}} \tag{3.24}$$

where L is the distance between stations and $(1/K_c\rho_o)^{1/2}$ is the propagation velocity, gives

$$U(x,s) = \frac{1}{\sinh(T_p s)}\Big(U(L,s)\,\sinh[s(K_c\rho_0)^{1/2}x] + U(0,s)\,\sinh[s(K_c\rho_0)^{1/2}(L-x))\Big) \tag{3.25}$$

In order to relate variables at x = 0 to variables at x = L equation (3.25) must be further manipulated. Substituting equation

(3.25) into equation (3.18) gives:

$$K_c sP(x,s) + \frac{d}{dx}\left(\frac{1}{\sinh(T_p s)} \left\{ U(L,s) \sinh[s(K_c\rho_o)^{1/2}x] + U(0,s) \sinh[s(K_c\rho_o)^{1/2}(L-x)] \right\} \right) = 0 \tag{3.26}$$

which after differentiation results in

$$K_c sP(x,s) + \frac{U(L,s)}{\sinh(T_p s)} s(K_c\rho_o)^{1/2} \cosh[s(K_c\rho_o)^{1/2}x] - \frac{U(0,s)}{\sinh(T_p s)} s(K_c\rho_o)^{1/2} \cosh[s(K_c\rho_o)^{1/2}(L-x)] = 0 \tag{3.27}$$

Setting x = L yields:

$$U(0,s) = \frac{1}{Z_o} \sinh(T_p s)P(L,s) + \cosh(T_p s)U(L,s) \tag{3.28}$$

where

$$Z_o = (\rho_o/K_c)^{1/2} \tag{3.29}$$

is called the characteristic impedance. A similar procedure for equation (3.20) leads to:

$$P(0,s) = \cosh(T_p s)P(L,s) + Z_o \sinh(T_p s)U(L,s) \tag{3.30}$$

Equations (3.28) and (3.30), relating Fourier-transformed pressure and velocity at x = 0 and x = L, may be rewritten in more versatile form. This can be done by using the volume velocity V instead of the velocity U, where V = U S. Morover, $T_p s$ can be

replaced by the product of the propagation constant and tube length, $T_p s = L(K_c \rho_o)^{1/2} i\omega = L \frac{1}{c} i\omega = \gamma L$. (Note: $\gamma = \alpha + ik$, here $\alpha = 0$). Using transfer matrix notation: equations (3.28) and (3.30) are reduced to:

$$\begin{bmatrix} P \\ V \end{bmatrix}_{x=0} = \begin{bmatrix} \cosh(\gamma L) & Z\sinh(\gamma L) \\ \frac{1}{Z}\sinh(\gamma L) & \cosh(\gamma L) \end{bmatrix} \begin{bmatrix} P \\ V \end{bmatrix}_{x=L} \tag{3.31}$$

where $Z = Z_o/S$ is called the acoustic impedance.

Equation (3.31) was derived for no-flow conditions. If mean flow is present, the value of γ has to be adjusted (the Mach number included) and the transfer matrix must be multiplied by $e^{-\gamma ML}$ where M is the Mach number of the moving medium. Therefore, for mean flow conditions, equation (3.31) takes the form:

$$\begin{bmatrix} P \\ V \end{bmatrix}_{x=0} = e^{-\gamma LM} \begin{bmatrix} \cosh(\gamma L) & Z\sinh(\gamma L) \\ \frac{1}{Z}\sinh(\gamma L) & \cosh(\gamma L) \end{bmatrix} \begin{bmatrix} P \\ V \end{bmatrix}_{x=L} \tag{3.32}$$

3.3 Practical Expressions for the Acoustic Properties

3.3.1 Acoustic Damping

Equation (3.32) presented in the previous section has not accounted for the dissipation of acoustic energy. In the case of a stationary medium this dissipation is caused by viscous effects,

heat transfer, and the exchange of molecular energy. For a moving medium, many formulae have been proposed to include the dissipation effects [47].

A convenient method to include the dissipation of acoustic energy is to express the parameters in the equations (3.31 and 3.32) as complex quantities [41,47,88]. They are as follows:

- Complex wavelength constant: $\bar{k} = k - i\alpha$,

  where α is the attenuation factor. Using the model presented in [41], when an acoustic wave propagates with speed c in medium of density ρ_o enclosed by a circular pipe of diameter d, α is given by:

  $\alpha = (0.01946/cd)(f/\rho_o)^{1/2}$ (no-flow)

  and $\alpha = \alpha(1 + M)^2$ (when flow is present)

- Complex speed of sound $\bar{c} = \frac{\omega}{\bar{k}}$.

- Complex propagation constant: $\bar{\gamma} = \frac{\alpha + ik}{1 - M^2}$, and

- Complex acoustic impedance: $\bar{Z} = \frac{\rho_o \bar{c}}{S}$

  The expansion of equation (3.32) to include acoustic damping can now be written:

$$\begin{bmatrix} P \\ V \end{bmatrix}_{x=0} = e^{-\bar{\gamma}LM} \begin{bmatrix} \cosh(\bar{\gamma}L) & \bar{Z}\sinh(\bar{\gamma}L) \\ \frac{1}{\bar{Z}}\sinh(\bar{\gamma}L) & \cosh(\bar{\gamma}L) \end{bmatrix} \begin{bmatrix} P \\ V \end{bmatrix}_{x=L} \qquad (3.33)$$

3.3.2 Acoustic Impedance

When sound propagation occurs in the form of plane waves, the acoustic impedance has the same value at every point of a particular cross-section of a pipe. The impedance is defined as the complex ratio of sound pressure to volume velocity through the cross-section. For example, consider a uniform pipe section with sta-

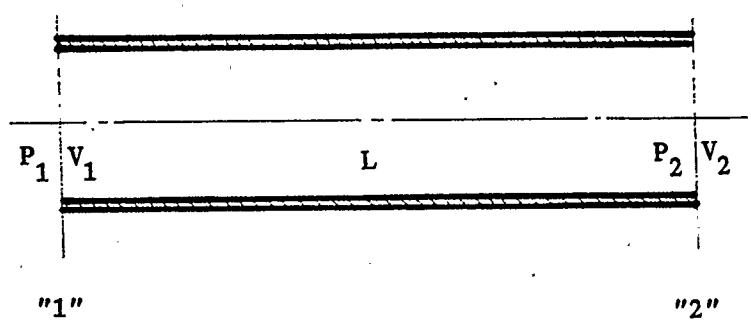

Figure 3.2 A Uniform Pipe Section

tions "1" and "2" as shown in Figure 3. The impedances at these stations are: $Z_1 = P_1/V_1$, and $Z_2 = P_2/V_2$ respectively. Using the four-pole parameter equation,

$$\begin{bmatrix} P_1 \\ V_1 \end{bmatrix} = \begin{bmatrix} A & B \\ C & D \end{bmatrix}_{1,2} \begin{bmatrix} P_2 \\ V_2 \end{bmatrix} \tag{3.34}$$

where A, B, C, and D are elements of transfer matrix $[T]_{12}$ (as in

equations (3.31), (3.32) or (3.33)), the volume velocities can be expressed as follows:

$$V_1 = \frac{P_2(B\ C - A\ D)}{B} + \frac{P_1 D}{B} \tag{3.35}$$

$$V_2 = \frac{(P_1 - A\ P_2)}{B} \tag{3.36}$$

Applying the reciprocal condition, det [T] = 1 (noflow), yields:

$$V_1 = \frac{(P_1 D - P_2)}{B} \tag{3.37}$$

$$V_2 = \frac{(P_1 - A\ P_2)}{B} \tag{3.38}$$

Therefore, the acoustic impedances Z_1 and Z_2 can be calculated from the pressures P_1 and P_2, and the matrix parameters A, B, C and D.

$$Z_1 = \frac{B}{D - P_2/P_1} \tag{3.39}$$

$$Z_2 = \frac{B}{(P_1/P_2) - A} \tag{3.40}$$

From the equations (3.39) and (3.40), it can be noticed that neither Z_1 nor Z_2 depend directly on the input and output pressures, but only on their ratio (P_1/P_2) which depends only on the downstream geometry and termination impedance. The above equations can be used to experimentally determine the impedance.

3.3.3 Discontinuity Correction Factor

A discontinuity such as a sudden expansion or contraction is usually corrected for by one of two methods. The first method is based on the physical fact that the gas beyond the open end of the smaller tube moves as a unit together with the gas enclosed in that tube [63]: The corrected length of the tube is then taken as $L_e = L + \Delta L$, where L is the actual tube length and ΔL is the Pollack correction factor given in Figure 3.2a. Hence, the transfer matrix in the equation (3.33) is written as

$$\begin{bmatrix} P_p \\ V_P \end{bmatrix}_{x=0} = e^{-\bar{\gamma}L_e} \begin{bmatrix} \cosh(\bar{\gamma}L_e) & \bar{Z}\sinh(\bar{\gamma}L_e) \\ \frac{1}{\bar{Z}}\sinh(\bar{\gamma}L_e) & \cosh(\bar{\gamma}L_e) \end{bmatrix} \begin{bmatrix} P_p \\ V_P \end{bmatrix}_{x=L} \tag{3.41}$$

In the second method, a separate transfer matrix representing the discontinuity is used [35].

$$\begin{bmatrix} T \end{bmatrix} = \begin{bmatrix} 1 & i\omega K_L \\ 0 & 1 \end{bmatrix} \tag{3.42}$$

where K_L is the Karal correction factor given in Figure 3.3b. In this work, the Karal correction factor was used.

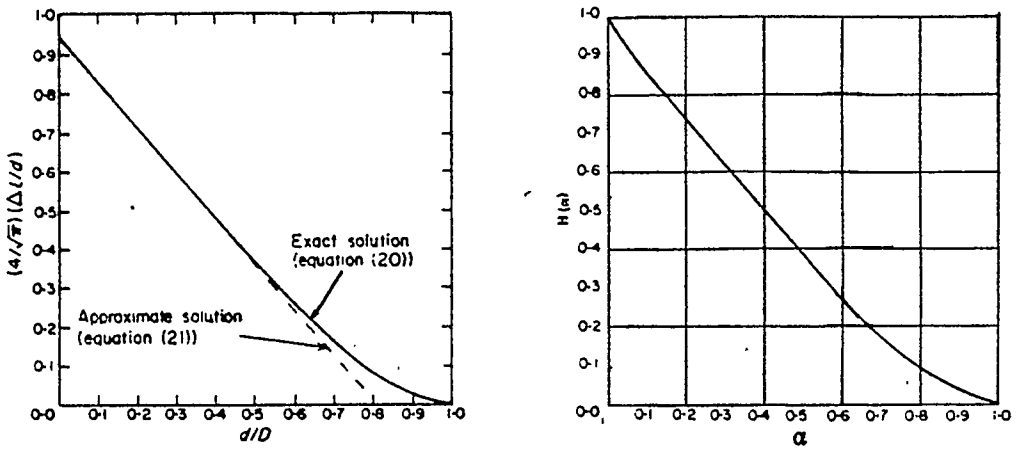

a) Pollack Correction Factor b) Karal Correction Factor

Figure 3.3 Correction Factors for Sudden Expansion and Sudden Contractions (d - diameter of the smaller tube, D - diameter of the large tube, ($\alpha = d/D$, $L = 8\rho[3\pi^2 d]\ H(\alpha)$)

CHAPTER 4

ARBITRARY BRIDGE NETWORK ANALYSIS

4.1 Mathematical Model of an Arbitrary Bridge Network

4.1.1 Transfer Matrix for a Bridge Network

The principle of applying the transfer matrix method to a bridge network is to express the overall transfer matrix in terms of the network's elements [83]. In this chapter transfer matrices for a network's elements are presented. The matrices for the fundamental elements such as a straight pipe, an elbow, a side branch, and an orifice plate are introduced first. Following this, the matrices for series-connected and parallel-connected elements are presented. Finally, the overall transfer matrix for an arbitrary bridge network is derived. Throughout this section, the transfer matrices are written for no flow conditions. The procedure to include mean flow involves only multiplication by a single factor and modifying the value of $\bar{\gamma}$ (as shown in section 3.2).

a) Straight Pipe

The expression for the no-flow transfer matrix, derived in section 3.2, is:

$$[T]_{1,2} = \begin{bmatrix} \cosh(\bar{\gamma}L) & \bar{Z}\sinh(\bar{\gamma}L) \\ \frac{1}{\bar{Z}}\sinh(\bar{\gamma}L) & \cosh(\bar{\gamma}L) \end{bmatrix} \tag{4.1}$$

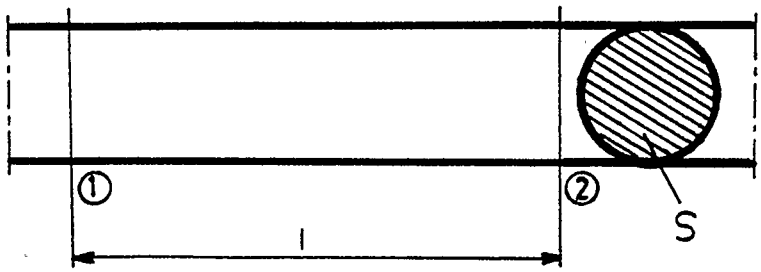

Figure 4.1 Straight Pipe

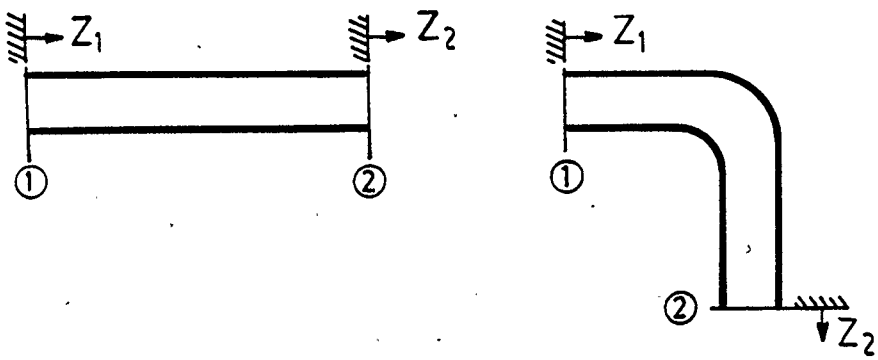

Figure 4.2 Straight Pipe and Elbow Elements

b) Elbow

In this work, an elbow is approximated by a straight pipe of equal length and cross-sectional area. An experiment was carried out to compare the behaviour of these two elements. For each, the following equation holds:

$$\begin{bmatrix} P_1 \\ V_1 \end{bmatrix} = \begin{bmatrix} A & B \\ C & D \end{bmatrix} \begin{bmatrix} P_2 \\ V_2 \end{bmatrix} \tag{4.2}$$

From this,

$$\frac{P_1}{P_2} = A + B/\bar{Z}_2 \tag{4.3}$$

For station 2 (see Figure 4.2) closed, the impedance $\bar{Z}_2$ is infinite. Consequently, it was possible to obtain the A parameters of the transfer matrices for both cases by measuring the port pressures. These parameters were plotted as a function of frequency. The graphs depicted in Figures 4.3 show that the adopted assumption is justified: effects of the distortion of waves by a duct bend are insignificant for frequencies below the cut-off frequency. In this work, the highest frequencies encountered are always lower than the cut-off frequency (plane wave propagation). The formula used to calculate the cut-off frequency [47] is given by:

$$f_c = 1.84\ c/(2\pi r) \tag{4.4}$$

For the above experiment, $f_c = 4945$ Hz.

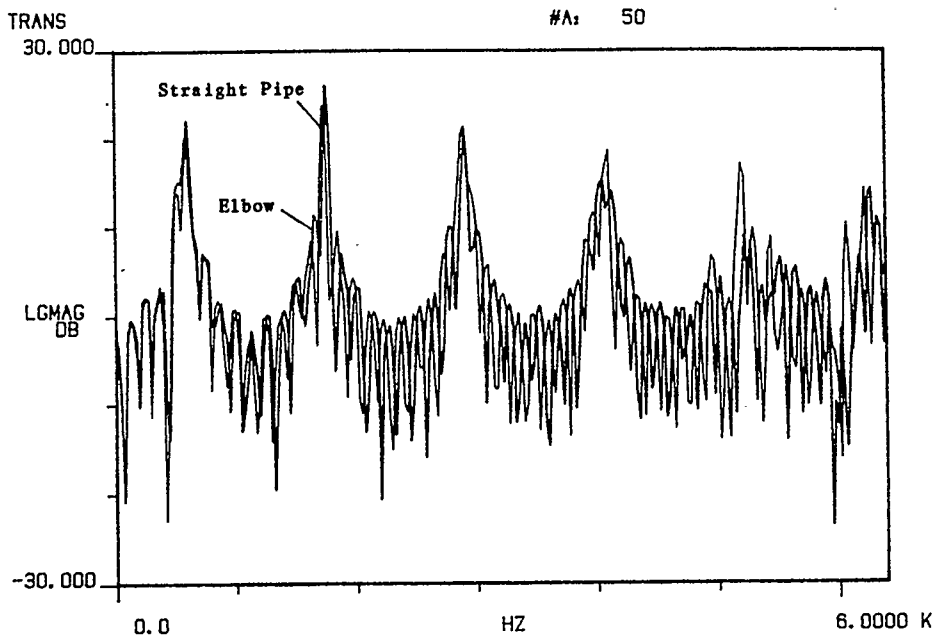

a) Range from 0 to 6000 Hz

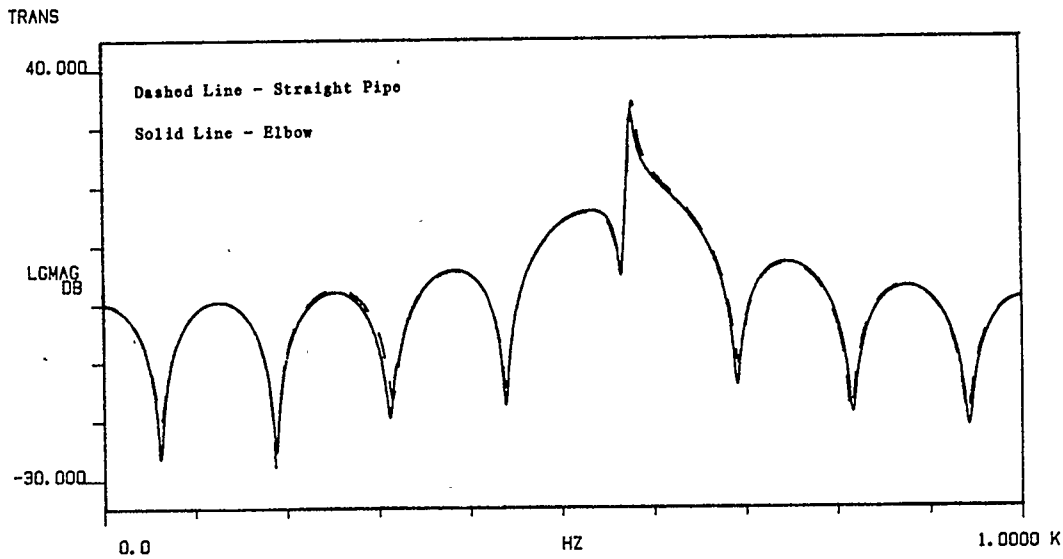

b) Range from 0 to 1000 Hz

Figure 4.3 The A Parameters of the Transfer Matrices for a Straight Pipe and Elbow

c) Side Branch

The transfer matrix of a side branch resonator is repeated here after reference [48]:

$$[T]_{1,2} = \begin{bmatrix} 1 & 0 \\ 1/\bar{Z} & 1 \end{bmatrix} \tag{4.5}$$

where $\bar{Z}$ (for closed end)is the ratio of the element A and C of the transfer matrix of the side branch.

d) Orifice Plate

An orifice plate and its model, tested at the University of Calgary, are depicted in Figure 4.5. The model, applicable for low flows, assumes that the orifice plate can be replaced by an equivalent system. The equivalent system is described by a short pipe of length given by:

$$l = 0.3d_{op} + l_{op} + 0.3d_{op} \tag{4.6}$$

and two side branches on each side of the pipe. The diameter and length of the branches are calculated as follow:

$$d_b = (d^2 - d_{op}^2)^{1/2} \tag{4.7}$$

$$l_b = 0.3\ d_{op}\ , \tag{4.8}$$

e) Series and Parallel Elements

Series-connected and parallel-connected elements are characterized by having two inlets and two outlets as shown in Figure

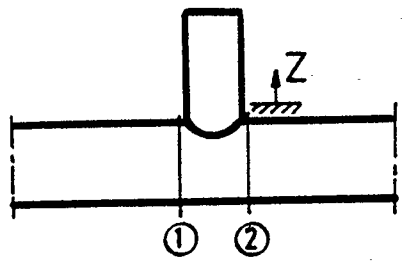

Figure 4.4 Side Branch Resonator

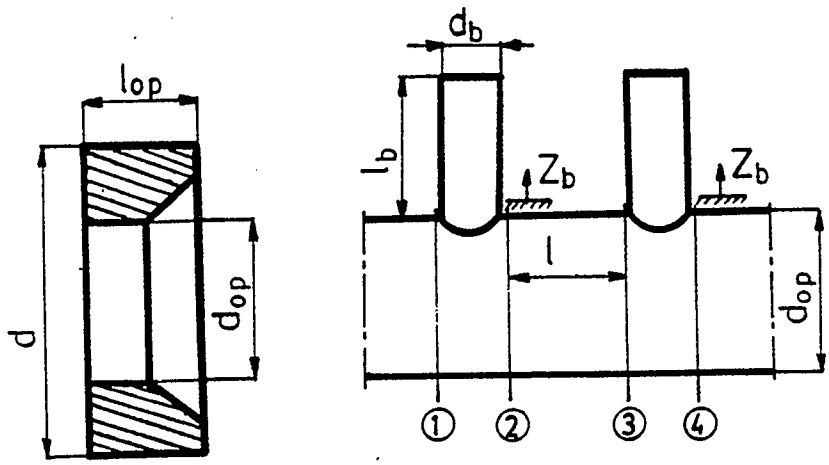

a) Orifice Plate b) Model

Figure 4.5 Orifice Plate and Its Acoustic Model

4.6. As a result, the transfer matrices between the input and output are four by four matrices. These matrices have been derived in

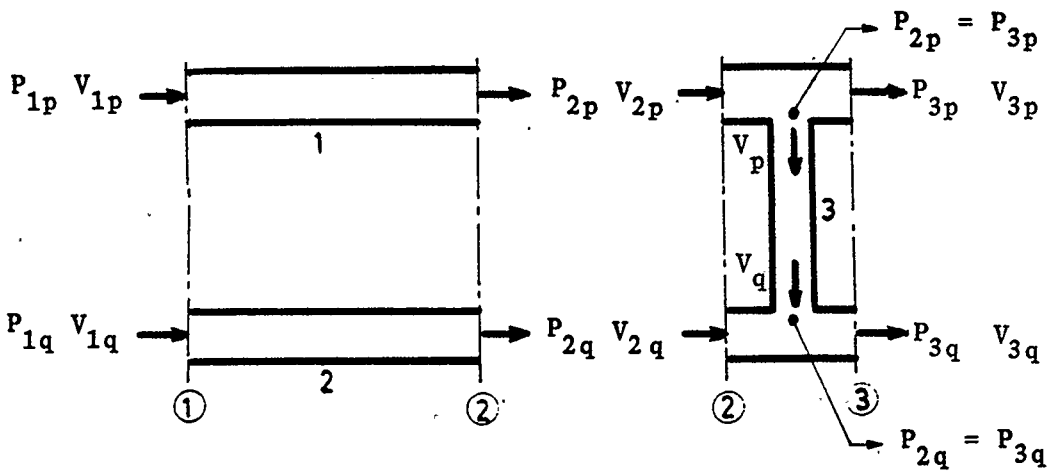

Figure 4.6 Series and Parallel Elements

references [6] and [47].

The transfer matrix for the series element was obtained by combining the matrices of the component elements. Consequently, the input-output equation for a series element is:

$$\begin{bmatrix} P_{1p} \\ V_{1p} \\ P_{1q} \\ V_{1q} \end{bmatrix} = \begin{bmatrix} A_1 & B_1 & 0 & 0 \\ C_1 & D_1 & 0 & 0 \\ 0 & 0 & A_2 & B_2 \\ 0 & 0 & C_2 & D_2 \end{bmatrix} \begin{bmatrix} P_{2p} \\ V_{2p} \\ P_{2q} \\ V_{2q} \end{bmatrix} \tag{4.9}$$

For the parallel-connected element the following continuity equations must hold:

$$P_{2p} = P_{3p} \tag{4.10}$$

$$P_{2q} = P_{3q} \tag{4.11}$$

$$V_{2p} = V_{3p} + V_p \tag{4.12}$$

$$V_{3q} = V_{2q} + V_q \tag{4.13}$$

The transfer matrix equation for element 3 is:

$$\begin{bmatrix} P_{2p} \\ V_p \end{bmatrix} = \begin{bmatrix} A_3 & B_3 \\ C_3 & D_3 \end{bmatrix} \begin{bmatrix} P_{2q} \\ V_q \end{bmatrix} \tag{4.14}$$

The transfer matrix for the parallel-connected element is obtained by combining equations (4.10) to (4.14). Hence, the input-output equation for a parallel element is:

$$\begin{bmatrix} P_{2p} \\ V_{2p} \\ P_{2q} \\ V_{2q} \end{bmatrix} = \begin{bmatrix} 1 & 0 & 0 & 0 \\ D_3/B_3 & 1 & -\Delta_3/B_3 & 0 \\ 0 & 0 & 1 & 0 \\ -1/B_3 & 0 & A_3/B_3 & 1 \end{bmatrix} \begin{bmatrix} P_{3p} \\ V_{3p} \\ P_{3q} \\ V_{3q} \end{bmatrix} \tag{4.15}$$

where, $\Delta_3 = A_3D_3 - B_3C_3$.

f) Overall Transfer Matrix

In this work an arbitrary bridge network was considered. Its schematic representation is depicted in Figure 4.7. The network is composed of k segments, each of which comprises a series type ele-

ment and a parallel type element. Segment k+1 includes a series type element only. The transfer matrix between station 1 and station m is a four by four matrix:

$$[N]_{4x4} = [S_1][P_1][S_2][P_2]\ldots[S_k][P_k][S_{k+1}] \tag{4.16}$$

where $[S]_i$ is a four by four matrix of the i-th series type element, and $[P]_i$ is a four by four matrix of the i-th parallel type

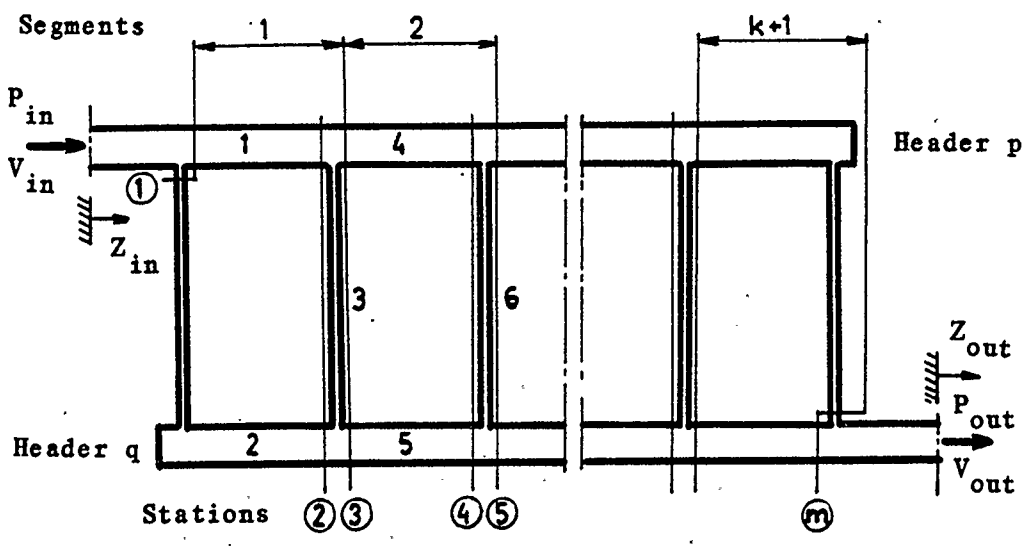

Figure 4.7 Arbitrary Bridge Network, Scheme

element.

To relate the network's input to its output, the overall matrix $[M]_{2x2}$ is used. It is obtained by substituting the continuity equations at the ends of the network into equation (4.16)

as is shown in [6]. Consequently, the input-output relation is:

$$\begin{bmatrix} P_{in} \\ V_{in} \end{bmatrix} = [M] \begin{bmatrix} P_{out} \\ V_{out} \end{bmatrix} \tag{4.17}$$

The parameters of matrix [M] which are expressed in terms of the elements of matrix [N] are as follows:

$$M_{11} = [(N_{11} + N_{13})K_2 - (N_{12} - N_{14})K_1]/K_2 \tag{4.18}$$

$$M_{12} = (N_{12}N_{34} - N_{14}N_{32})/K_2 \tag{4.19}$$

$$M_{21} = (K_2K_3 - K_1K_4)/K_2 \tag{4.20}$$

$$M_{22} = [(N_{22} + N_{42})K_2 - (N_{12} - N_{32})K_4]/K_2 \tag{4.21}$$

where

$$K_1 = N_{11} + N_{13} - N_{31} - N_{33}$$

$$K_2 = N_{12} - N_{14} - N_{32} + N_{34}$$

$$K_3 = N_{21} + N_{23} + N_{41} + N_{43}$$

$$K_4 = N_{22} - N_{24} + N_{42} - N_{44}$$

If some of the valves in the network are closed, the transfer matrix [N] must be modified. For example, if a valve of run i is closed, the corresponding parallel type element must be replaced by a series type element with side branches:

$$[N]' = [S_1][P_1]\ldots[S_i][P_i]'\ldots[S_k][P_k][S_{k+1}] \tag{4.22}$$

Here,

$$[P_i]' = \begin{bmatrix} T_{iu} & 0 \\ 0 & T_{il} \end{bmatrix} \tag{4.23}$$

where T_{iu} and T_{il} are transfer matrices for upper and lower side branches created as a result of shutting the valve in element i. T_u and T_l are calculated from eq. (4.5). In the case when the very first run is closed, the procedure becomes more complex. The modified transfer matrix [N] is:

$$[N]' = ([S_1][P_1])' \ldots [S_2]'[P_2] \ldots [S_k][P_k][S_{k+1}] \tag{4.24}$$

where

$$([S_1][P_1])' = [I] \tag{4.25}$$

and

$$[S_2]' = \begin{bmatrix} T_4 & 0 \\ 0 & T_3 T_{2l} T_5 \end{bmatrix} \tag{4.26}$$

Additionally, the overall 2x2 matrix [M] must be modified, namely, premultiplied by $([T_{2u}][T_1])$. Matrices T_1, T_4 and T_5 are transfer matrices for elements 1, 4 and 5 respectively, and are calculated by chain multiplication of the component elements (refer to Figures 4.7 and 4.8). The situation when the last run is closed, is analogous to the case with the first run closed. Closing of several valves involves combining several required modifications.

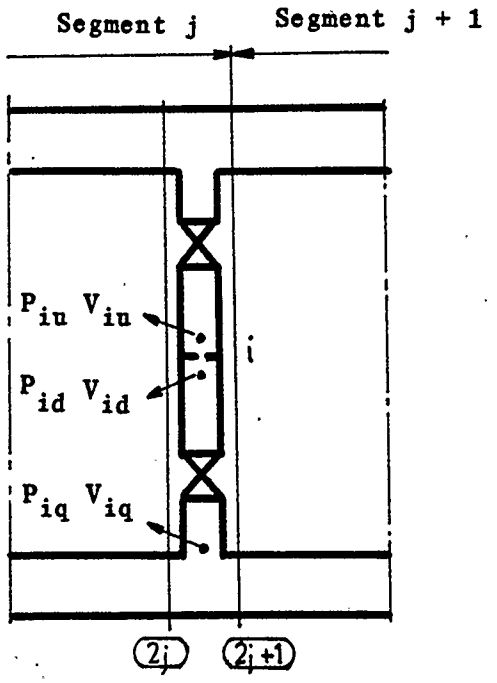

Figure 4.8 Bridge Element Including an Orifice Plate

4.1.2 Volume Velocities and Pressures at Orifice Plate Locations

The transfer matrices presented in section 4.1.1 were used for calculating volume velocities and pressures, both upstream and downstream of the orifice plates. The following procedure was followed:

a) For a given input value of pressure P_{in}, the input volume velocity V_{in} was calculated using:

$$\begin{bmatrix} P_{in} \\ V_{in} \end{bmatrix} = [M] \begin{bmatrix} P_{out} \\ V_{out} \end{bmatrix} \tag{4.27}$$

from which

$$\frac{P_{in}}{V_{in}} = \frac{M_{11}Z_{out} + M_{12}}{M_{21}Z_{out} + M_{22}} \tag{4.28}$$

In the above expression, the impedance $Z_{out} = P_{out}/V_{out}$ was evaluated from the anechoic end condition:

$$Z_{out} = \frac{\rho c}{S_{out}} \tag{4.29}$$

b) The output values of pressure and volume velocity were calculated from:

$$\begin{bmatrix} P_{out} \\ V_{out} \end{bmatrix} = [M]^{-1} \begin{bmatrix} P_{in} \\ V_{in} \end{bmatrix} \tag{4.30}$$

c) The pressures and volume velocities at stations 1 and m

(see Figure 4.7) were evaluated from:

$$\begin{bmatrix} P_{1p} \\ V_{1p} \\ P_{1q} \\ V_{1q} \end{bmatrix} = [N] \begin{bmatrix} P_{mp} \\ V_{mp} \\ P_{mq} \\ V_{mq} \end{bmatrix} \tag{4.31}$$

and the continuity equations:

$$P_{in} = P_{1p} = P_{1q} \tag{4.32}$$

$$P_{out} = P_{mp} = P_{mq} \tag{4.33}$$

$$V_{in} = V_{1p} + V_{1q} \tag{4.34}$$

$$V_{out} = V_{mp} + V_{mq} \tag{4.35}$$

The pressure values were obtained directly from equations (4.32) and (4.33). The expressions obtained for the volume velocities are as follows:

$$V_{mq} = P_{in} - (N_{31} + N_{33}P_{out} - N_{32}V_{out}/N_{34} - N_{32} \tag{4.36}$$

$$V_{1q} = (N_{41} + N_{43})P_{out} + N_{42}V_{out} + (N_{44} - N_{42})V_{mq} \tag{4.37}$$

$$V_{1p} = V_{in} - V_{1q} \tag{4.38}$$

$$V_{mp} = V_{out} - V_{mq} \tag{4.39}$$

d) The pressures and volume velocities at the remaining stations were evaluated going backwards from segment k+1 to 1. For odd numbered stations the following matrix equation was used:

$$\begin{bmatrix} P_{(2j+1)p} \\ V_{(2j+1)p} \\ P_{(2j+1)q} \\ V_{(2j+1)q} \end{bmatrix} = [S_{j+1}] \begin{bmatrix} P_{(2j+2)p} \\ V_{(2j+2)p} \\ P_{(2j+2)q} \\ V_{(2j+2)q} \end{bmatrix} \tag{4.40}$$

and for even numbered stations:

$$\begin{bmatrix} P_{(2j)p} \\ V_{(2j)p} \\ P_{(2j)q} \\ V_{(2j)q} \end{bmatrix} = [P_j] \begin{bmatrix} P_{(2j+1)p} \\ V_{(2j+1)p} \\ P_{(2j+1)q} \\ V_{(2j+1)q} \end{bmatrix} \tag{4.41}$$

where j decrements from station k to station 1.

e) The pressures and volume velocities downstream of the orifice plate placed in the i-th element (see Figure 4.8) were calculated using:

$$\begin{bmatrix} P_{id} \\ V_{id} \end{bmatrix} = [T_{id}] \begin{bmatrix} P_{(2j)q} \\ V_{(2j+1)q} - V_{(2j)q} \end{bmatrix} \tag{4.42}$$

where $[T_{id}]$ is the transfer matrix for the downstream part of element i. The continuity equations used in equation (4.42) are as follows:

$$P_{iq} = P_{(2j)q} = P_{(2j+1)q} \tag{4.43}$$

$$V_{iq} = V_{(2j+1)q} - V_{(2j)q} \tag{4.44}$$

The upstream values of pressure and volume velocity were obtained from:

$$\begin{bmatrix} P_{iu} \\ V_{iu} \end{bmatrix} = [T_{io}] \begin{bmatrix} P_{id} \\ V_{id} \end{bmatrix} \tag{4.45}$$

where $[T_{io}]$ is the transfer matrix for the orifice plate.

4.2 Verification of the Model

The mathematical model introduced above was verified by conducting laboratory tests with one-bridge and two-bridge networks. No flow and random excitation of the system was used.

4.2.1 Instrumentation

Two bridge network models made from ABS plastic tubes and fittings were tested. A schematic representation of the testing apparatus is depicted in Figure 4.9. A loudspeaker (1) was connected at the input of the network model; the output of the network was either closed or open. The loudspeaker was driven by a random noise generator from the Structural Digital Analyzer (6) through a power amplifier (3). There were two microphones (7,8) for which the calibration factors had been previously determined. One of the microphones (7) was placed at the inlet tube, the other (8) was located either at the outlet or at points inside the network. These points are indicated in plots included in Figures 4.11, 4.13 and 4.14. The acoustic signals sensed by the microphones were amplified (amplifiers 4 and 5) and transmitted to the DSA (6). Transfer functions between microphones were stored on magnetic tape for subsequent plotting and analysis.

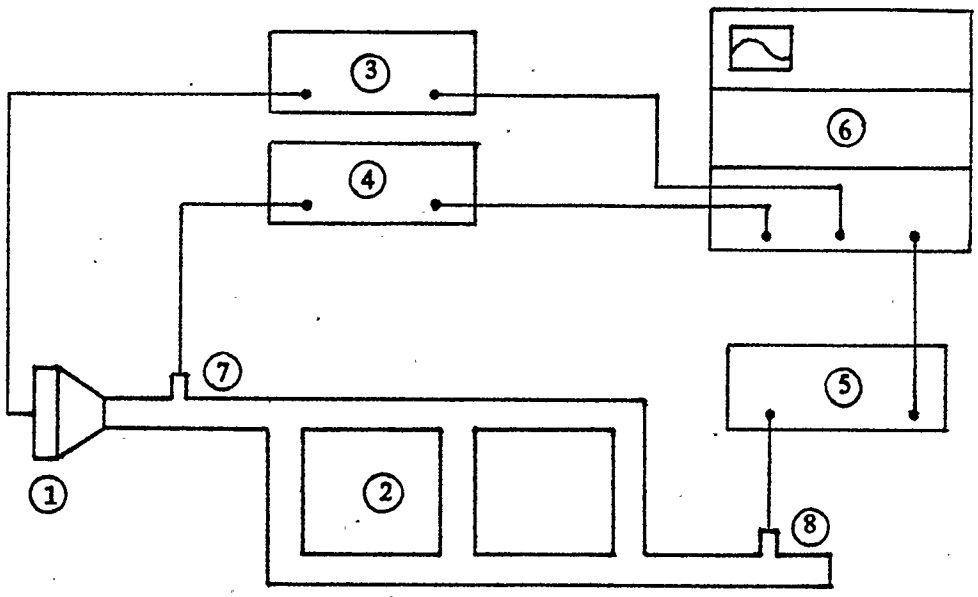

1) Loudspeaker (30 W)
2) Bridge Network Being Tested (Two- or One-Bridge Network)
3) Power Amplifier (Holiday Model - 7100 Stereo)
4) Amplifier (B & K 2608)
5) Amplifier (B & K 2608)
6) Structural Digital Analyzer (HP 5423A)
7) Condenser Microphone (B & K 4133)
8) Condenser Microphone (B & K 4133)

Figure 4.9 Diagram of Testing Apparatus

4.2.2 One-Bridge Network Model

Dimensions of the one-bridge network model are given in Figure 4.10. Experimental pressure ratios were obtained for four different locations (indicated with arrows in Figure 4.11) in the bridge network model (P_i/P_{in}, i = 1,2,3) with all valves open. Both theoretical and experimental results for closed end are shown in Figure 4.11. An excellent agreement can be observed between the shape of the curves. Similar results were obtained for an open termination. The slight shift along the frequency axis, for higher frequencies, is most likely due to inaccuracies in calculating the speed of sound (see Chapter 2). The measurement of bridge dimensions, temperature and pressure could also introduce errors.

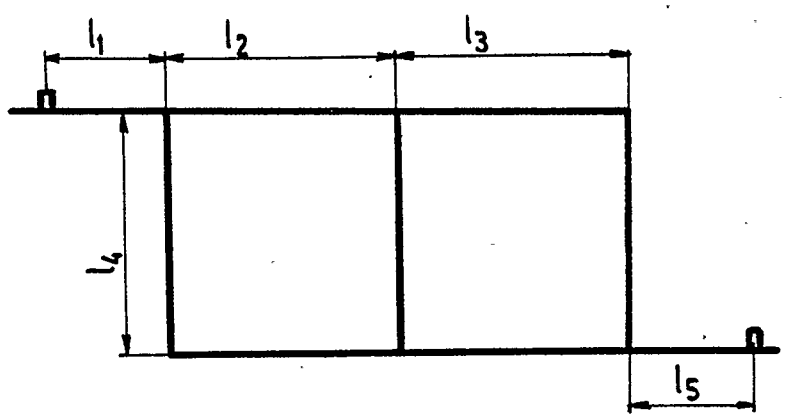

Dimensions:

l_1 = 0.895m l_4 = 0.669m Pipe ID = 0.041m
l_2 = 0.669m l_5 = 0.893m
l_3 = 0.669m

Figure 4.10 One-Bridge Network Model

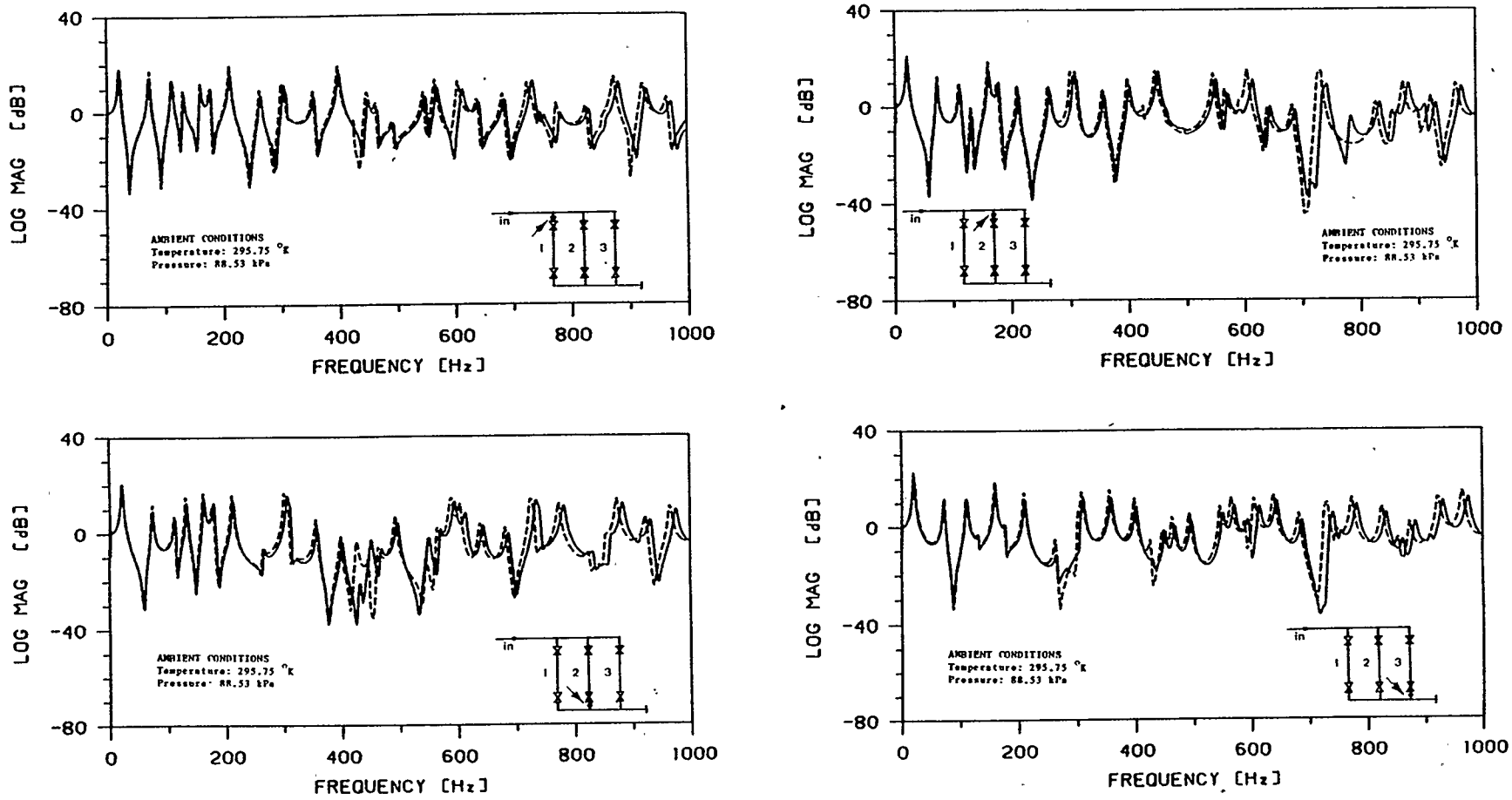

Figure 4.11 Pressure Levels in the One-Bridge Network at Chosen Locations Indicated by Dots, (theory - dashed line, experiment - solid line). All valves open

4.2.3 Two-Bridge Network Model

Dimensions of the two-bridge network model are given in Figure 4.12. Experimental pressure ratios were obtained at four different locations in the bridge network while all valves were open. Both theoretical and experimental results obtained for the given ambient conditions are shown in Figure 4.13. Also, the pressure ratios at different locations for all possible combinations of valve closing were determined. Some representative results for a closed end are depicted in Figure 4.14. Other results, not presented here, showed analogous behaviour. Again, a very good agreement between theoretical and experimental curves can be observed. The shapes of the curves are preserved, but there is a small shift proportional to frequency. As explained earlier, this is most likely caused by inaccuracies in calculating the speed of sound and by possible measuring errors.

The results of these experiments prove the model to be valid and useful in predicting pressure levels in bridge networks, with any combination of valve closure.

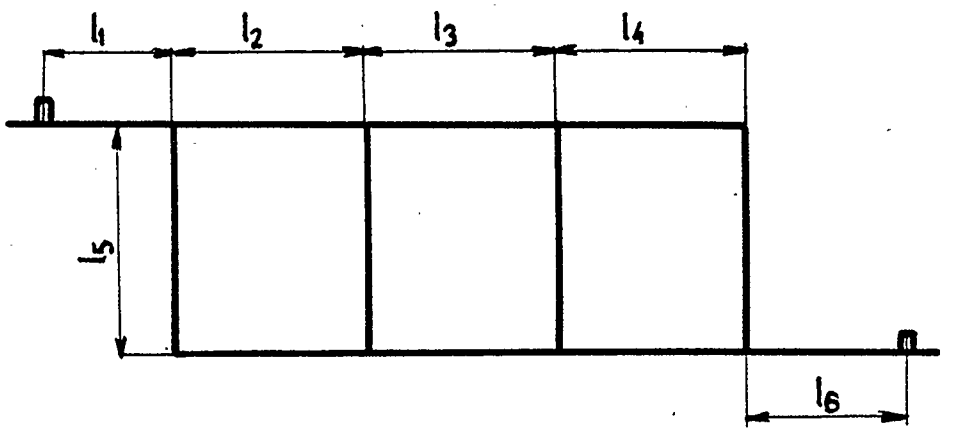

Dimensions:

l_1 = 0.893m	l_4 = 0.671m	Pipe ID = 0.041m
l_2 = 0.671m	l_5 = 0.492m	
l_3 = 0.671m	l_6 = 0.895m	

Figure 4.12 Two-Bridge Network Model

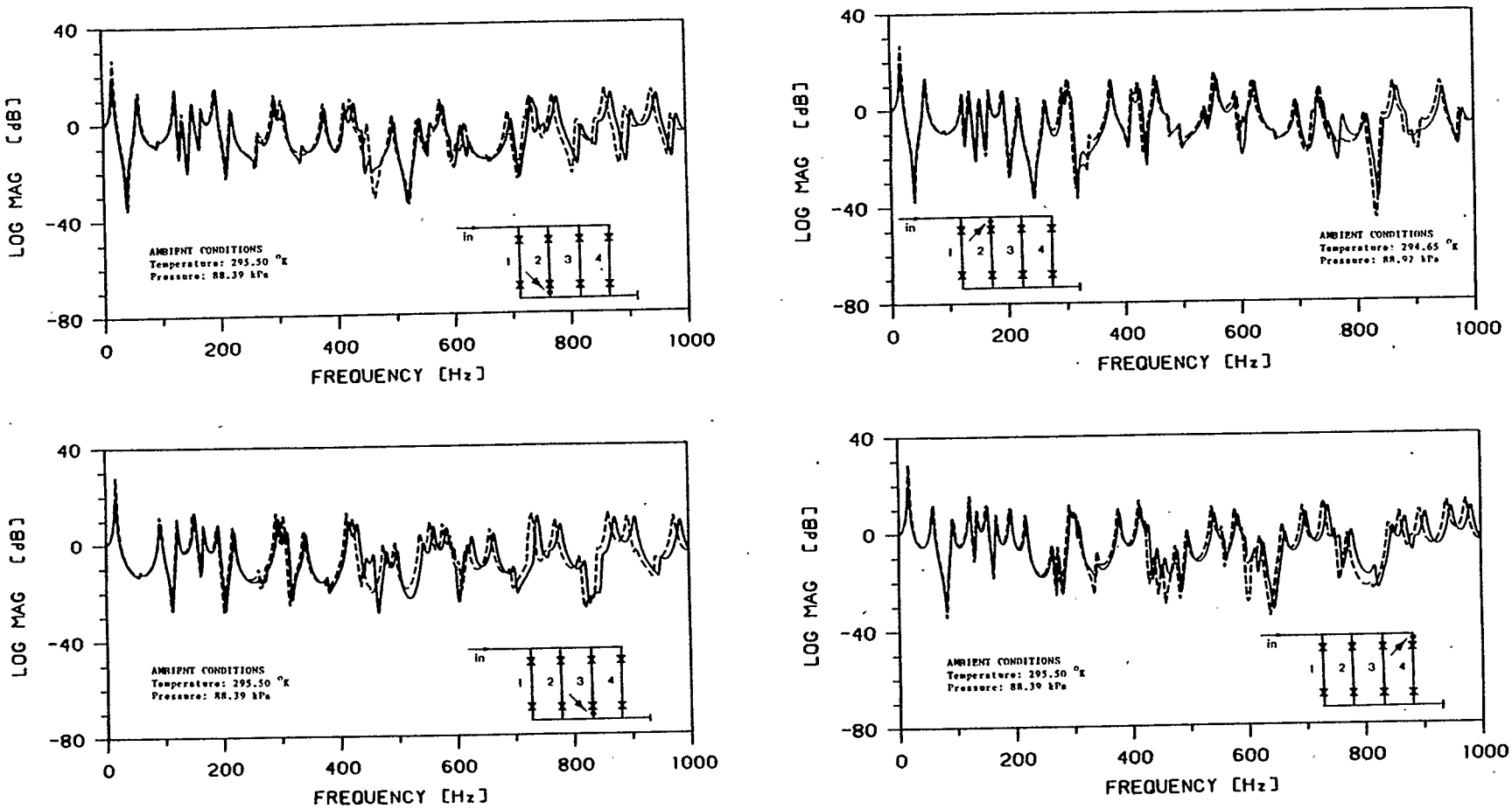

Figure 4.13 Pressure Levels in the Two-Bridge Network at Chosen Locations Indicated by Dots, (theory - dashed line, experiment - solid line). All valves open

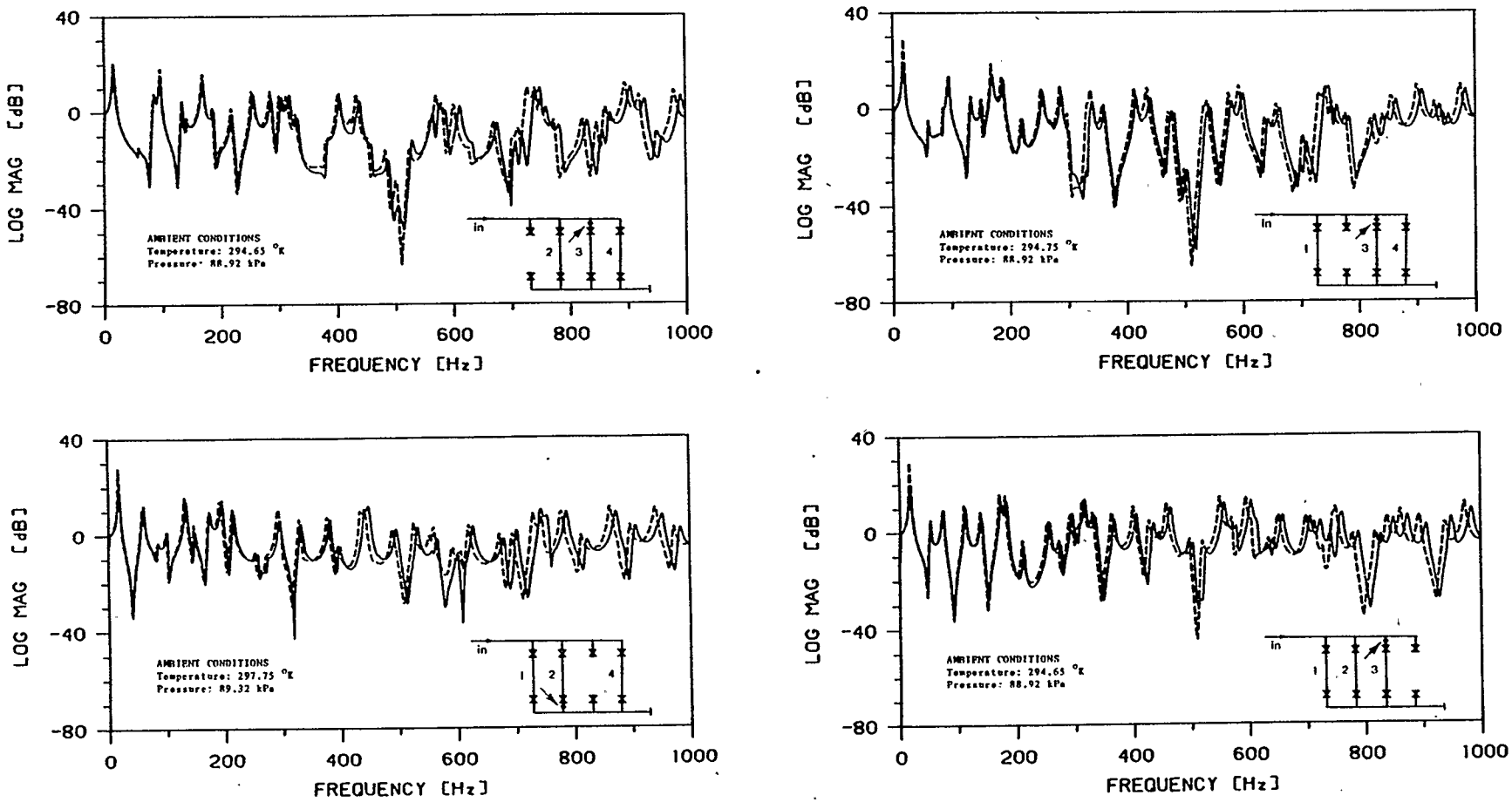

Figure 4.14 Pressure Levels in the Two-Bridge Network at Chosen Locations Indicated by Dots for Various Combinations of Open or Closed Valves, (theory - dashed line, experiment - solid line)

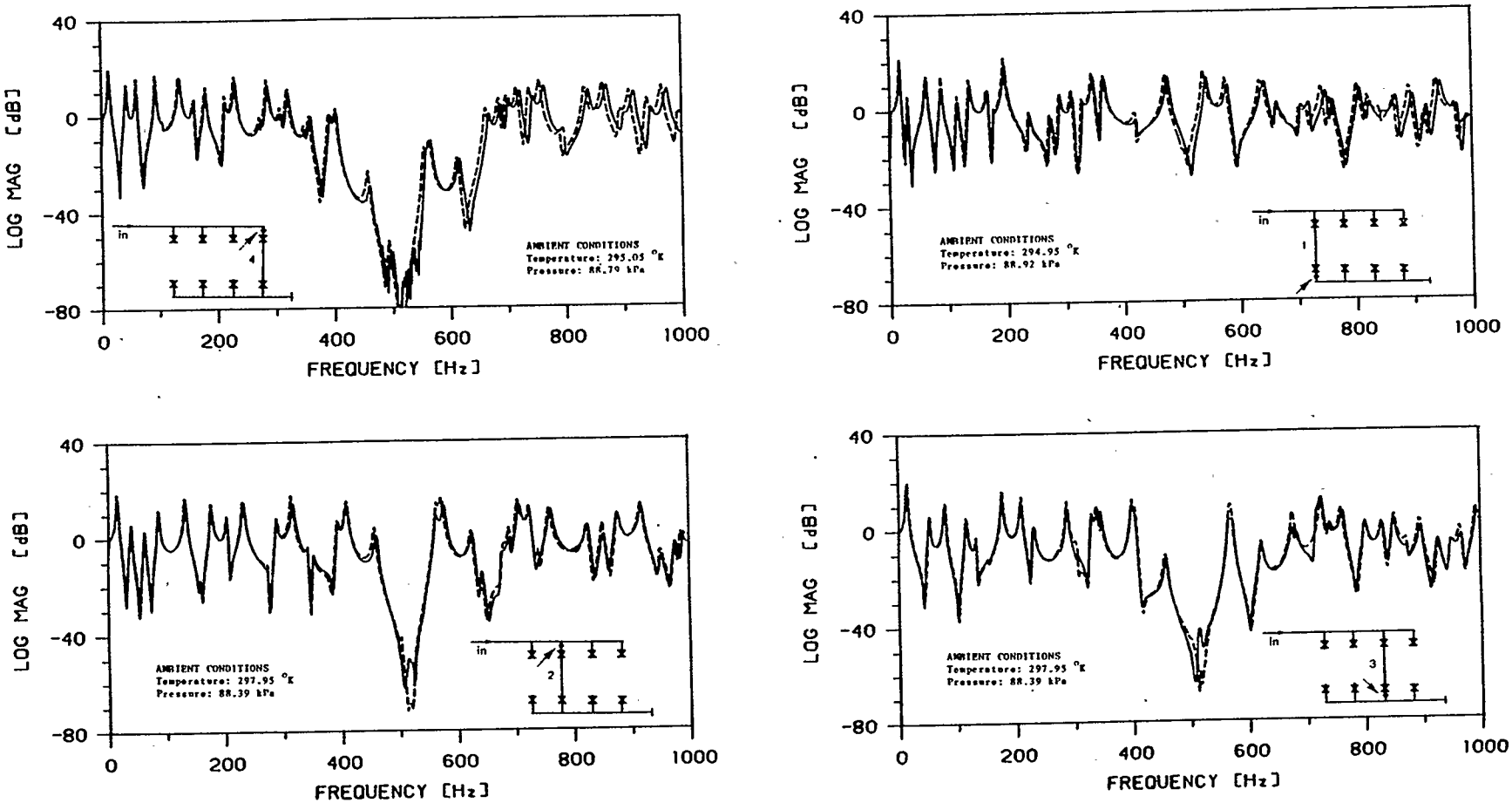

Figure 4.14 (continued)

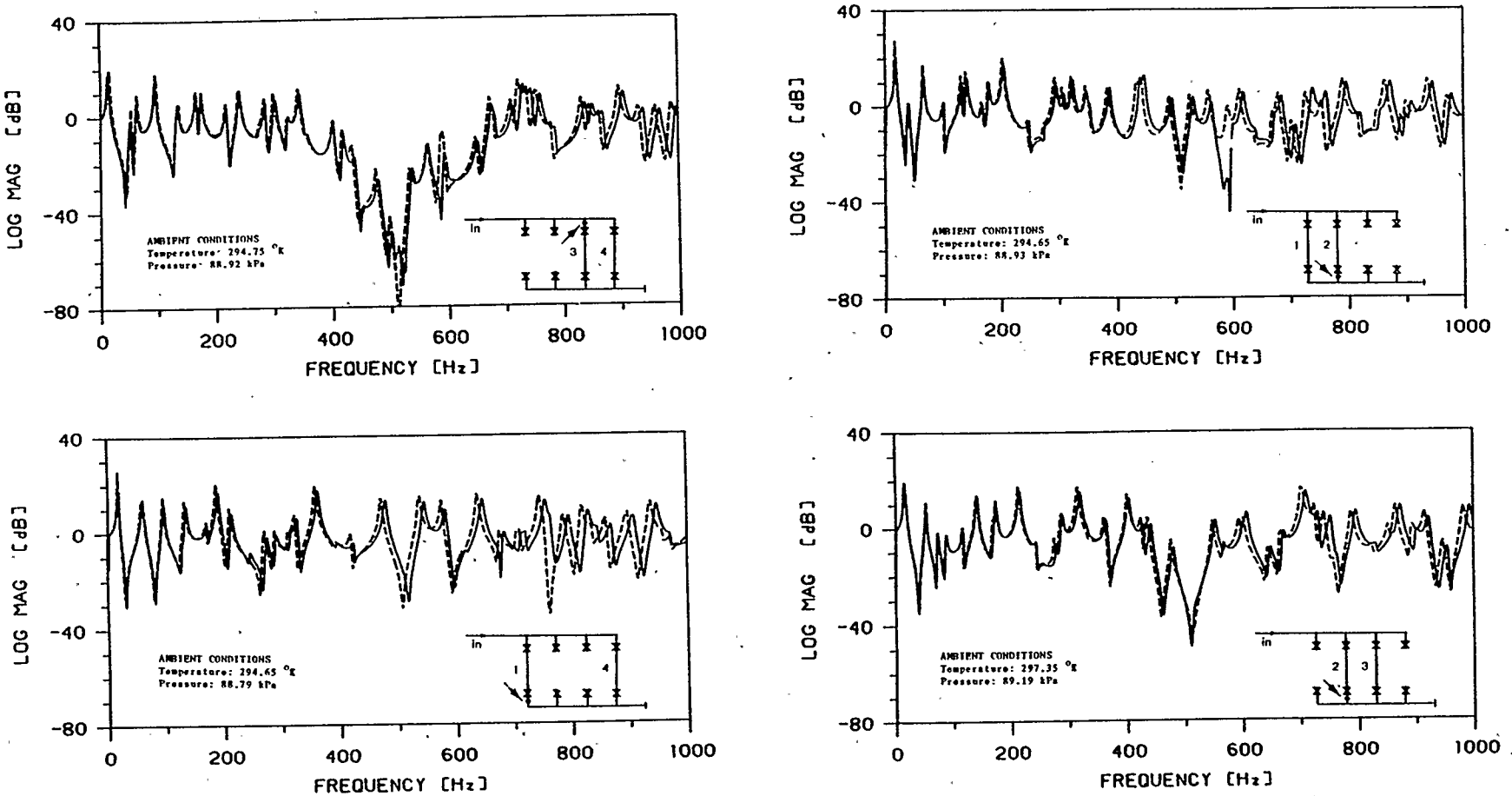

Figure 4.14 (continued)

4.3 Methods of Analysis

Different dimensions of the bridge network, as well as various flow conditions and gas compositions were used as input data to the computer programs which calculated the levels of pressure and volume velocity and corresponding RMS values at chosen locations. The following locations of interest were chosen: the output and input of the bridge network, and points in the vicinity of orifice plates. The latter points were chosen because pulsations produced in the vicinity of orifice plates affect flow measurement. The influence is especially significant if large oscillations happen to be at the frequencies close to the natural frequencies of the pressure meters.

The pulsations were evaluated with regard to two aspects: i) the levels of the peak oscillatory pressure and volume velocity amplitudes together with their associated frequencies, and ii) the RMS values of the pressure, volume velocity and also input impedance.

The pulsation pressure levels and volume velocity levels were determined in each band of a set of contiguous frequency bands and were plotted as a function of the center frequency of the band. The component bands were of equal width $\Delta f = 0.2$ Hz; the width of the integral-frequency-band was 200 Hz. The levels, as is usual, were given in decibels, shown above or below the reference level which is determined by the reference quantity. In this case, the

reference levels were chosen to be those associated with the input to the bridge network. The pressure level was then defined as:

$$L_P = 20\log_{10}(\frac{P}{P_{ref}}) \text{ dB} \tag{4.46}$$

and the volume velocity level was defined as:

$$L_V = 20\log_{10}(\frac{V}{V_{ref}}) \text{ dB} \tag{4.47}$$

where P, P_{ref}, V and V_{ref} are Fourier-transformed pressures and volume velocities respectively. (Note that the volume velocity levels can be used for comparisons since all the runs have the same cross-sectional areas).

Pulsation in a piping network can be assumed as random in nature. For a random signal q(t), the average value $\bar{q}(t)$ given by:

$$\bar{q}(t) = \lim_{T\to\infty} \frac{1}{T} \int q(t)dt \tag{4.48}$$

is a deterministic feature but does not describe the size of fluctuations which is of main interest. Any numerical measurement of $\bar{q}(t)$ is by necessity a statistical estimate whose uncertainty can be reduced only by increasing T. For a purely random signal, the average $\bar{q}(t)$ is zero which is of no use in the evaluation of the signal. The most widely used measure of the magnitude of random fluctuations is the mean-squared value $q^2(t)$ defined by

$$q^2(t) = \lim_{T\to\infty} \frac{1}{T} \int q^2(t)dt \tag{4.49}$$

Since it is desirable to use a quantity having the same physical dimensions as the signal, the root-mean-square (RMS) value was used

in this work:

$$q_{RMS} = \overline{(q^2)}^{1/2} \tag{4.50}$$

Here, the q_{RMS} values were used to compare the fluctuation magnitudes of several random signals in a gross way without judging them

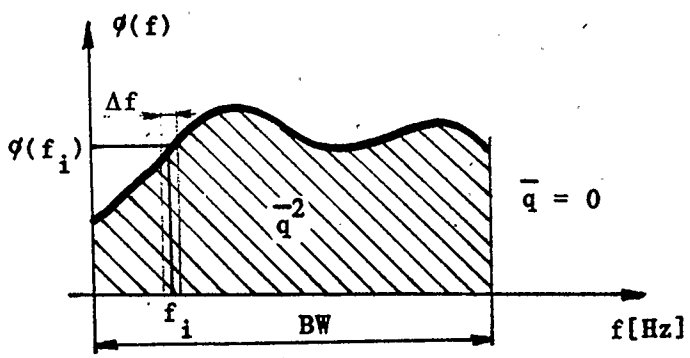

Figure 4.15 Mean-Square Spectral Density

individually. The values of q_{RMS} were computed from frequency spectra using the mean-square spectral density $\phi(f)$ concept [15]. $\phi(t)$ is a per-unit-frequency quantity that when integrated with respect to frequency between any two frequencies gives the contribution of that frequency band to the total mean square value. Taking a narrow increment Δf and assuming that $q(f_i)$ is constant over

the range of Δf, the mean square spectral density $\phi(f_i)$ was computed

$$\phi(f_i) = \frac{q^2(f_i)}{\Delta f} \tag{4.51}$$

The square root of the integral of $\phi(f)$ over the total frequency band gave the values of q_{RMS}:

$$q_{RMS} = (\int \phi(f)\,df)^{1/2} \tag{4.52}$$

Using the above expressions, the RMS values for pressure, volume velocity and input impedance signals were computed.

4.4 Results

4.4.1 Reference Network Behaviour

The reference network is one example of a gas metering station built by NOVA, An Alberta Corporation. A schematic representation of the station is depicted in Figure 4.16. The station includes a two-bridge network consisting of four runs and headers (collectors). There is also a place for a fifth run for future development. Dimensions of the network as well as flow conditions and typical gas compositions are gathered in Table 4.1.

Pressure levels as well as the corresponding volume velocity levels at points upstream of the orifice plates and at the bridge output are shown in Figure 4.17. The complex shape of the pressure level curves, which is the result of numerous interactions, is dif-

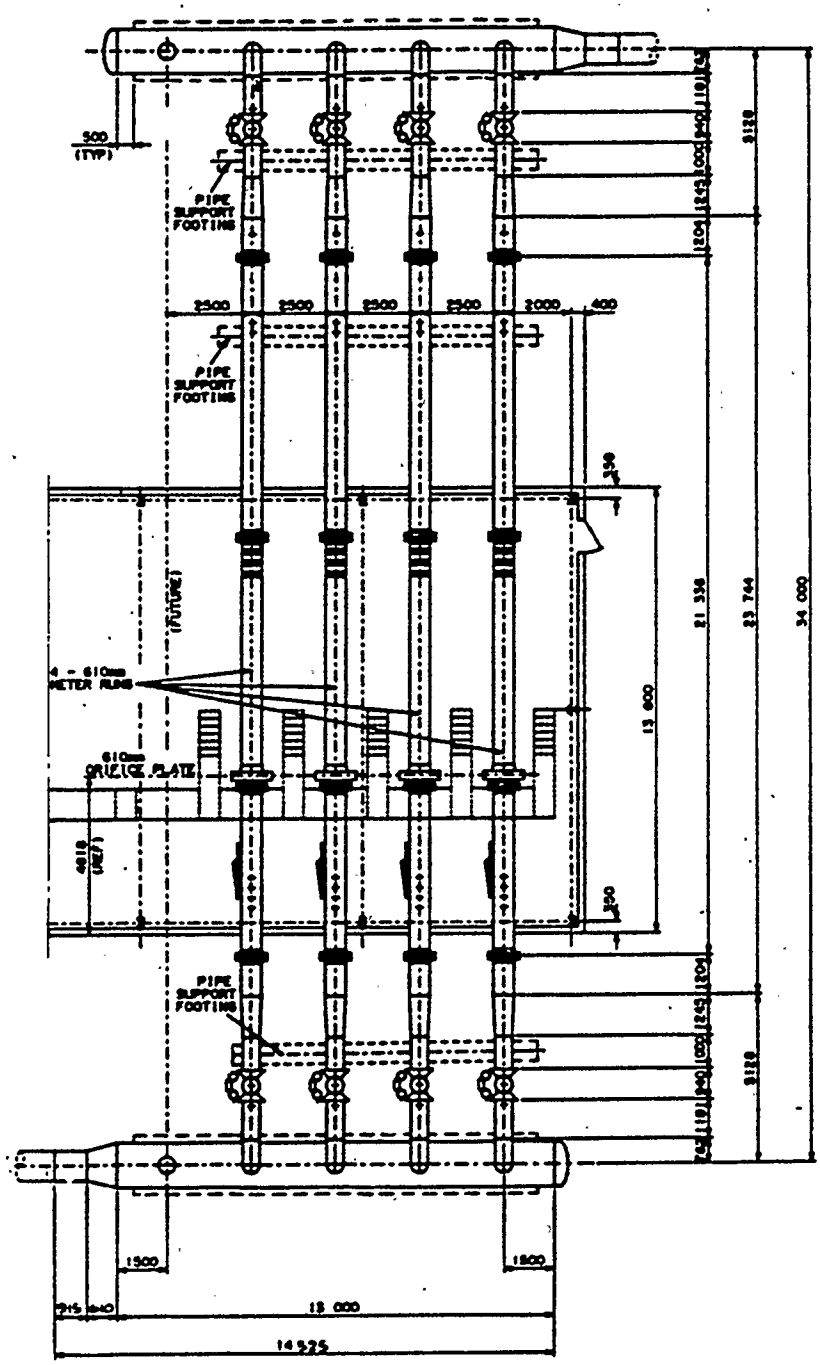

Figure 4.16 Schematic Representation of the Reference Network

Table 4.1 Basic Dimensions, Flow Conditions and Gas Composition for Reference Network

Basic Dimensions *	
Collector Pipe	1.372 x 0.025 [m]
Run Pipe	0.610 x 0.0222 [m]
Collector-Run Connection Pipe	0.508 x 0.0151 [m]
$m = (d\ D)^2$ Ratio for Used Orifice Plate	0.586
Flow Conditions	
Temperature	307.15 [^{o}K]
Pressure	3700 [kPa]
Density	25.05 [kg m^3]
Speed of Sound	436.02 [m s^2]
Mach Number	0.1
Gas Composition	
C_1	0.9556
C_2	0.0208
C_3	0.0010
nC_4	0.0001
N_2	0.0185
CO_2	0.0004

* For Missing Dimensions See Figure 4.16

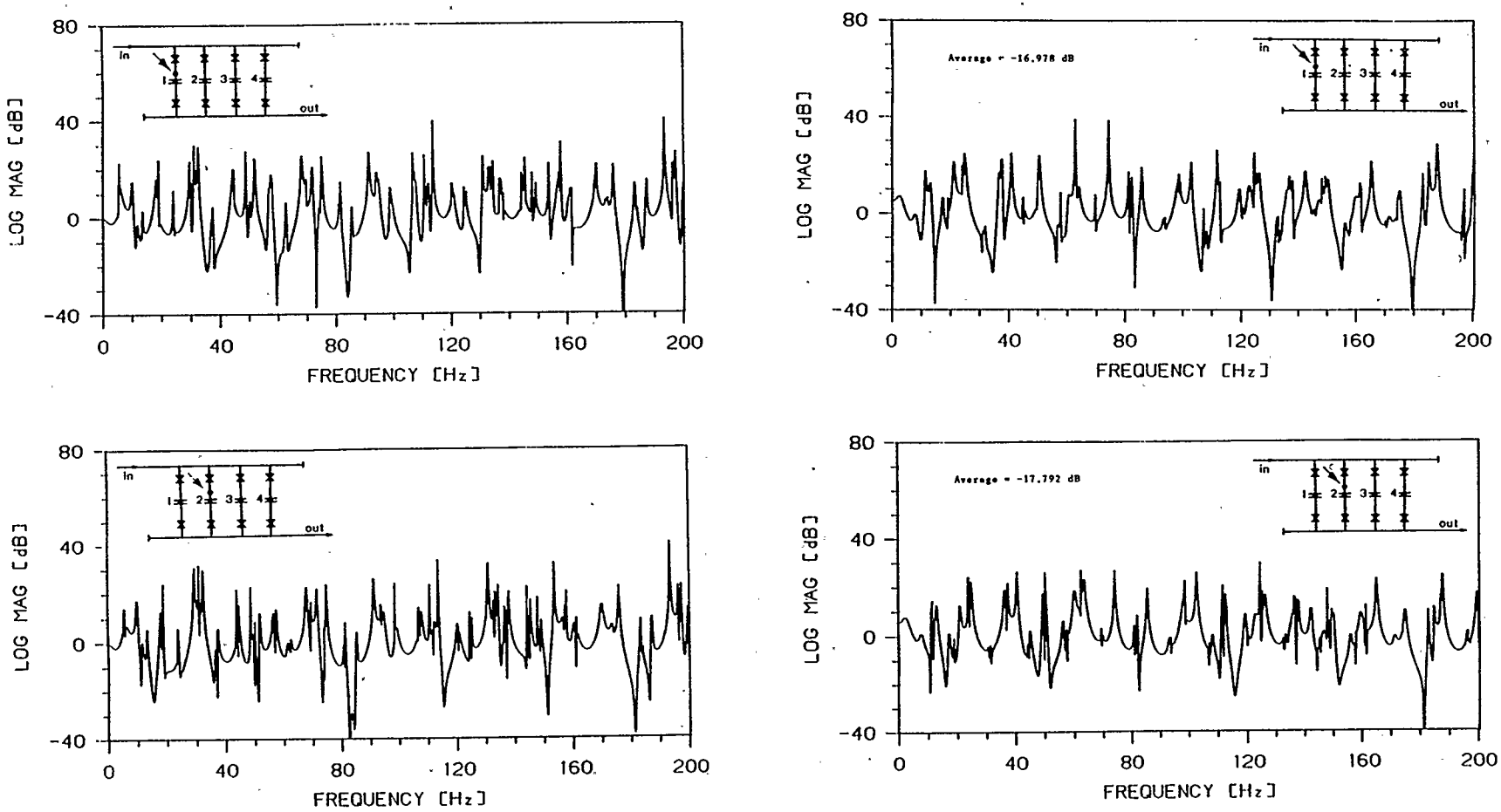

a) Pressure Levels

b) Volume Velocity Levels

Figure 4.17 Reference Pressure Volume Velocity, and Input Impedance Levels Upstream of Orifice Plates

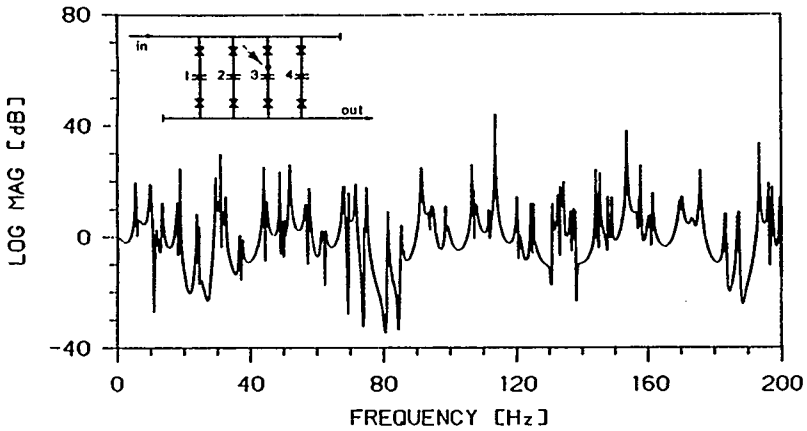

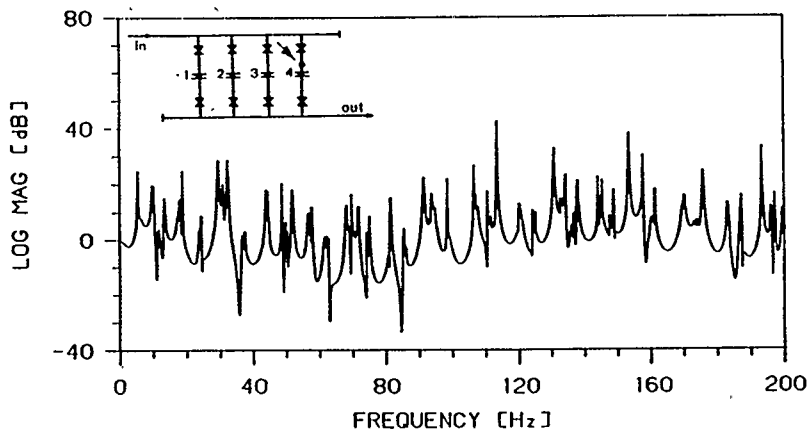

a) (continued)

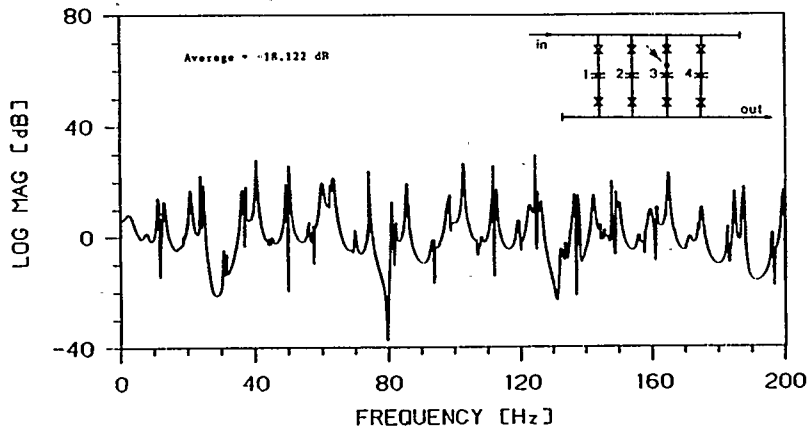

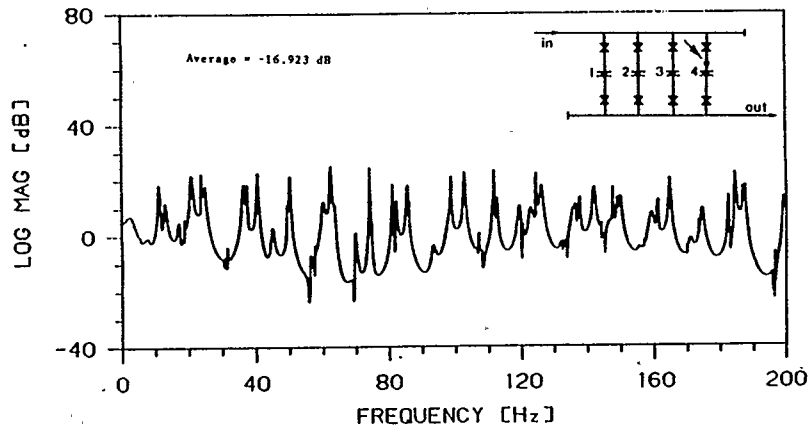

b) (continued)

Figure 4.17 (continued)

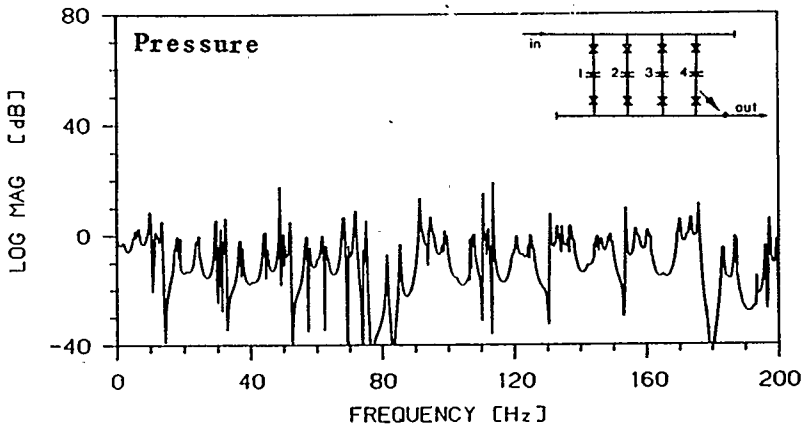

a) (continued)

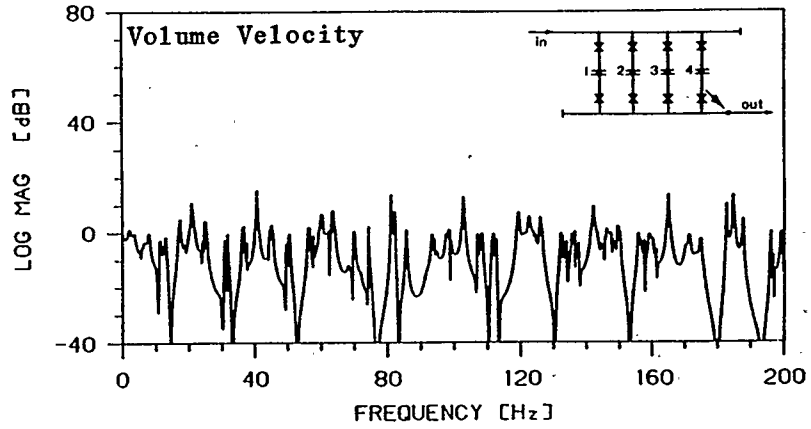

b) (continued)

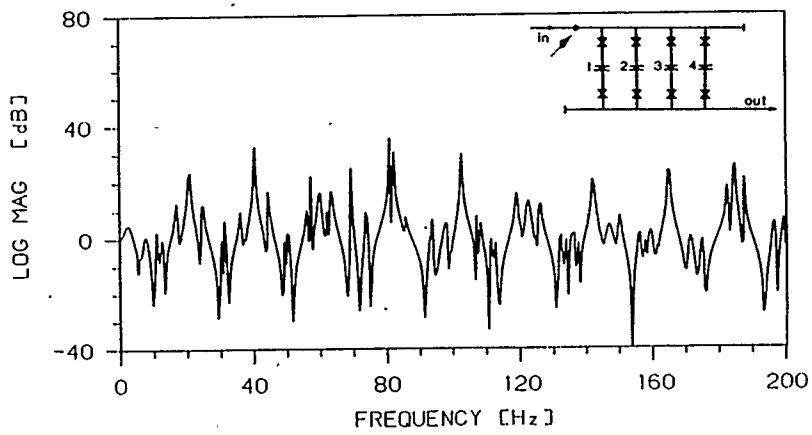

c) Input Impedance Levels

Figure 4.17 (continued)

ficult to explain in general. Only some of the minima can be predicted from the lengths of the side branches. For example, the valley at approximately 72 Hz, noticed for all locations, is associated with the effect of the 1.52 m-long side branch resonators created at the ends of collectors. The shapes of the curves are similar for all locations, but the values reached by the peaks are different. Generally, high peak values are present for lower frequencies; for the range from 6 to 40 Hz, the pressure level reaches 30 dB. These large amplifications can easily produce a pulsation problem and influence flow measurement. In all curves, the pressures vary about zero dB mean.

Volume velocity levels do not have mean value of zero dB. This is because the medium flow divides and goes through several runs. The volume velocity levels are generally very low, averaging about -17 dB. The curves, however, were shifted so that their arithmetic averages are at zero dB (the true averages are indicated). This shift was done in order to obtain the same scale for all the plots and to be able to compare the magnitudes of the oscillations. The highest velocity levels are for the first run; they occur at 62 and 73 Hz. The lowest levels are for the fourth run. The shapes of the curves are equally complex as for the pressure levels and again difficult to explain in general.

The pressure RMS values upstream and downstream of the orifice plates and at the output are shown in Table 4.2 (p.121). Since the mean square pressure value (consequently, also RMS) is related to

the power carried by the signal, it can be noticed that the most unfavourable conditions for the reference system are for the third run. It is also evident that the orifice plates act as acoustic attenuation devices which cause a significant drop in the RMS of the passing signal. As a result of this and other damping effects, the whole bridge structure attenuates the incoming disturbances to a high degree (typically 20 to 30 dB). The RMS volume velocity values are gathered in Table 4.3. They show that the highest fluctuations are for the first run, lower for the second, and even lower for the third and fourth runs. There is an insignificant drop in volume velocity RMS values across the orifice plates. The input impedance RMS value for the reference system can be found in Table 4.4.

4.4.2 Influence of Change in Flow Conditions

The system was examined while one of the flow conditions changed and the remaining parameters retained their reference values. First, the Mach Number was set to zero (no mean flow); then, the temperature of the medium was reduced to 286.48 ^{o}K (13.33 ^{o}C); finally, the gas pressure was increased to 4439 kPa from 3700 kPa. Pressure and volume velocity levels for the altered conditions are depicted in Figures 4.19 through 4.21. Input impedance levels are shown in Figures 4.33a, b and c. Behaviour of RMS values can be found in Tables 4.2 through 4.4.

For lower frequencies, up to 20 Hz, all the curves remain basically unchanged no matter what conditions were used. However, above this range there were noticeable changes in values reached by both the peaks and average fluctuations (RMS). Pressure peaks observed at about 30 Hz, which were consistently present in the tested network, were magnified for no-flow, reduced temperature (except for the third run), and increased pressure. This amplification at such a low frequency can produce a pulsation problem, and, consequently, affect flow measurement. As shown in Chapter 5, the pressure gauges most frequently used for differential flow measurement have their mechanical or acoustic resonant frequencies in the range of 10 to 50 Hz. The volume velocity levels and average fluctuations are not much affected by flow condition changes. On the other hand, the input impedance RMS visibly grows when the temperature or pressure is changed. The increase in pressure does not cause any shift on the frequency axis, but for no-flow condition or reduced temperature such a shift occurs. The general character of the curves, however, does not change significantly for a particular position in the network. For no-flow, the pressure, volume velocity and input impedance level curves are shifted towards higher frequencies; the shift can be explained by lower acoustic damping (see section 3.3.1) due to absence of mean flow (the relationship between the presence of flow and acoustic damping is explained by Ingard [29]). There is an opposite effect for reduced temperature conditions, the curves are shifted towards

lower frequencies. In this case, the reason why the shift occurs is difficult to explain because there are changes in many properties of medium in different directions and to a different degree. As a result, simple relationships involving frequency are not available.

4.4.3 Influence of Change in Medium Composition

The same chemical species as for the reference system were used but their mole fractions were altered to values listed below (reference values are repeated in brackets).

$C_1 = 0.9163$	(0.9556)
$C_2 = 0.0455$	(0.0208)
$C_3 = 0.0091$	(0.0010)
$nC_4 = 0.0021$	(0.0001)
$N_2 = 0.0192$	(0.0185)
$CO_2 = 0.0078$	(0.0004)

Pressure and volume velocity levels are shown in Figure 4.21; input impedance levels are presented in Figure 4.33d. RMS values for pressure, volume velocity, and input impedance are gathered in Tables 4.2, 4.3 and 4.4 respectively.

For this particular gas composition, pressure levels are generally lower, higher peaks being especially affected. Conversely, volume velocity levels become higher than those for the reference

medium. All curves, however, remain unchanged for low frequencies, up to 15 Hz. The pressure, volume velocity and input impedance level curves, all exhibit a significant shift towards lower frequencies. The described behaviour shows that even in a very well designed network, pulsation problems can be easily encountered because the medium itself is a decisive factor in producing the pulsation.

4.4.4 Influence of Changes in Bridge Network Arrangement

a) Absence of Orifice Plates

The system analogous to the reference system but having no orifice plates was examined. Pressure and volume velocity levels are shown in Figure 4.22, while the input impedance levels are depicted in Figure 4.33e. RMS values are gathered in Tables 4.2 through 4.4.

Pressure levels as well as their average fluctuations are lower. This could be expected because the orifice plates, major obstacles for the flow, were removed and less reflections were produced in the system. Associated with the above are also lower levels of input impedance, which can be expected.

b) Absence of End Pipes

In this case, the reference system was changed by removing the end pipes (branch resonators). The level curves are depicted in Figures 4.23 and 4.33f. The RMS values can be found in Tables 4.2

through 4.4.

A new feature, not observed in the case of previous changes, is now present. Namely, the pressure, volume velocity and input impedance level curves change both their character and their values reached at the peaks. There is no uniform tendency in lowering or increasing the peaks. Instead, the peaks are damped or amplified only at certain frequencies. Also, for the pressure level curves, the valley near 72 Hz which was formed by the side branch resonator vanishes.

c) Closing of Valves

Here, very important maintenance situations are simulated. If there is an increase or decrease in flow through the pipeline the orifice plates have to be consecutively exchanged, and, consequently, the corresponding runs have to be shut down. In emergency situations, more than one run can be turned off. Such situations are highly undesirable since they change the geometry of the bridge resulting in additional side branch resonators. In most situations, flow measurement is highly affected in the open runs.

At most locations pressure and volume velocity levels are higher. As it can be noticed in Figures 4.24 through 4.30 some peaks are much higher than those encountered in the reference system. However, there is no uniform tendency in their behaviour. It depends on the particular bridge configuration. Generally, the

average fluctuations of pressure, volume velocity and input impedance grow significantly, which can be observed in Tables 4.3 through 4.4.

d) Changing the Number of Runs

Two bridge networks, one with a decreased and the other with an increased number of runs, are examined.

Pressure and volume velocity levels for a one-bridge network are shown in Figure 4.31. Input impedance levels are depicted in Figure 4.33n. RMS values are gathered in Tables 4.2 through 4.4. The level curves exhibit a less jagged character and have different shapes although some similarities to the reference curves (Figure 4.17) can be observed. For example, the valley near 72 Hz associated with end pipe resonators is still present. All the peaks are magnified and average fluctuations of pressure, volume velocity and input impedance are significantly higher. This can be explained by the smaller number of reflections cancelling out each other than in the reference system.

Just the opposite behaviour can be noticed for a three-bridge network. The peaks and valleys are more numerous, the values reached by the peaks are not so high and the average fluctuations are also decreased. Pressure and volume velocity levels for three-bridge network are presented in Figure 4.32, and the input impedance levels are shown in Figure 4.33. The RMS values are

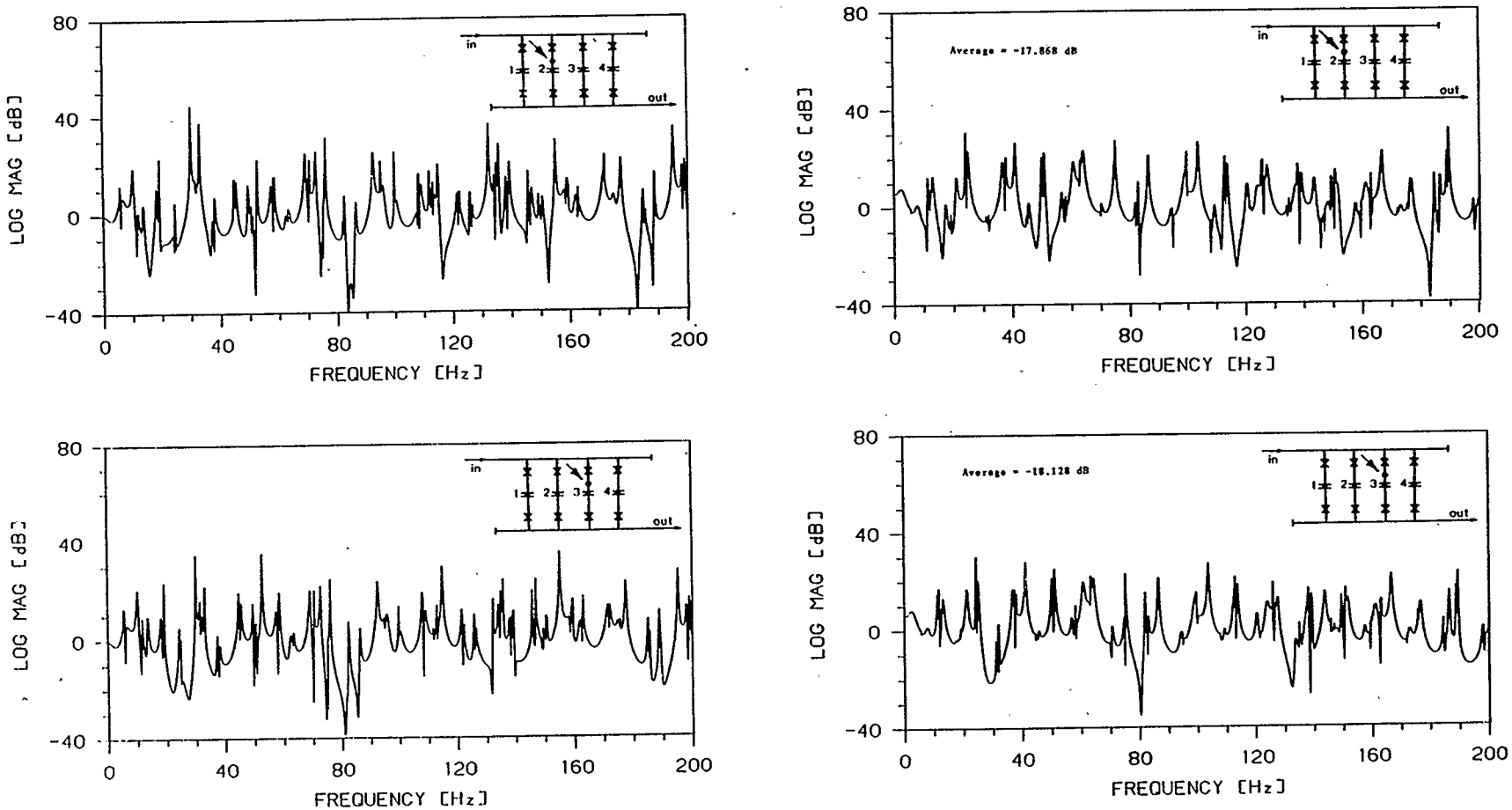

a) Pressure Levels

b) Volume Velocity Levels

Figure 4.18 Pressure and Volume Velocity Levels Upstream of Orifice Plate on the Second and Third Runs for No-Flow Conditions

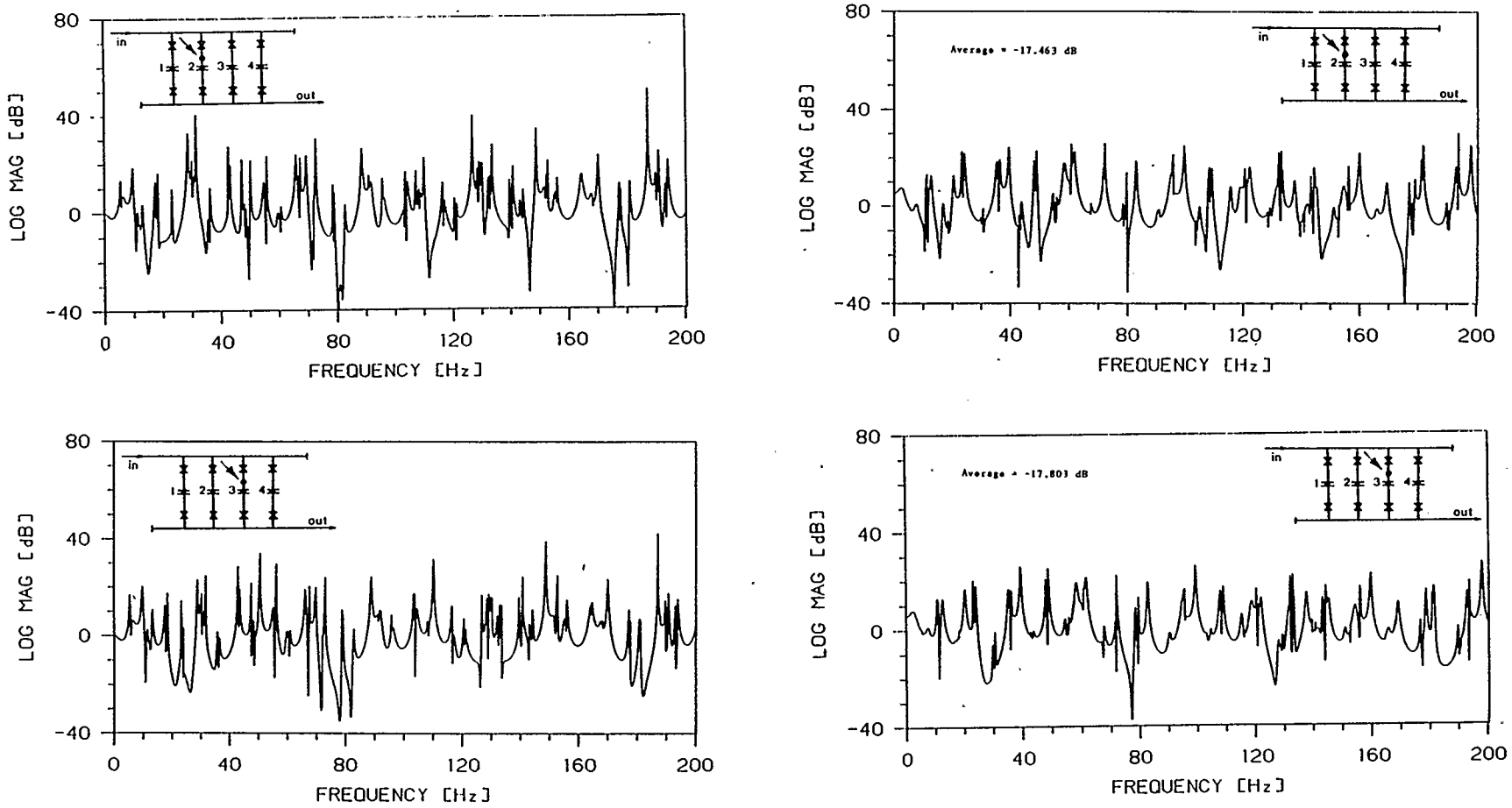

a) Pressure Levels

b) Volume Velocity Levels

Figure 4.19 Pressure and Volume Velocity Levels Upstream of Orifice Plate on the Second and Third Runs for Lowered Temperature

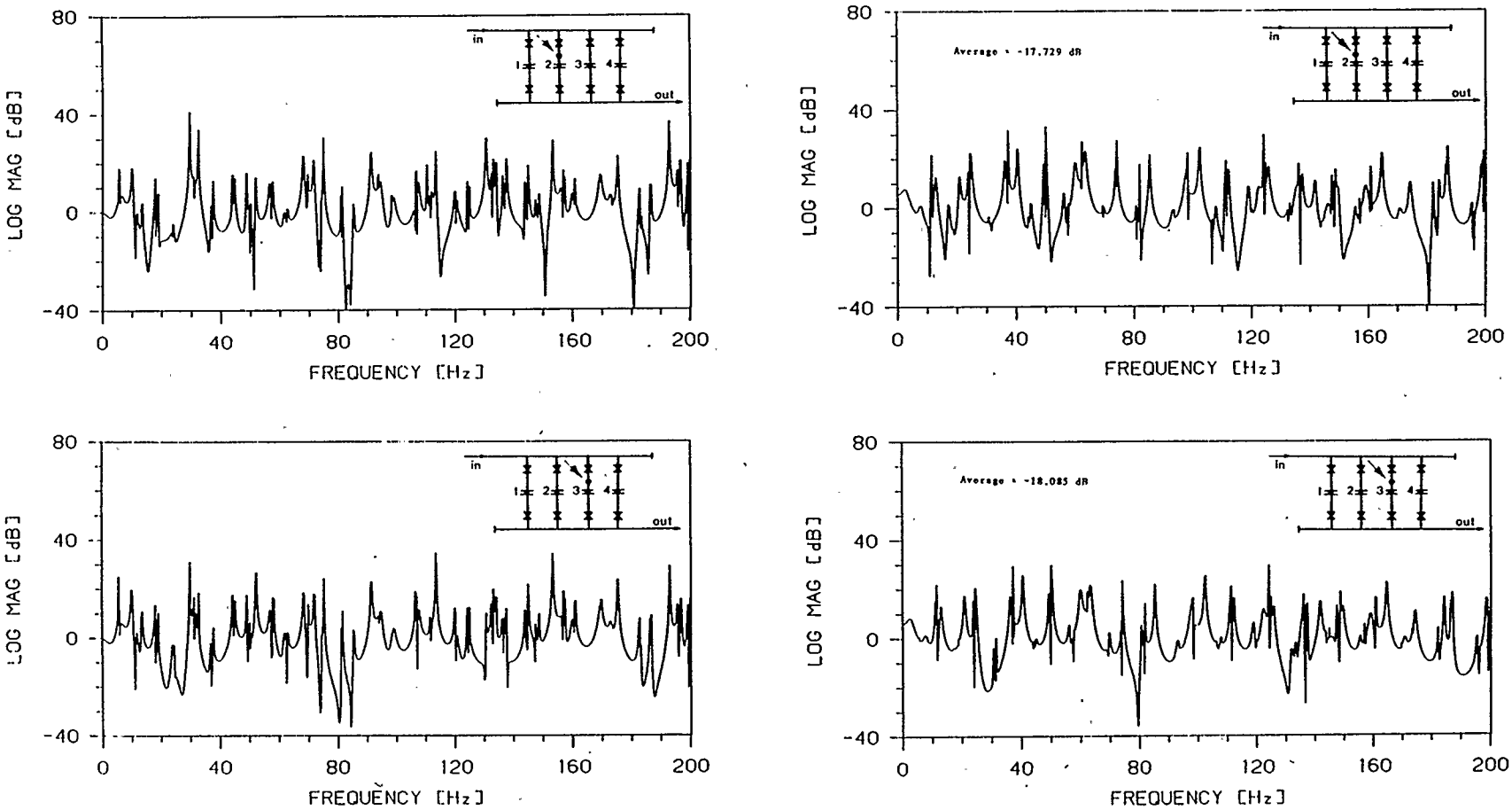

a) Pressure Levels

b) Volume Velocity Levels

Figure 4.20 Pressure and Volume Velocity Levels Upstream of Orifice Plate on the Second and Third Runs for Increased Pressure

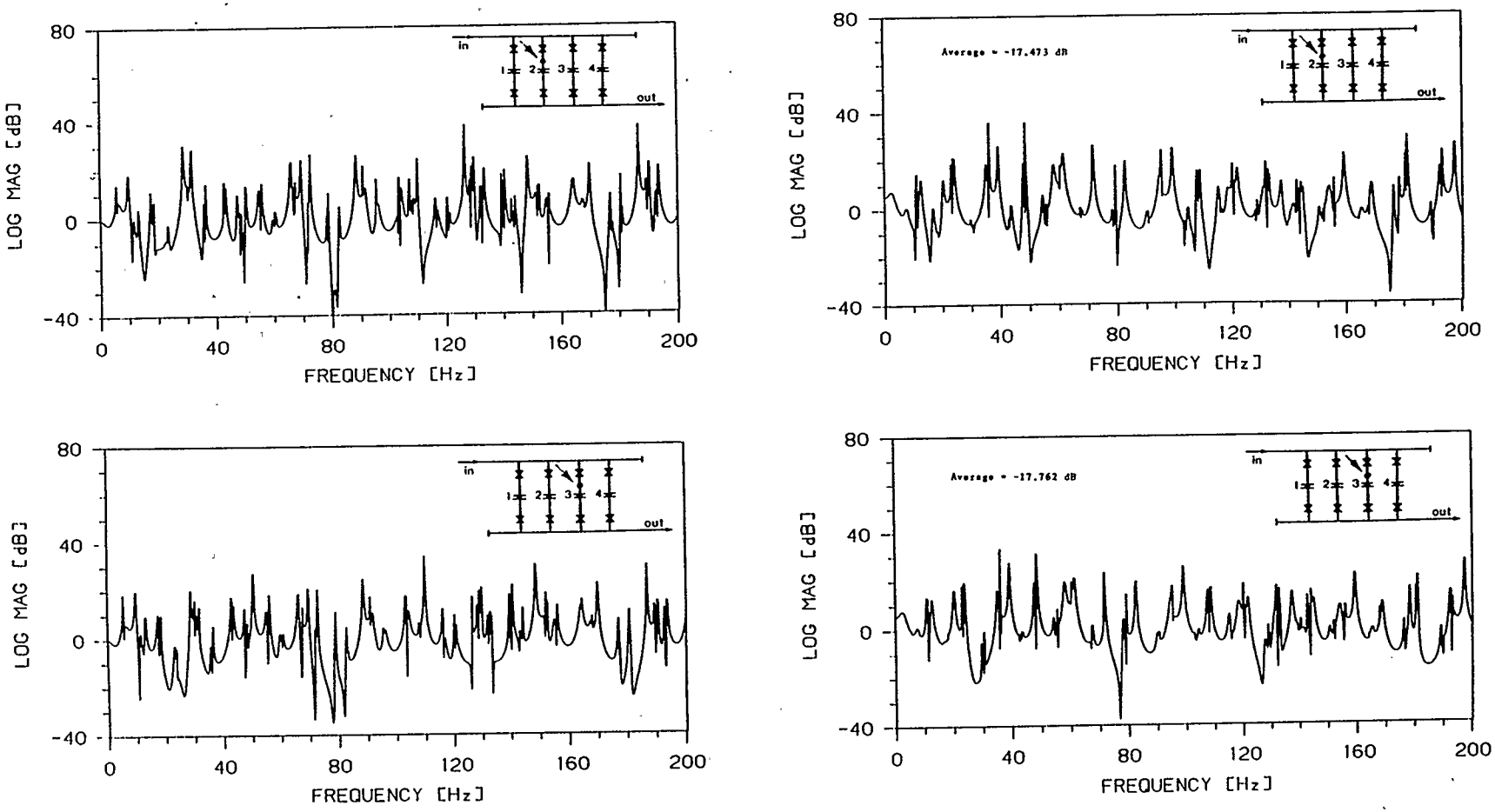

a) Pressure Levels

b) Volume Velocity Levels

Figure 4.21 Pressure and Volume Velocity Levels Upstream of Orifice Plate on the Second and Third Runs for Changed Medium Composition

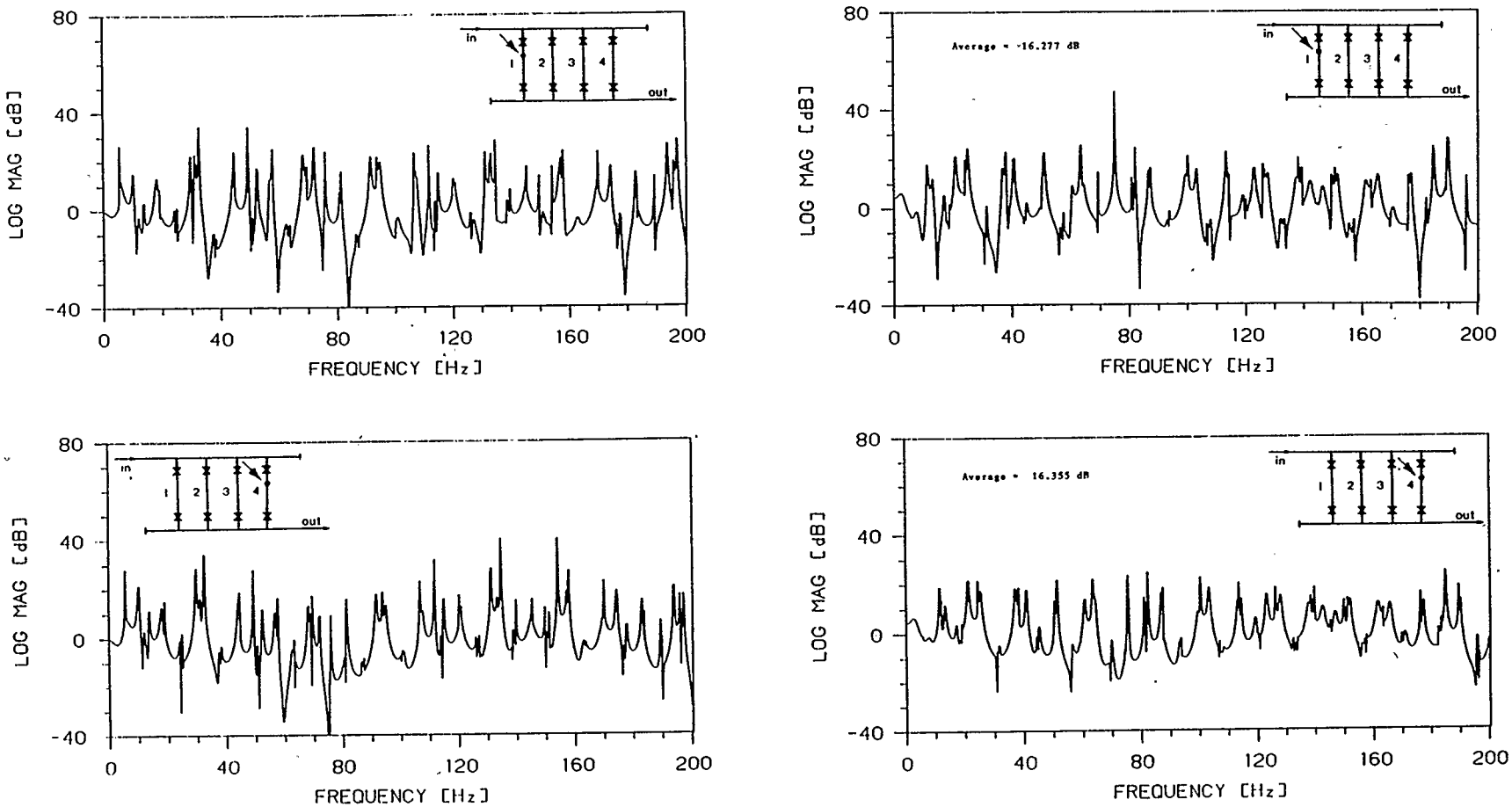

a) Pressure Levels

b) Volume Velocity Levels

Figure 4.22 Pressure and Volume Velocity Levels on the First and Fourth Runs When Orifice Plates Are Absent

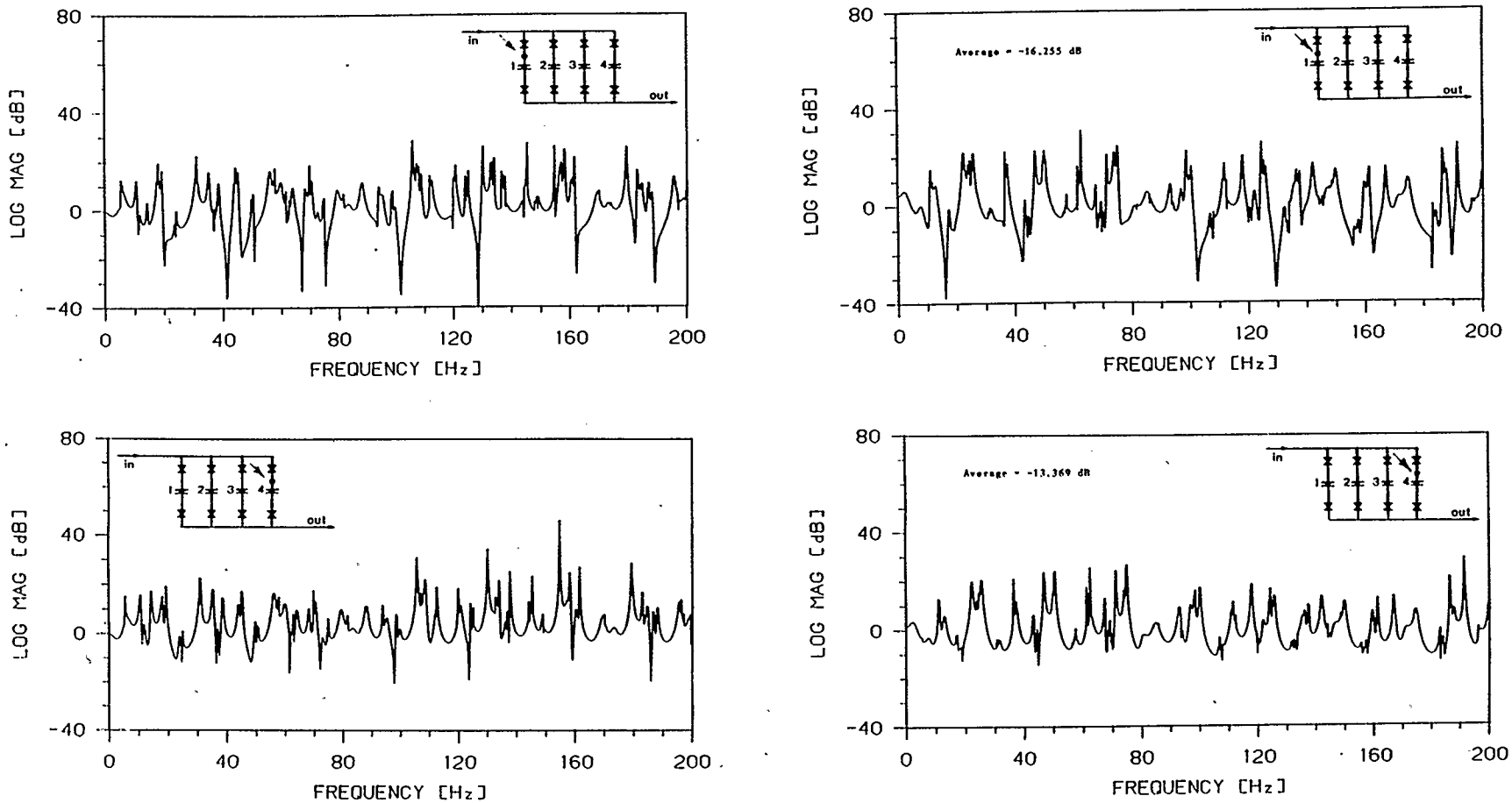

a) Pressure Levels

b) Volume Velocity Levels

Figure 4.23 Pressure and Volume Velocity Levels Upstream of Orifice Plate on the First and Fourth Runs When End Pipes Are Absent

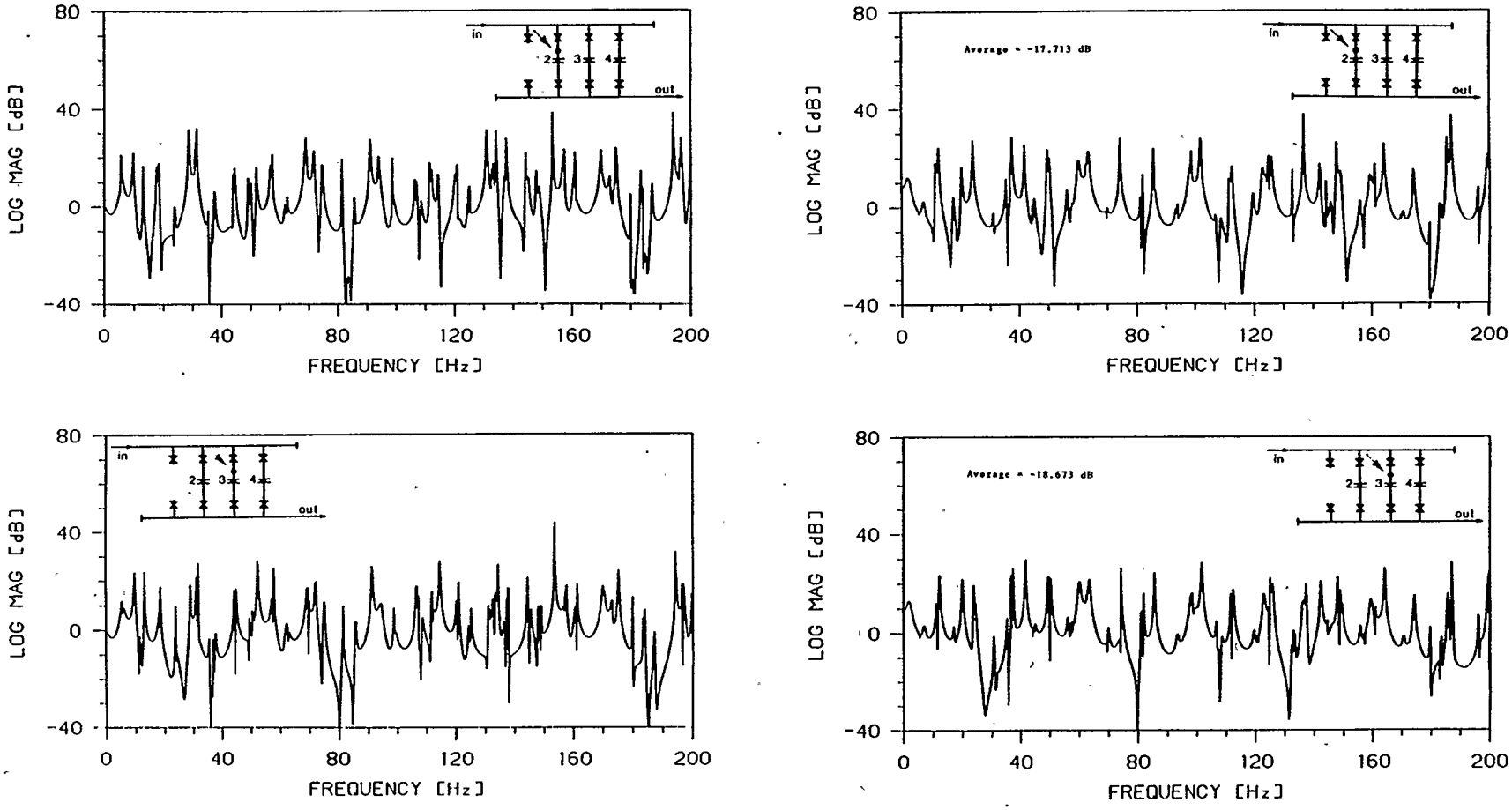

a) Pressure Levels

b) Volume Velocity Levels

Figure 4.24 Pressure and Volume Velocity Levels Upstream of Orifice Plate on the Second and Third Runs When the First Run Is Closed

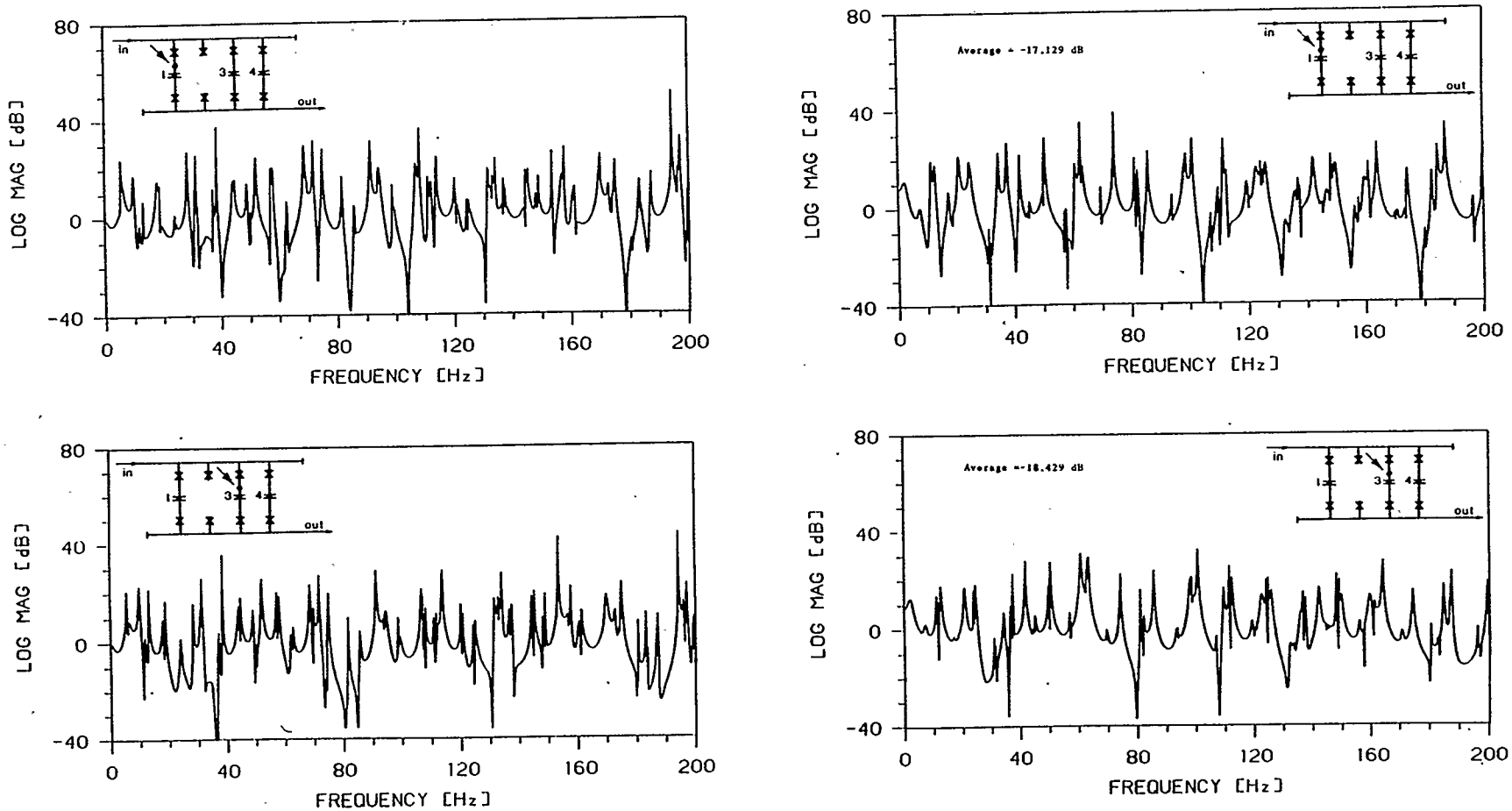

a) Pressure Levels

b) Volume Velocity Levels

Figure 4.25 Pressure and Volume Velocity Levels Upstream of Orifice Plate on the First and Third Runs When the Second Run Is Closed

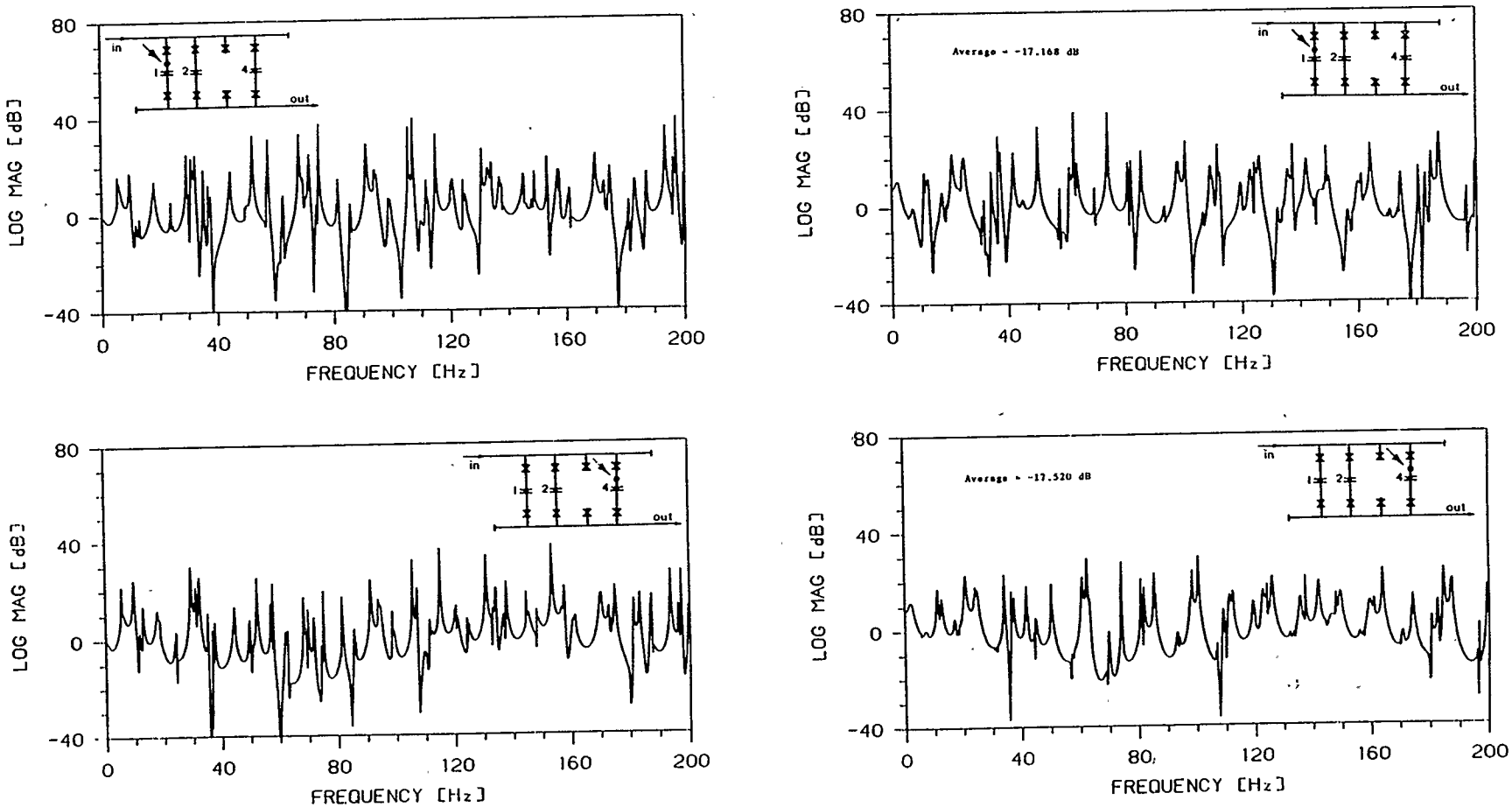

a) Pressure Levels

b) Volume Velocity Levels

Figure 4.26 Pressure and Volume Velocity Levels Upstream of Orifice Plate on the First and Fourth Runs When the Third Run Is Closed

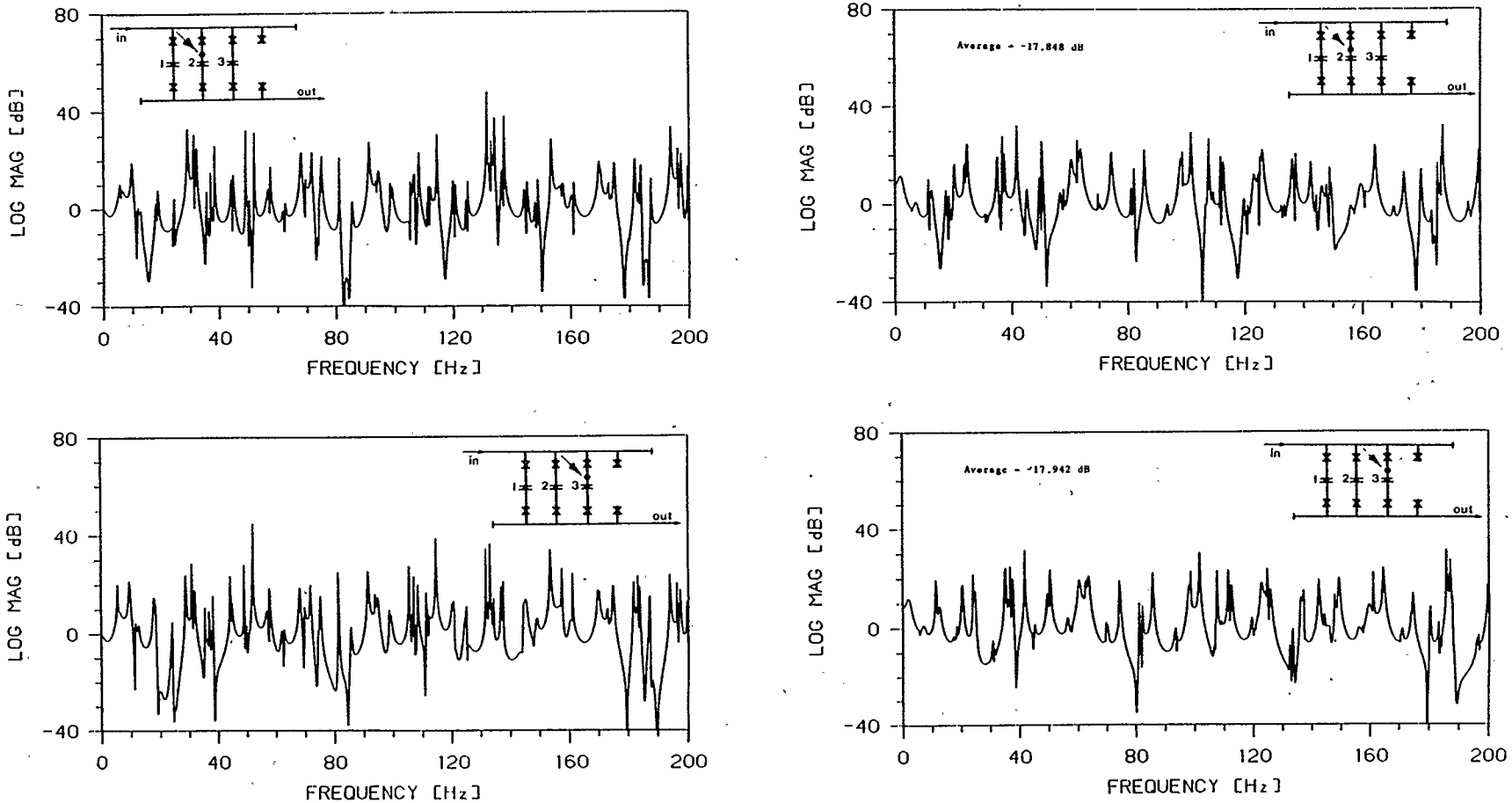

a) Pressure Levels

b) Volume Velocity Levels

Figure 4.27 Pressure and Volume Velocity Levels Upstream of Orifice Plate on the Second and Third Runs When the Fourth Run Is Closed

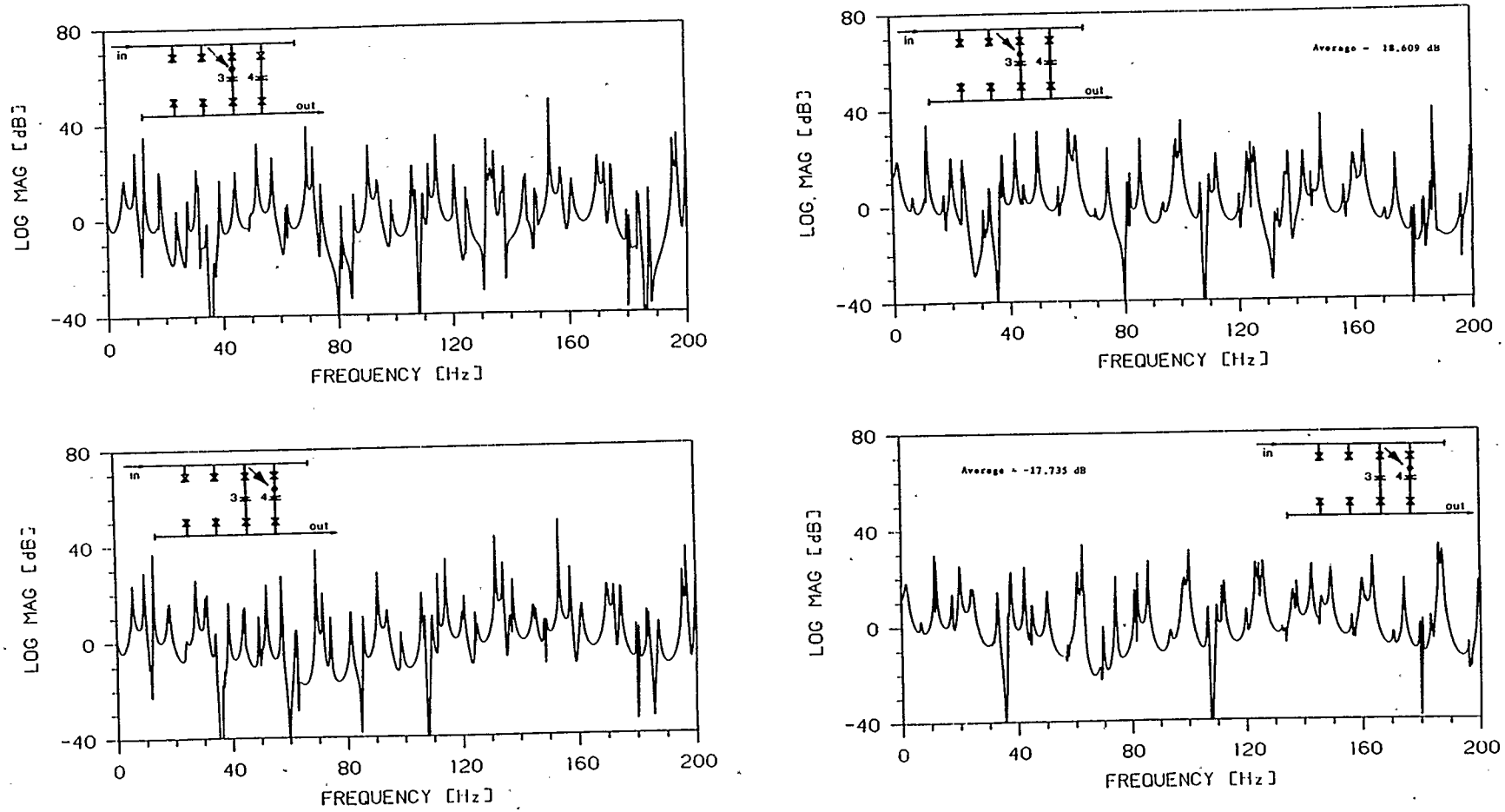

a) Pressure Levels

b) Volume Velocity Levels

Figure 4.28 Pressure and Volume Velocity Levels Upstream of Orifice Plate on the Third and Fourth Runs When the First and Second Runs Are Closed

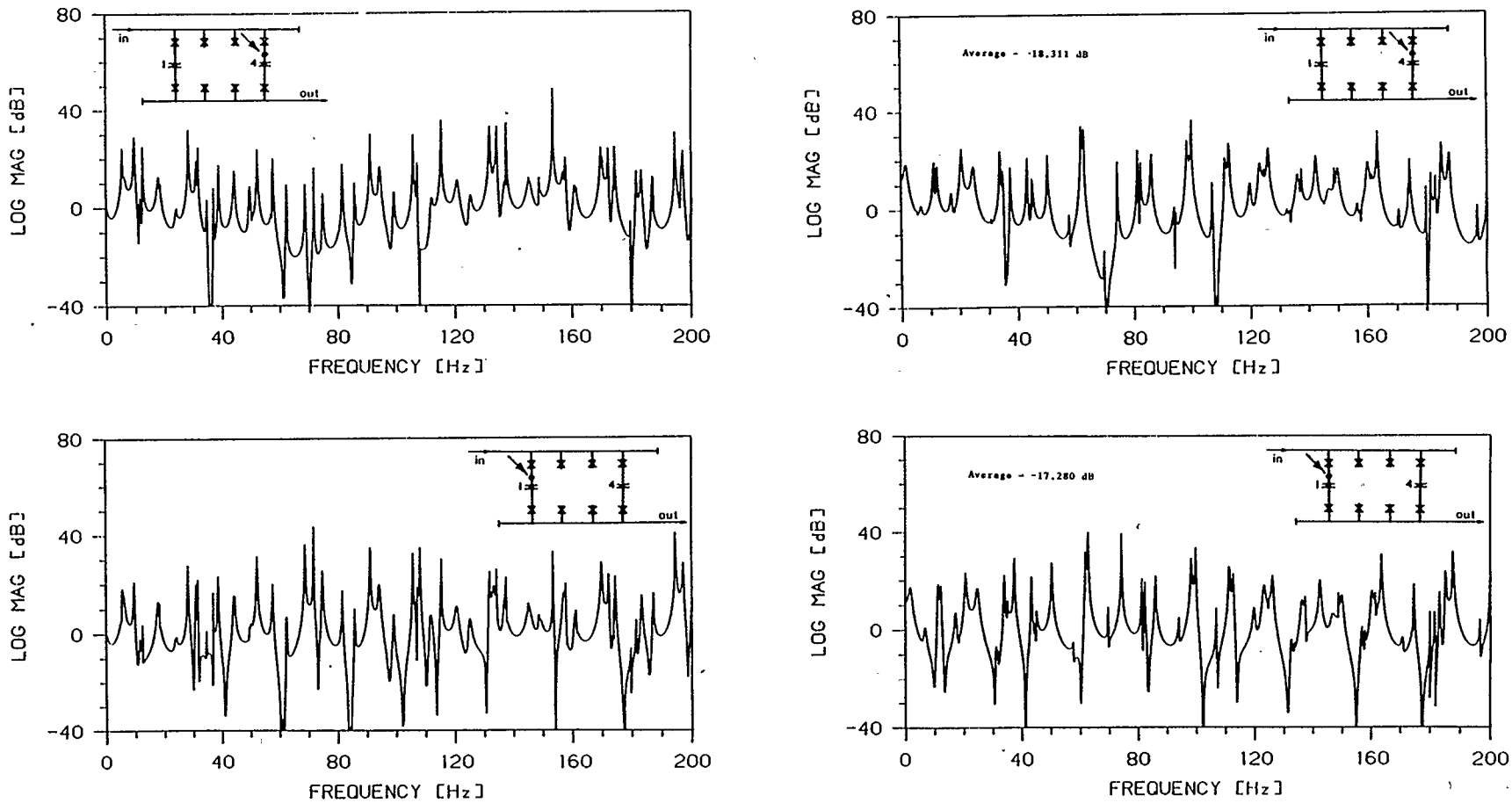

a) Pressure Levels

b) Volume Velocity Levels

Figure 4.29 Pressure and Volume Velocity Levels Upstream of Orifice Plate on the First and Fourth Runs When the Second and Third Runs Are Closed

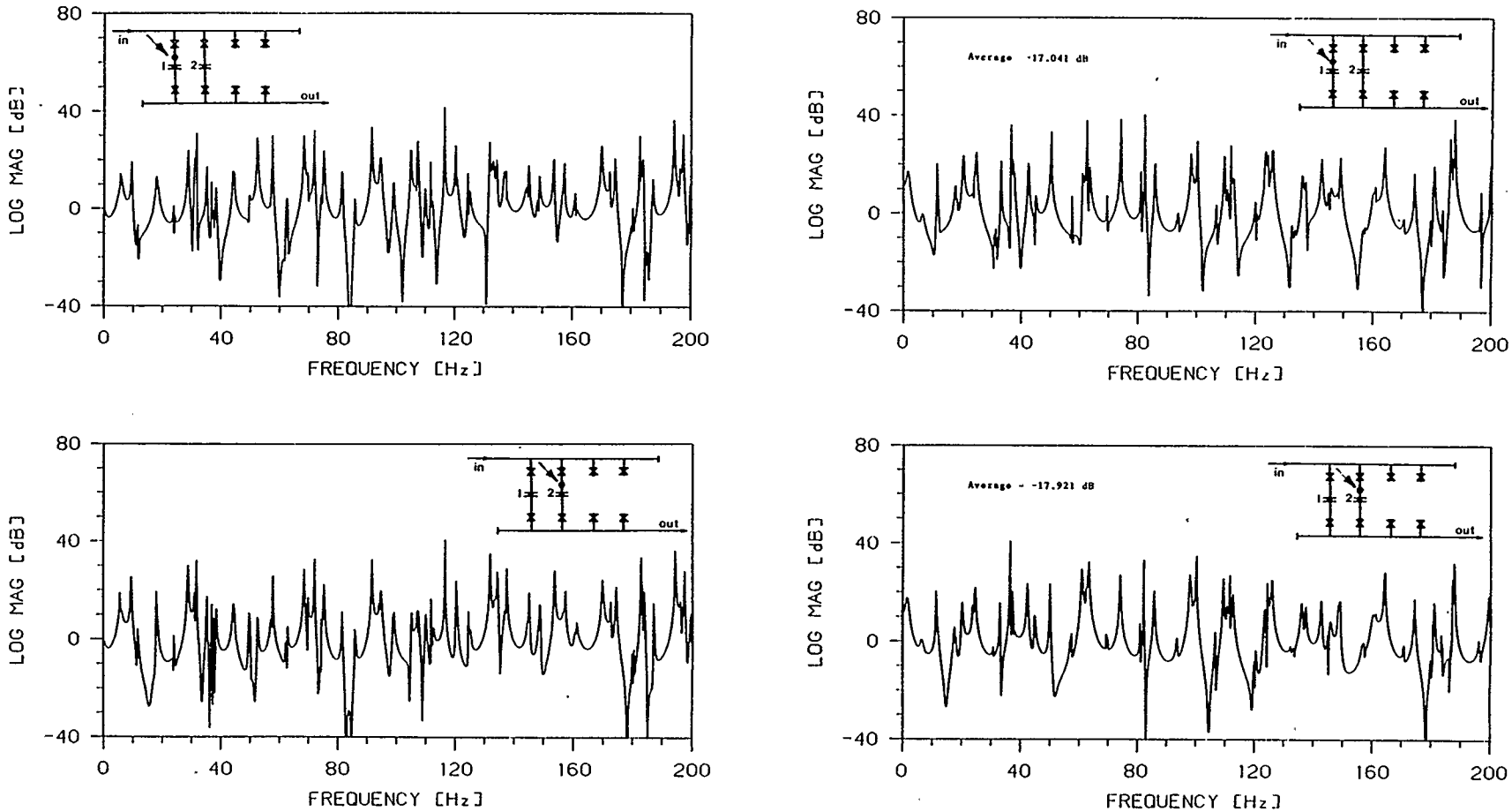

a) Pressure Levels

b) Volume Velocity Levels

Figure 4.30 Pressure and Volume Velocity Levels Upstream of Orifice Plate on the First and Second Runs When the Third and Fourth Runs Are Closed

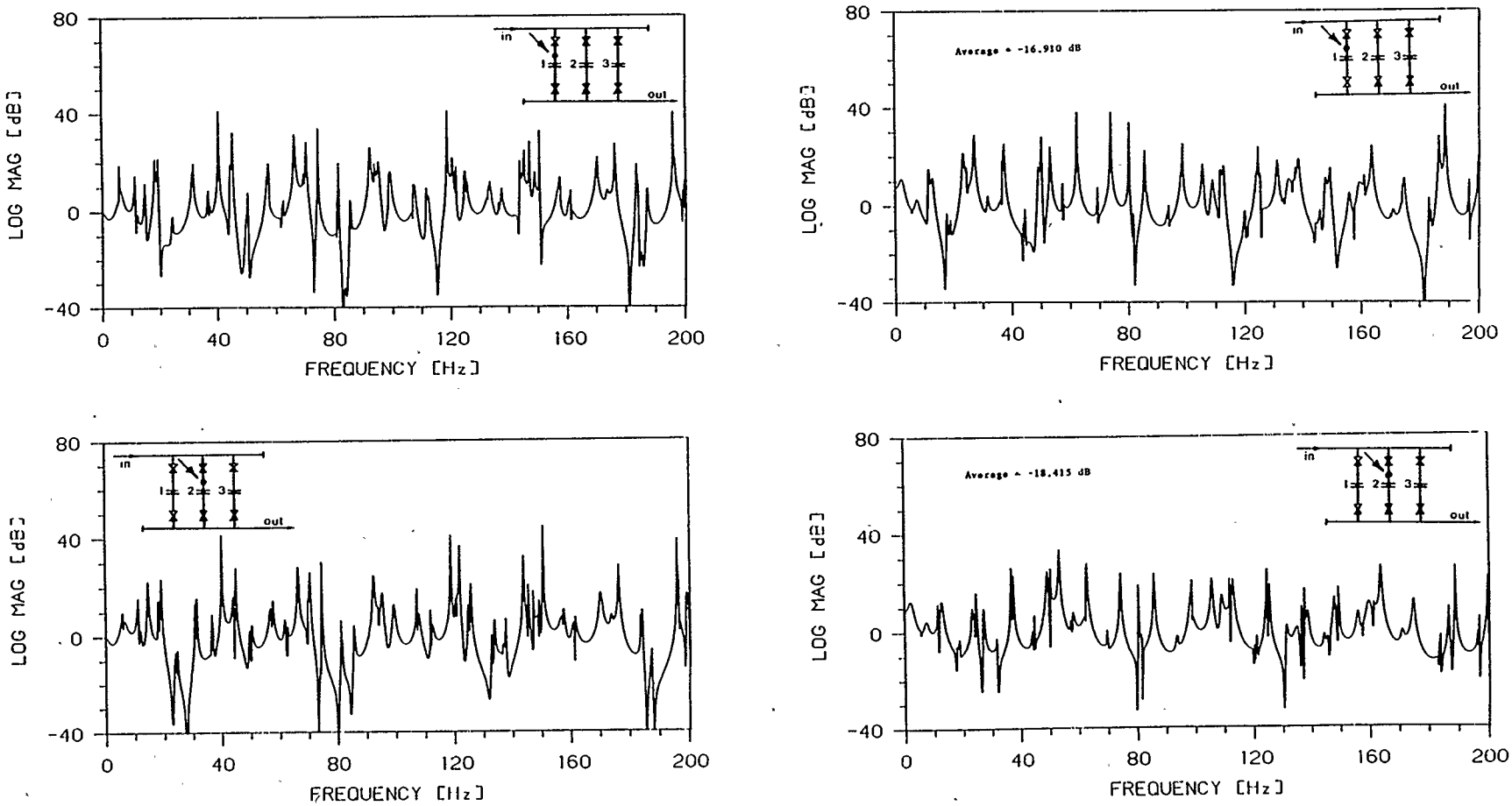

a) Pressure Levels

b) Volume Velocity Levels

Figure 4.31 Pressure and Volume Velocity Levels Upstream of Orifice Plate on the First and Second Runs for One-Bridge Network

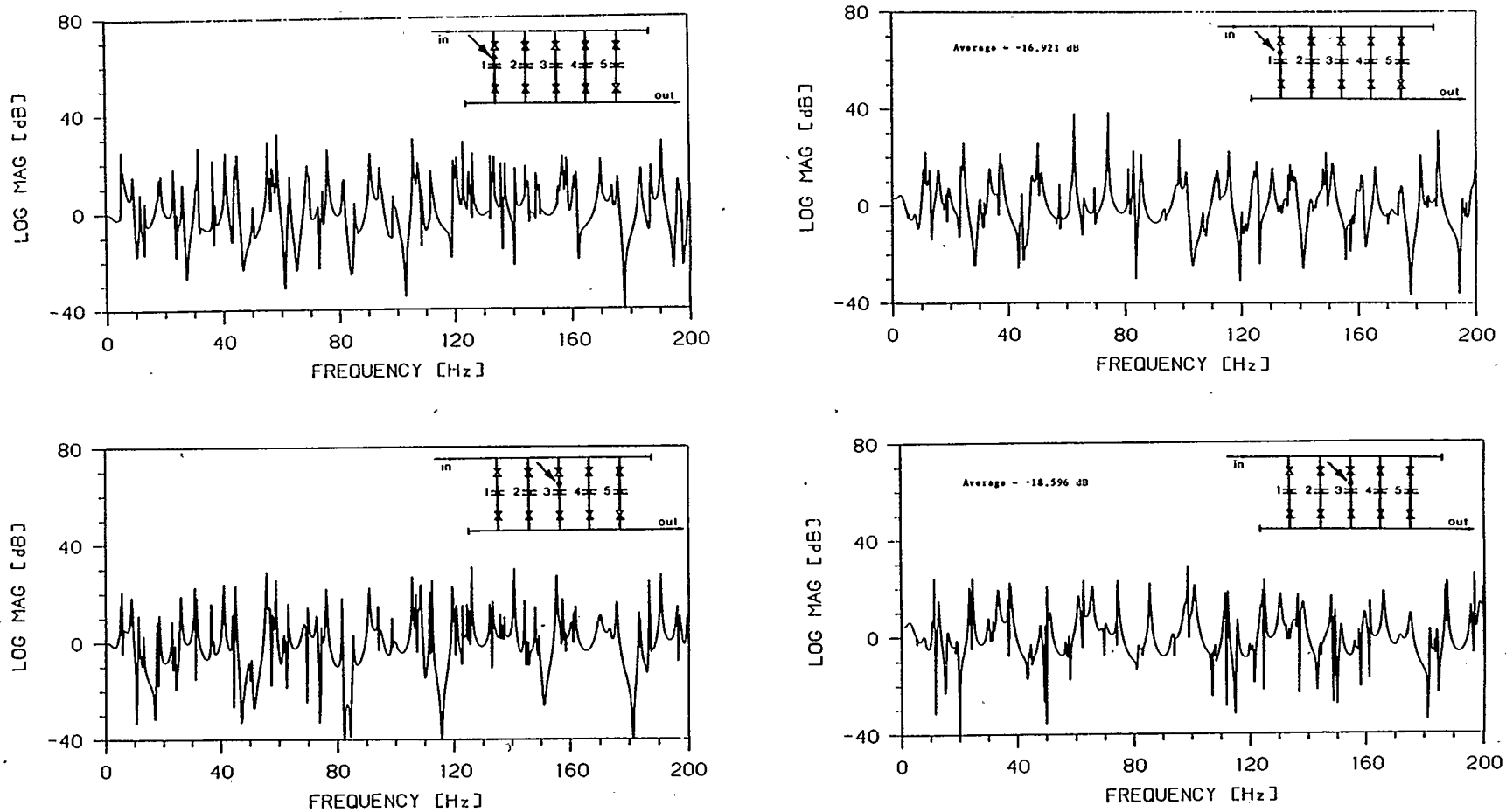

a) Pressure Levels

b) Volume Velocity Levels

Figure 4.32 Pressure and Volume Velocity Levels Upstream of Orifice Plate on the First and Third Runs for Three-Bridge Network

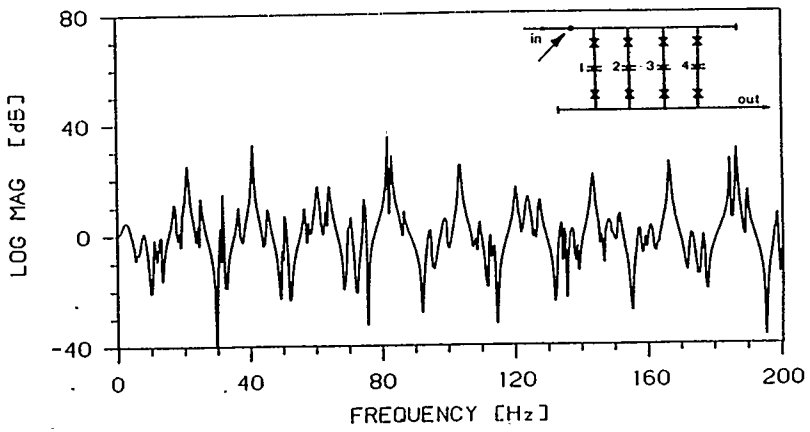

a) No Flow

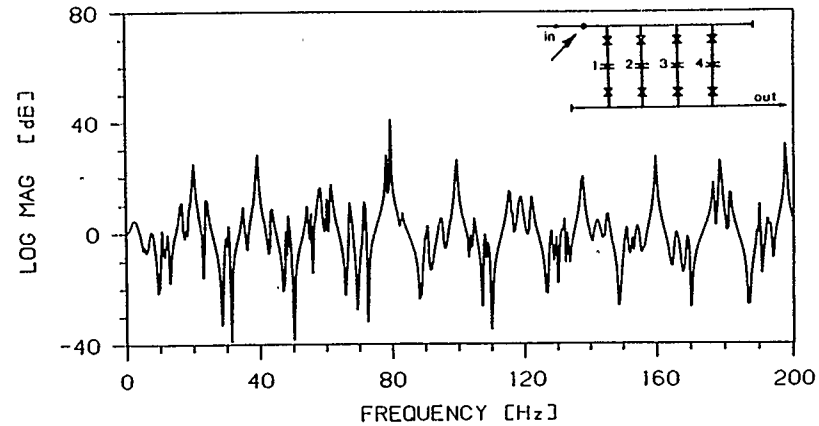

b) Temperature Reduced

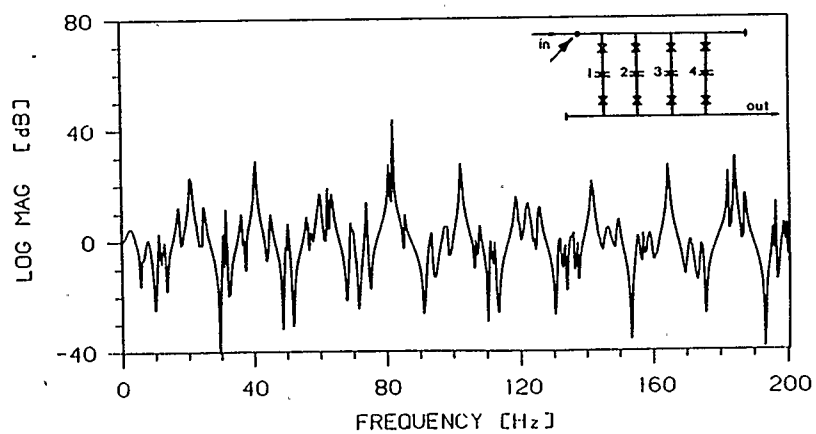

c) Pressure Increased

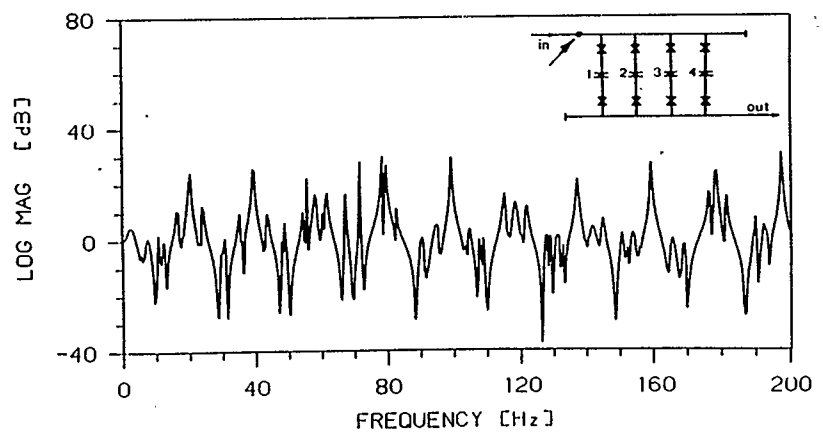

d) Medium Changed

Figure 4.33 Input Impedance for Various Conditions

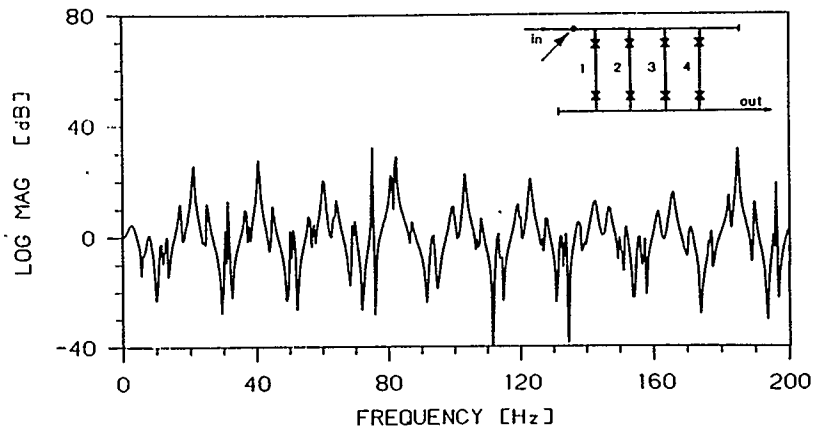

e) Orifice Plates Absent

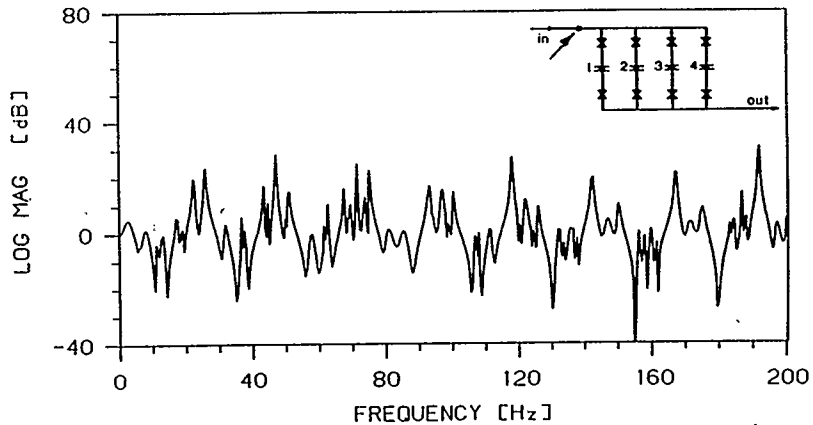

f) End Pipes Absent

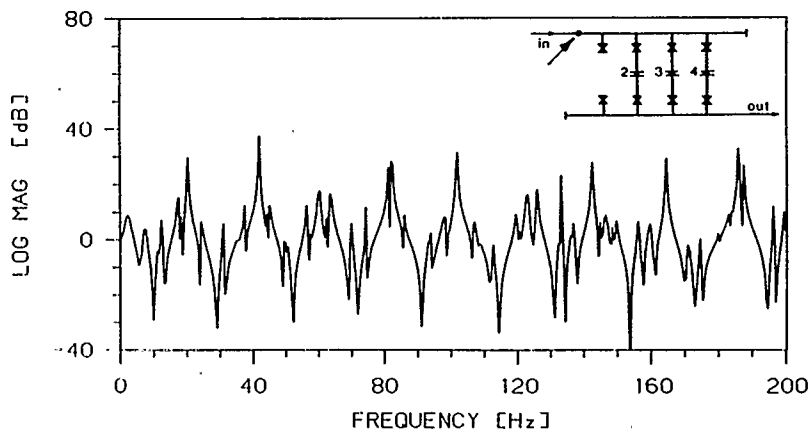

g) First Run Closed

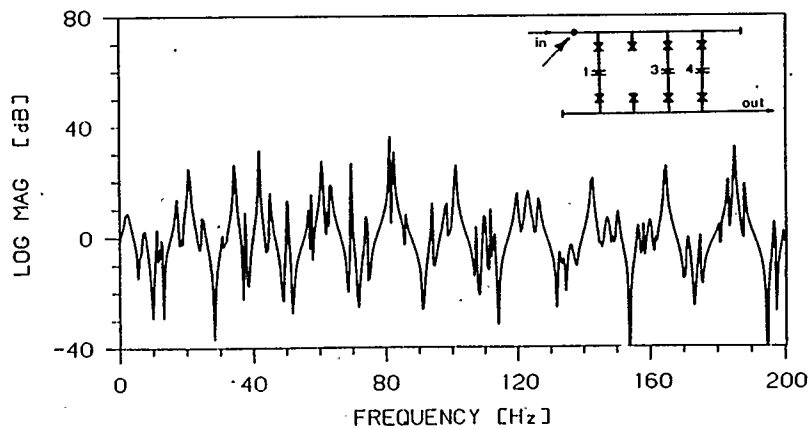

h) Second Run Closed

Figure 4.33 (continued)

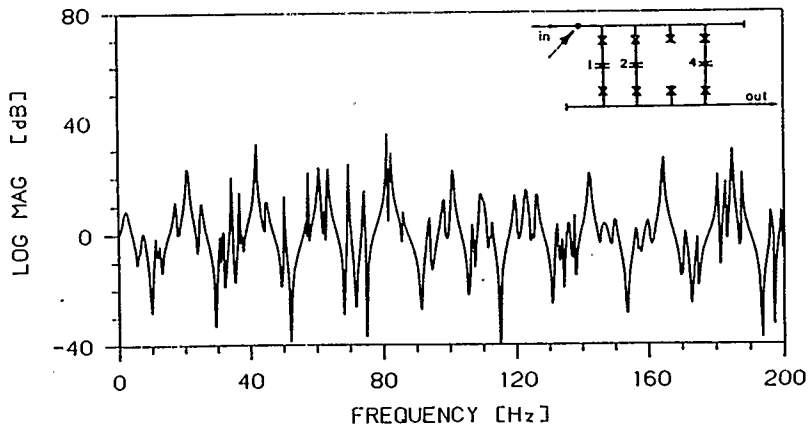

i) Third Run Closed

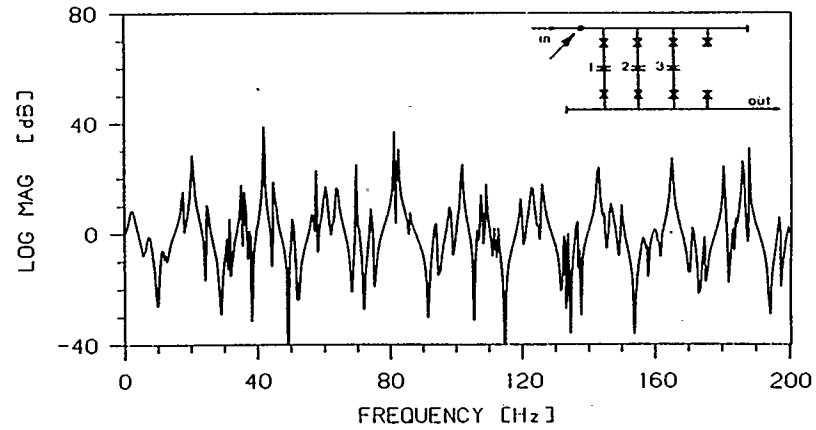

j) Fourth Run Closed

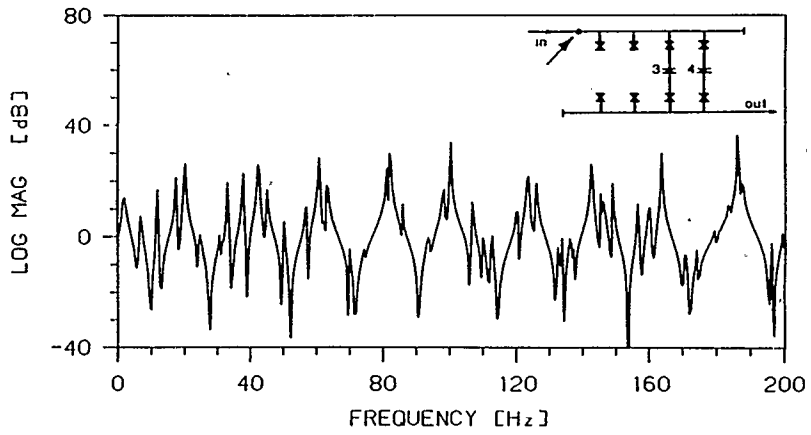

k) First and Second Runs Closed

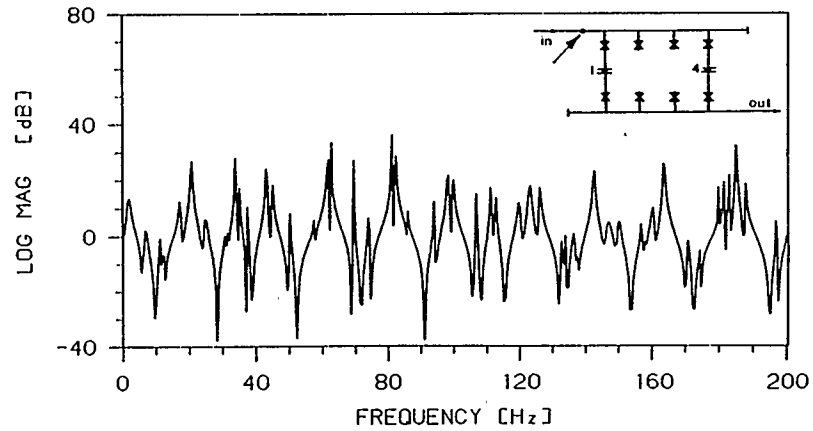

l) Second and Third Runs Closed

Figure 4.33 (continued)

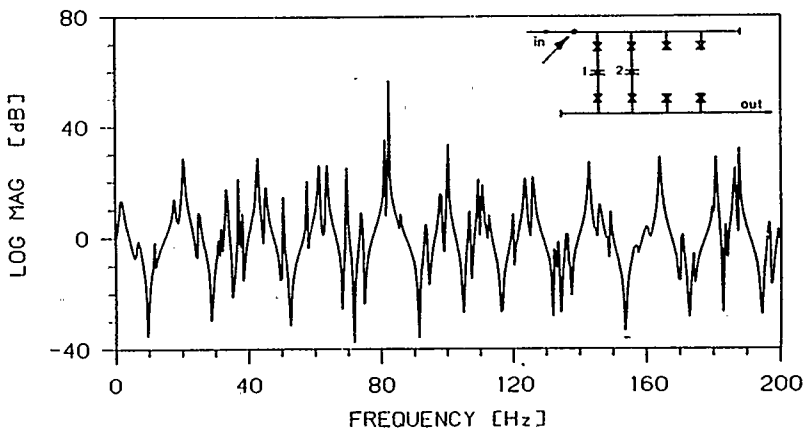

m) Third and Fourth Runs Closed

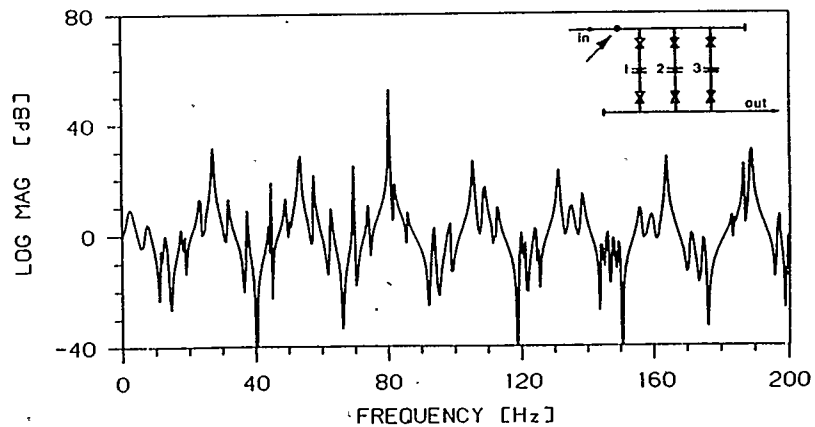

n) One-Bridge Network

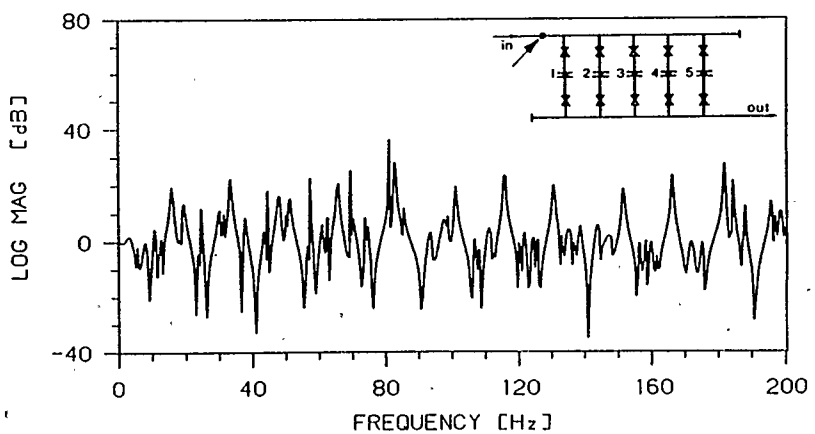

o) Three-Bridge Network

Figure 4.33 (continued)

Table 4.2 RMS Values of Pressures for Different Conditions

Conditions \ Orifice Plate	1		2		3		4		5	
	Up.	Dn.	Up.	Dn.	Up.	Dn.	Up.	Dn.	Up.	Dn.
Reference	189.5	139.9	177.4	129.8	203.3	124.8	196.7	124.5	---	---
No Flow	173.1	144.5	235.0	207.9	135.9	102.6	199.9	172.9	---	---
Temperature Changed	339.7	197.9	365.2	217.3	197.4	132.9	236.0	168.0	---	---
Pressure Changed	151.9	126.1	179.1	151.3	121.1	93.1	158.2	131.4	---	---
Medium Changed	138.9	111.5	155.5	116.8	107.8	78.1	143.0	106.1	---	---
Orifice Plate Absent	136.3	138.4	172.7	174.7	149.9	149.2	183.8	184.0	---	---
End Pipe Absent	94.7	88.3	131.1	103.3	194.8	130.8	234.1	151.3	---	---
First Run Closed	---	---	186.2	159.0	192.3	117.4	217.8	154.8	---	---
Second Run Closed	374.5	244.5	---	---	241.2	154.1	227.5	145.2	---	---
Third Run Closed	221.3	202.7	172.2	159.7	---	---	163.4	115.1	---	---
Fourth Run Closed	246.0	237.2	303.2	256.0	249.4	235.4	---	---	---	---
First and Second Runs Closed	---	---	---	---	338.1	224.1	367.4	244.6	---	---
Second and Third Runs Closed	258.5	317.5	---	---	---	---	313.6	174.4	---	---
Third and Fourth Runs Closed	210.7	177.9	210.1	184.6	---	---	---	---	---	---
One-Bridge Network	238.3	196.3	288.3	195.6	348.9	205.0	---	---	---	---
Three-Bridge Network	125.3	116.6	124.4	111.9	113.2	106.9	119.6	116.6	123.9	119.3

Up. - Upstream Orifice Plate
Dn. - Downstream Orifice Plate

Table 4.3 RMS Values of Volume Velocity for Different Conditions

Conditions \ Orifice Plate	1		2		3		4		5	
	Up.	Dn.	Up.	Dn.	Up.	Dn.	Up.	Dn.	Up.	Dn.
Reference	22.5	22.5	13.2	13.1	12.0	11.8	12.2	12.1	---	---
No Flow	17.5	17.4	13.5	13.3	11.9	11.7	12.0	11.9	---	---
Temperature Changed	22.1	22.1	13.8	13.6	11.8	11.5	11.8	11.8	---	---
Pressure Changed	23.2	23.3	15.1	15.1	12.6	12.5	12.5	12.6	---	---
Medium Changed	34.0	34.1	17.6	17.4	13.9	13.6	12.9	13.1	---	---
Orifice Plate Absent	38.7	38.6	14.1	14.1	11.4	11.4	12.3	12.0	---	---
End Pipe Absent	14.8	14.6	12.7	12.6	14.0	13.7	17.9	17.5	---	---
First Run Closed	---	---	20.9	20.8	13.5	13.3	16.0	16.1	---	---
Second Run Closed	22.6	22.6	---	---	15.5	15.3	13.5	13.4	---	---
Third Run Closed	23.9	23.9	19.7	19.6	---	---	13.5	13.5	---	---
Fourth Run Closed	26.4	26.4	15.6	15.3	15.1	15.0	---	---	---	---
First and Second Runs Closed	---	---	---	---	24.3	24.1	20.4	20.4	---	---
Second and Third Runs Closed	29.2	29.2	---	---	---	---	19.4	19.4	---	---
Third and Fourth Runs Closed	33.7	34.9	26.0	26.0	---	---				
One-Bridge Network	29.0	28.1	13.8	13.5	20.7	19.4	---	---	---	---
Three-Bridge Network	21.6	21.6	11.9	11.8	10.9	10.7	10.2	9.9	11.5	11.4

Up. - Upstream Orifice Plate
Dn. - Downstream Orifice Plate

Table 4.4 RMS Values of Input Impedance for Different Conditions

Conditions	Input Impedance
Reference	113.7
No Flow	110.5
Temperature Changed	147.8
Pressure Changed	177.3
Medium Changed	99.7
Orifice Plate Absent	93.9
End Pipe Absent	80.3
First Run Closed	441.1
Second Run Closed	101.4
Third Run Closed	132.7
Fourth Run Closed	121.4
Second and Third Runs Closed	130.9
Third and Fourth Runs Closed	709.5
One-Bridge Network	441.1
Third-Bridge Network	101.4

found in Tables 4.2 through 4.4.

4.5 Conclusions

Table 4.5 shows in a condensed way how the pressure, volume velocity, and imput impedance respond to various changes introduced into a typical two-bridge network. From this table and previously discussed plots the following can be concluded.

1) The shape of the pressure and volume velocity curves is quite unpredictable. Only the presence of the side branch resonator (created by end pipes) can be readily detected.

2) High pressure levels are often noticed for lower frequency ranges in which the mechanical or acoustic resonant frequencies of the secondary device can be present.

3) For specific conditions, the level curves are different in every run although they may be similar in shape.

4) When all four runs are open (reference system and the first six alterations) the highest pressure fluctuations are present in the second and fourth runs. Volume velocity fluctuations are highest in the first run except when end pipes are absent.

5) The pressure and volume velocity levels drop at the bridge output by about 20 to 30 dB because the system acts as an attenuation device. As a result, measurement of pressure and volume velocity at the output of the bridge gives little information about the behaviour of those values inside the

bridge (see Figure 4.17).

6) From among different flow conditions (see upper part of Table 4.5), reduced temperature has the most dramatic effect on pressure fluctuations, magnifying them most in the first and second runs.

7) Closing the first run has only a slight effect on fluctuations in the remaining runs. On the other hand closing up the second or the fourth run results in much higher fluctuations in the open runs.

8) Rearranging the bridge network by increasing the number of runs results in lower fluctuations. Decreasing the number of runs causes a meaningful rise in pressure and volume velocity fluctuations. In general, the effect of adding a run has less impact on fluctuations compared to the effect of eliminating a run. The negative influence is more significant.

9) The second part of Table 4.5 indicates that when the flow conditions and medium remain unchanged, and orifice plates as well as end pipes are present, the input impedance can be a good indicator of the behaviour of pressure and volume velocity fluctuations inside the bridge network. If the input impedance grows the fluctuations in pressure and volume velocity grow too. Consequently, the effects of shutting down one or more runs as well as rearranging the bridge network by adding or eliminating one run can be easily estimated.

Table 4.5 Behaviour of RMS Values of Pressure, Volume Velocity and Input Impedance

Conditions	Input Impedance	Orifice Plate Number							
		1	2	3	4	1	2	3	4
		Pressure				Volume Velocity			
No Flow	~	↓	↑↑	↓↓	~	↓↓	~	~	~
Temperature Reduced	↑↑	↑↑↑	↑↑↑	~	↑↑	~	↑	~	↓
Pressure Increased	↑↑	↓↓	~	↓↓	↓↓	↑	↑↑	↑	~
Medium Changed	↓	↓↓	↓↓	↓↓	↓↓	↑↑↑	↑↑	↑↑	↑
Orifice Plates Absent	↓	↓↓	~	↓↓	↓	↑↑↑	↑	↓	~
End Pipes Absent	↓	↓↓	↓↓	~	↑↑	↓↓	↓	↑↑	↑↑↑
First Run Closed	↑		~	~	↑↑		~	↑↑	↑↑
Second Run Closed	↑	↑↑↑		↑↑	↑↑	~		↑↑	↑↑
Third Run Closed	~	↑↑	~		↓↓	↑	↑↑↑		↑↑
Fourth Run Closed	↑↑	↑↑	↑↑↑	↑↑		↓↓	↑↑	↑↑	
First and Second Runs Closed	↑			↑↑↑	↑↑↑			↑↑↑	↑↑↑
Second and Third Runs Closed	↑	↑↑			↑↑↑	↑↑			↑↑↑
Third and Fourth Runs Closed	↑↑↑	↑↑	↑↑			↑↑↑	↑↑↑		
One-Bridge Network	↑↑↑	↑↑	↑↑↑	↑↑↑		↑↑	↑	↑↑↑	
Three-Bridge Network	↓	↓↓	↓↓	↓↓	↓↓	↓	↓	↓↓	↓↓

LEGEND

Fluctuation Changes:

About the Same	~	
Small	↑	↓
Moderate	↑↑	↓↓
Significant	↑↑↑	↓↓↓

CHAPTER 5

DIFFERENTIAL-PRESSURE TRANSMITTER ANALYSIS

5.1 Description of Three Types of Differential-Pressure Transmitters

Typically, the transmitter is connected across a primary device, an orifice plate, and the pressure difference is measured. Differential-pressure transmitters are difficult to design since they need to sense small differences in large pressures while they also have to be able to withstand high line pressure overload. Described below are two electrical and one mechanical differential-pressure transmitters.

5.1.1 Rosemount Transmitter

A model 1151DP Alphaline D-PT with a range from 0 - 750 " H_2O (193 kPa) was tested. Figure 5.1 shows a diagram of the sensing unit called a δ-cell. Pressure is transmitted through isolating diaphragms and silicone oil fill fluid to a sensing diaphragm in the centre of the δ-cell. The sensing diaphragm is a spring element which deflects in response to differential pressure across it. The displacement of the sensing diaphragm is proportional to the differential pressure. The position of the sensing diaphragm is detected by capacitor plates on both sides of the sensing diaphragm. The differential capacitance between the sensing

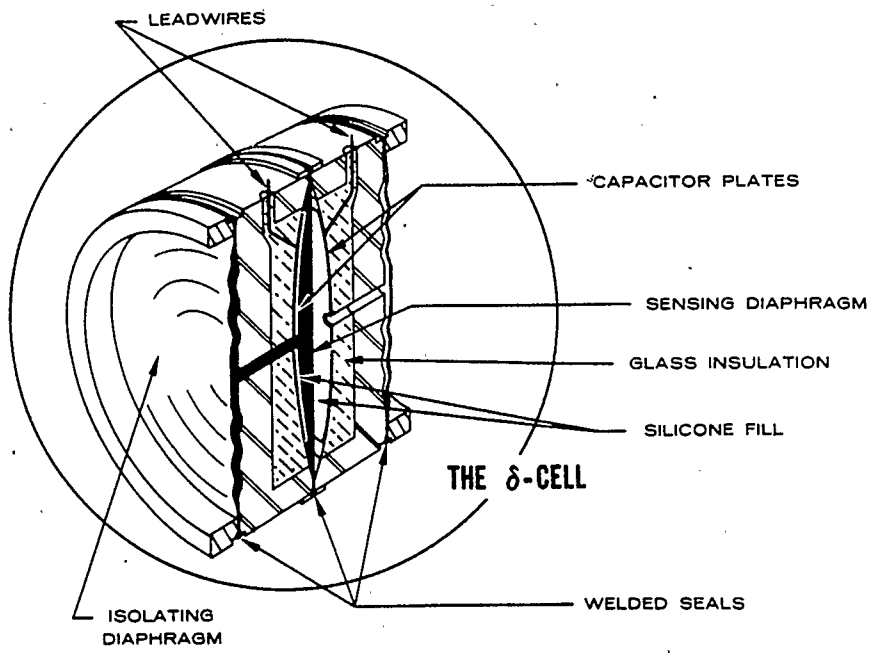

Figure 5.1 Rosemount, Capacitive Differential-Pressure Transmitter

diaphragm. The differential capacitance between the sensing diaphragm and the capacitor plates is converted electronically to either 4-20 milliamps DC or 10-50 milliamps DC current. The δ-cell is completely sealed. Welded stress isolation clamping in the sensor housing prevents errors introduced by stresses and torques on the process flanges and minimizes the effects of line pressure and overpressure up to 2000 psi (13790 kPa).

5.1.2 Gould Transmitter

A model PD 3000 with a range from 0-100" H_2O (25.7 kPa) was tested. The sensor of the Gould Transmitter consists of a beam-diaphragm assembly, with a thin film strain gauge bridge circuit

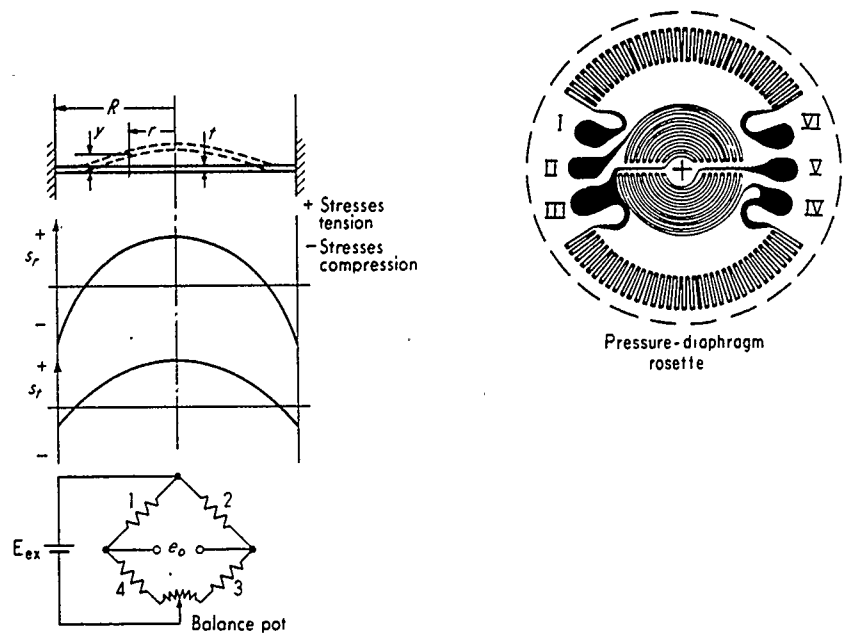

Figure 5.2 Beam Assembly with a Diaphragm-Type Strain Gauge

located on the bending beam (Figure 5.2). This strain gauge offers the stability and resistance characteristics required for high stability and dependable performance. No bonding agents are used, minimizing the effects of stress and temperature. Differential pressure is transmitted to the sensing diaphragm by a silicone oil fill fluid. The displacement of the sensing diaphragm is transmitted to the beam assembly, whose strain gauges are electrically

connected to the amplifier circuit. A change in differential pressure causes a corresponding change in the resistance of the strain gauge bridge and the transmitter 4-20 milliamps DC output of the transmitter.

5.1.3 Barton Transmitter

A model 199 DPU with a range from 0-100"H_2O (25.7 kPa) was tested. Figure 5.3 shows a cutaway view of the differential pres-

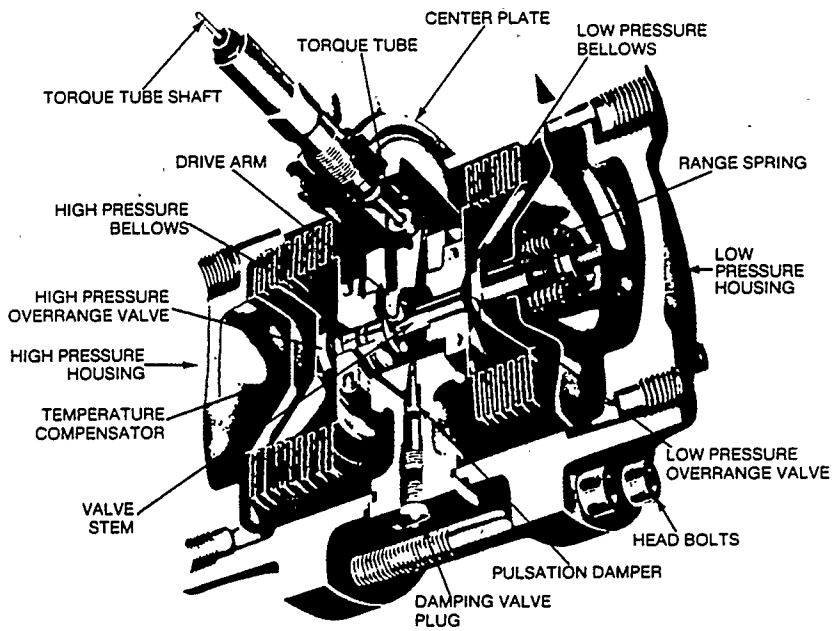

Figure 5.3 Barton, Differential Bellows Pressure Transmitter, Cutaway View

sure unit. The unit consists of two bellows, each of which is

sealed at one end and open at the other. The open ends are sealed to both sides of a centre plate. The bellows and centre plate are filled with a liquid. An opening through the centre plate allows the liquid to flow between the two bellows. There is a possibility to restrict flow for cases when a higher damping of the transmitter is desirable. The bellows are connected internally by a valve stem that passes through the opening in the centre plate. Each bellows is enclosed by a separate housing, one housing for the high pressure (HP) connection and one housing for the low pressure (LP) connection. The housings are connected by pipe or tubing to the high and low pressure sides of an orifice plate in the process system. Any pressure change within the housings causes the bellows to contract or expand laterally, forcing the fill liquid through the centre plate. As the bellows move, the connecting valve stem follows the motion of the bellows. The valve stem movement is transmitted through the drive arm to twist the torque tube. Consequently, the rotation of the torque tube's shaft provides the DPU's mechanical output.

5.2 Model of the Pressure Sensing Device

Each of the transmitters described in section 5.1 consists of a volume enclosed in the transmitter's housing and sensing diaphragm which equally divides this volume. The diaphragm is exposed to pressures which are transmitted by the connecting tubing to the volumes on both sides of the diaphragm.

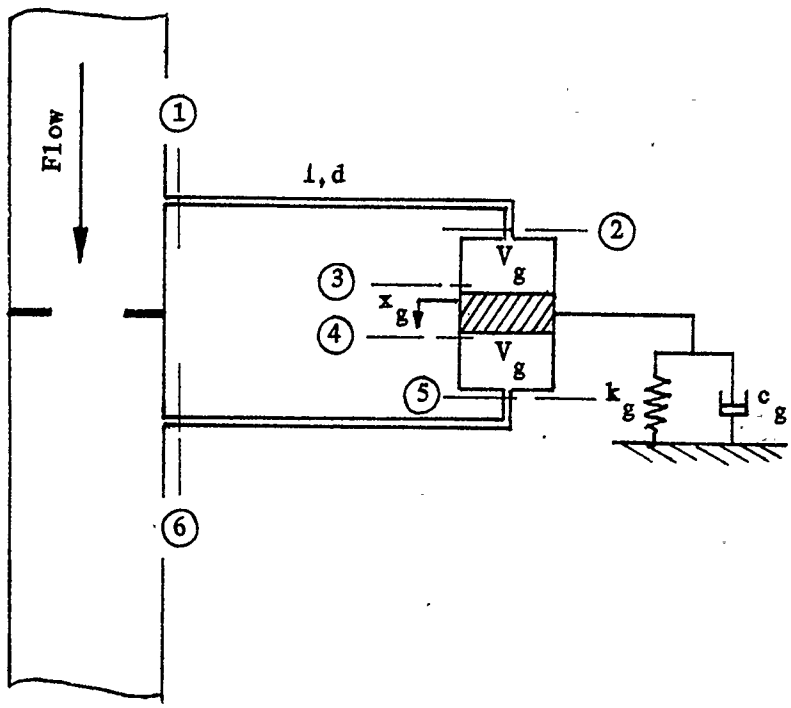

Figure 5.4 Model of the Differential-Pressure Sensing Device

The model of the pressure-sensing device is depicted in Figure 5.4. The system is modelled as an assembly of acoustic and mechanical elements. The acoustic part is composed of two tubes (representing the connecting tubing) and a chamber (representing the interior of the transmitter's housing). The volume included in the tubes is normally small compared to that inside the chamber, but is nevertheless taken into account in the model. The mechanical part is modelled as a piston, representing the sensing diaphragm, whose motion in the chamber is restricted by a spring and damper. The mechanical stiffness is considered to be large compared to that of the acoustic system.

The actual volume V_g was modelled as a cylinder whose dimensions were similar to the actual chamber dimensions. The differential-pressure-sensing device was characterized by a transfer function relating the differential pressure at the primary device to the linear displacement of the sensing element:

$$TF_g = X_g/\Delta P = X_g/(P_1-P_6) \tag{5.1}$$

This transfer function was derived using transfer matrices to represent the system. Relationships among the acoustic variables at stations 1 and 3, and 4 and 6 are:

$$\begin{bmatrix} P_1 \\ V_1 \end{bmatrix} = [T]_{13} \begin{bmatrix} P_3 \\ V_3 \end{bmatrix} \tag{5.2}$$

$$\begin{bmatrix} P_4 \\ V_4 \end{bmatrix} = [T]_{46} \begin{bmatrix} P_6 \\ V_6 \end{bmatrix} \tag{5.3}$$

where $[T]_{13}$ and $[T]_{46}$ are the overall or combined transfer matrices between the stations indicated. For example,

$$[T]_{13} = [T]_1[T]_2 = \begin{bmatrix} A_{13} & B_{13} \\ C_{13} & D_{13} \end{bmatrix}$$

The volume velocity V_3 equals V_4 and both are related to the mechanical element's dispacement by:

$$V_3 = V_4 = i\omega S_g X_g \tag{5.4}$$

Using equations (5.2), (5.3) and (5.4), Fourier-transformed pressures P_3 and P_4 were derived as functions of the transfer matrix parameters:

$$P_3 = 1/A_{13}(P_1 - B_{13}S_g i\omega X_g) \tag{5.5}$$

$$P_4 = 1/D_{46}(P_6 - B_{46}S_g i\omega X_g) \tag{5.6}$$

In order to relate P_3 and P_4, the four-pole equation for the mechanical element, derived in Appendix B, was used:

$$\begin{bmatrix} P_3 \\ X_3 \end{bmatrix} = \begin{bmatrix} 1 & (k_g/S_g)(1 - r^2 + i2\eta r) \\ 0 & 1 \end{bmatrix} \begin{bmatrix} P_4 \\ X_4 \end{bmatrix} \tag{5.7}$$

from which, the pressure P_3 was obtained:

$$P_3 = P_4 + (k_g/S_g)(1 - r^2 + i2\eta r)X_4 \tag{5.8}$$

or

$$P_3 = P_4 + B_{34}X_4 \tag{5.9}$$

Substituting equations (5.5) and (5.6) into (5.9) gives:

$$\frac{P_1}{A_{13}} - \frac{P_6}{D_{46}} = \left[\frac{B_{13}}{A_{13}} i\omega S_g + \frac{B_{46}}{D_{46}} i\omega S_g + B_{34} \right] X_g \tag{5.10}$$

The system is reciprocal (there is no mean flow) which results in the following identities:

$$A_{13} = D_{13}, \; A_{46} = D_{46} \tag{5.11}$$

Also, for a symmetrical system,

$$A_{13} = A_{46}, \quad B_{13} = B_{46}, \quad C_{13} = C_{46}, \quad D_{13} = D_{46} \tag{5.12}$$

Substituting equations (5.11) and (5.12) into (5.10) gives the following expression for the transfer function:

$$\frac{X_g}{P_1 - P_6} = \frac{1}{(2B_{13} i\omega S_g + A_{13}B_{34})} \tag{5.13}$$

Equation (5.13) is used in the subsequent sections to predict the acoustic and mechanical behaviour of the secondary system.

The model of a secondary device presented above can also be simplified and used to predict the Helmholtz frequency only. This procedure is included in Appendix C.

5.3 Prediction of Transfer Function Based on the Model

The influence of variations in four parameters, which are important in secondary device design, was examined using the model introduced in section 5.2. These parameters are: stiffness and

damping of the sensing diaphragm, volume of the transmitter's chamber and the length of the connecting lines. The reference parameters of the hypothetical secondary device were chosen based on realistic typical values, and are given in Fig. 5.5 through 5.8.

5.3.1 Influence of the Transmitter Stiffness

The stiffness (k_g) of the spring restricting the piston's motion (see model in section 5.2) was varied in the range from 3.16e7 to 3.16e3 N/m . Figure 5.5 shows how the transfer function behaves for two cases: i) when the piston's motion is undamped, and ii) when the piston's motion is slightly damped. Three resonant frequencies are apparent, two acoustic and one mechanical. To visually identify the mechanical resonant frequency, the frequency response curves were ploted with and without mechanical damping. The peak associated with mechanical resonance was decreased significantly when mechanical damping was present. The fundamental resonant acoustic frequency, the so-called Helmholtz frequency, results from the oscillatory motion of the mass of fluid in the line. The higher acoustic frequencies originate from standing waves in the cavity, and are not harmonically related to the fundamental frequency. When the mechanical stiffness is varied, the behaviour of the Helmholtz and mechanical acoustic frequencies is analogous to that of a two-degree of freedom mechanical system composed of two masses connected by a spring. As the spring stiffness decreases,

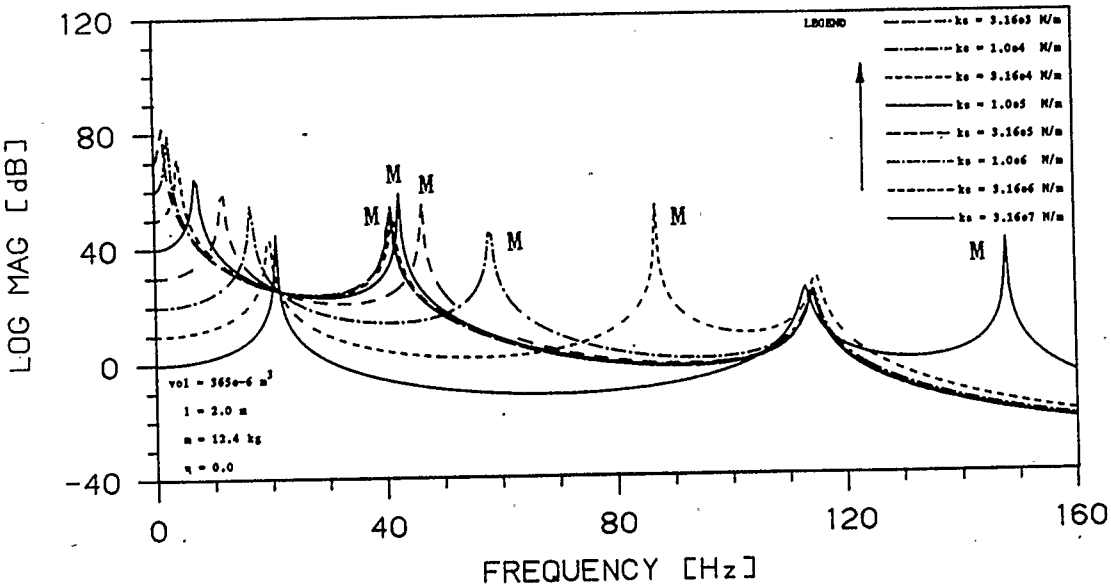

a) Mechanical Damping Absent

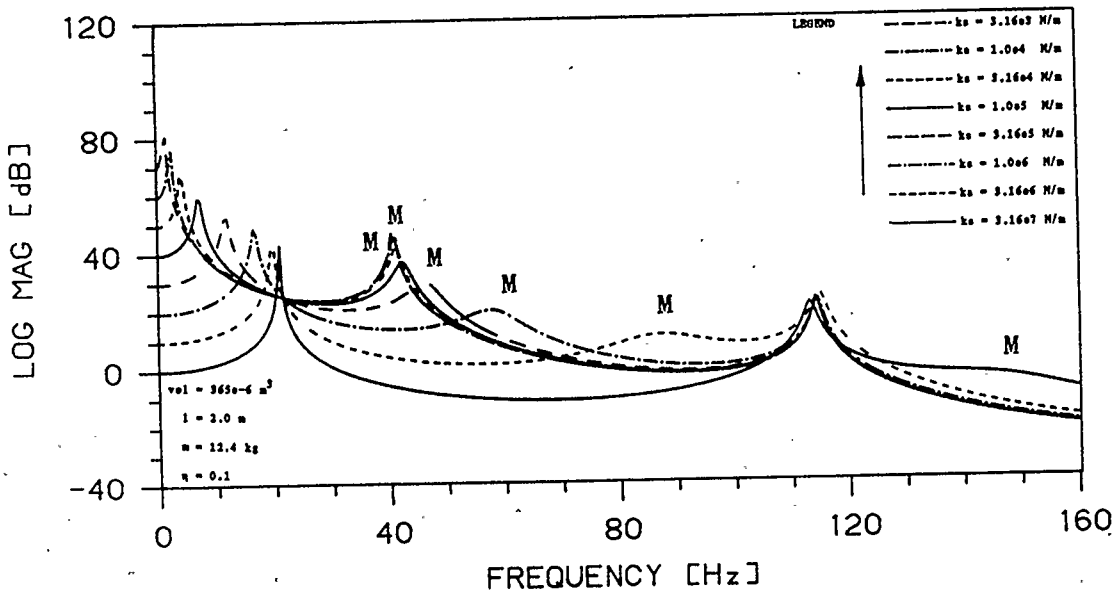

b) Mechanical Damping Present

Figure 5.5 Transmitter's Frequency Responses for Varied Mechanical Element's Stiffness

the amplitude of the mechanical element vibration grows, opposite to that of the acoustic element. At the same time the resonant frequencies shift towards lower values, the Helmholtz frequency moving considerably slower. Simultaneously with the decreasing mechanical resonant frequency, a decrease in the actual damping coefficient in the mechanical element is also observed (note that the non-dimensional damping factor η is constant).

5.3.2 Influence of the Transmitter Damping

The influence of varying the damping factor of the mechanical element on the transmitter's frequency response is shown in Figure 5.6. Two secondary devices having preset stiffnesses of 10^7 N/m (high stiffness) and 10^5 N/m (moderate stiffness) were subjected to five different damping factors. Here again, the interaction between the mechanical and the acoustic elements was noticed. For moderate stiffness, an increase in the mechanical damping factor causes a significant decrease in the amplitude not only of the mechanical resonant peak, but also of the adjacent, lower frequency acoustic resonant peak. The higher frequency acoustic resonant peak is relatively unaffected, so are the locations of all the resonances in the given frequency range.

The similar pattern can be observed for high stiffness case. Decrease in both the mechanical and the adjacent acoustic amplitudes when the mechanical damping factor increases is evident.

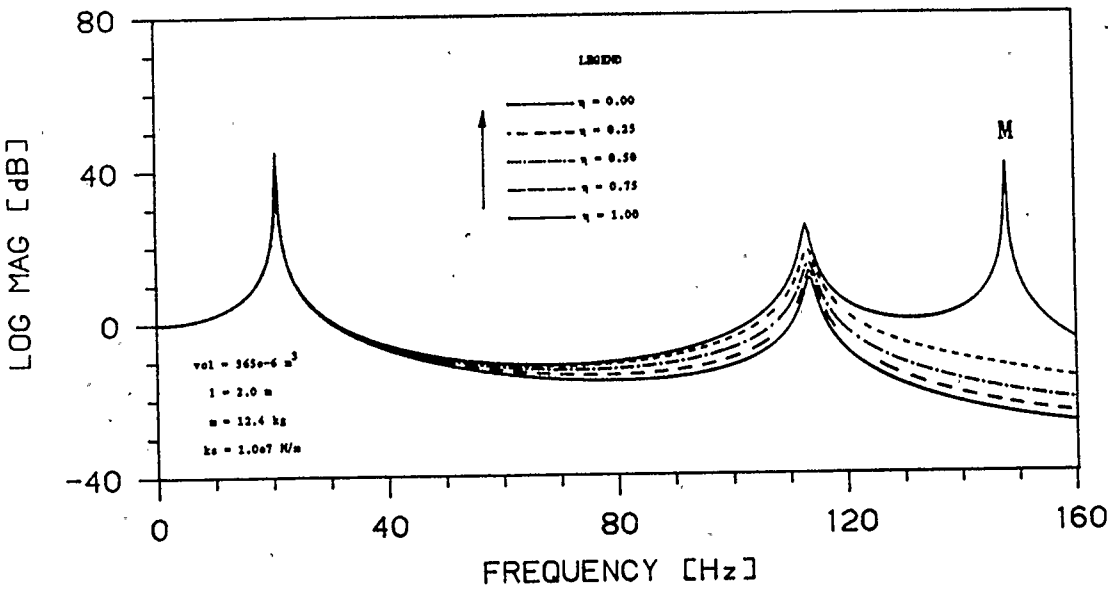

a) High Stiffness

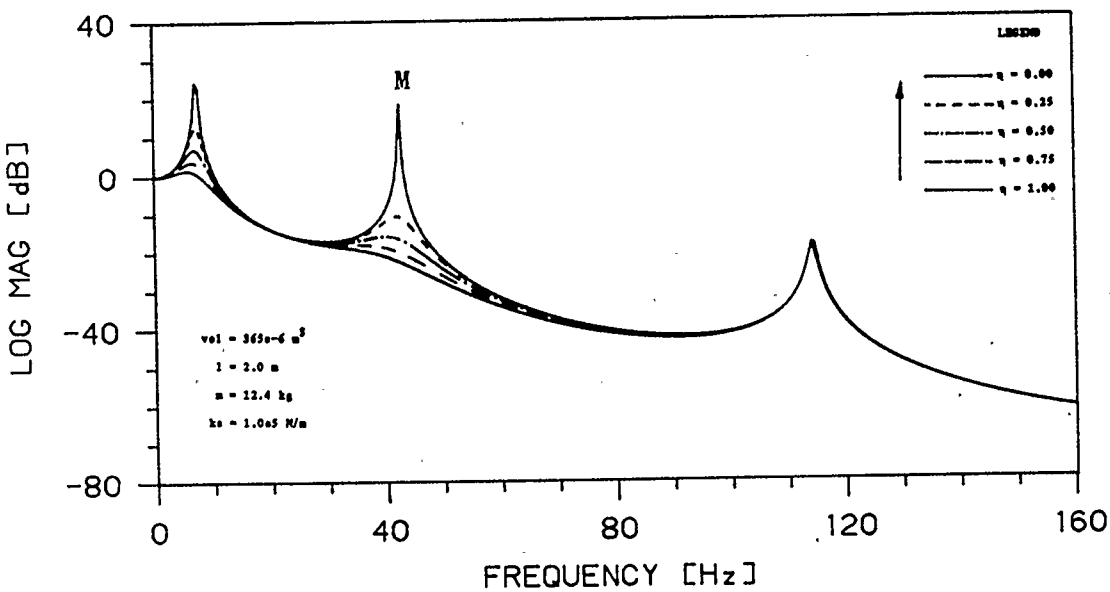

b) Moderate Stiffness

Figure 5.6 Transmitter's Frequency Responses for Varied Mechanical Element's Damping

5.3.3 Influence of the Transmitter Volume Space

A change in volume of the transmitter influences its characteristics. Three cases for three different transmitter volume spaces were tested: 365e-6 m^3 (Barton), 34e-6 m^3 (Gould), and 23e-6 m^3 (Rosemount). The corresponding curves are depicted in Figure 5.7. It can be observed that the increase in the volume at the end of the transmitter line causes a shift of the peaks towards lower frequencies. When the increase in volume is small, the shift is also small, particularly for the peaks in the lower frequency ranges; for example, the Helmholtz resonant frequency basically retains its value. However, when the volume increase is large the shift of the peaks is significant.

In Figure 5.8, it is shown how the resonant frequencies depend on the transmitter's volume. The volume was normalized to the Barton transmitter's volume V_o. Three curves correspond to two acoustic and one mechanical resonances. It can be observed that the resonant frequencies tend to be lower when the volume increases. For small volumes, therefore stiffer systems, the acoustic resonant frequencies become higher, and, at the same time, increase the mechanical resonant frequencies. In practice, the plot can give a general idea how to choose the proper volume of a transmitter when the length of transmission lines is fixed.

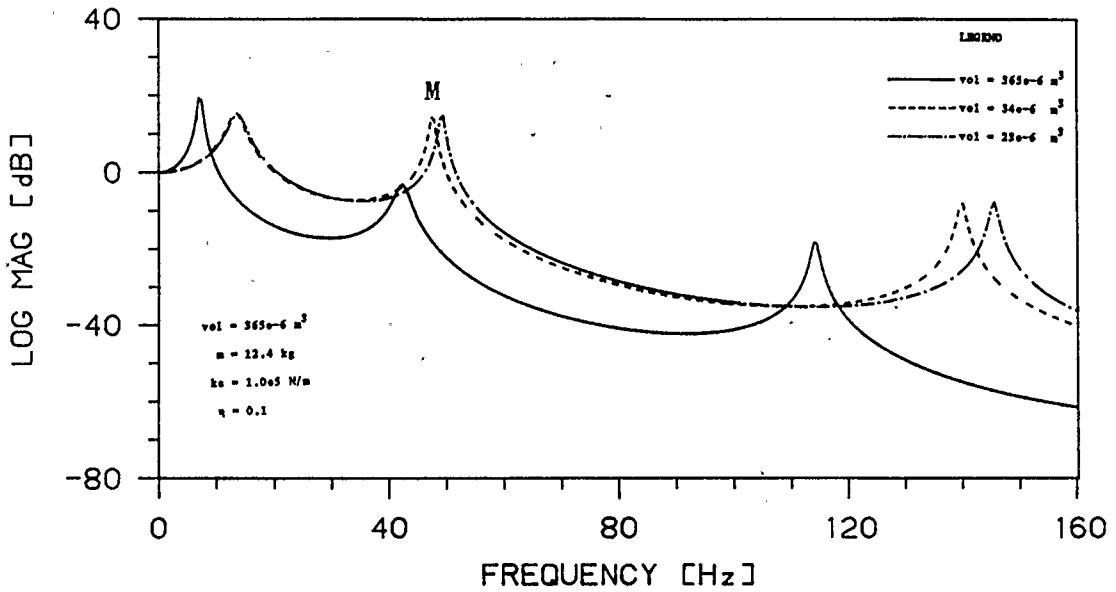

Figure 5.7 Effect of Transmitter Volume Space on Frequency Response

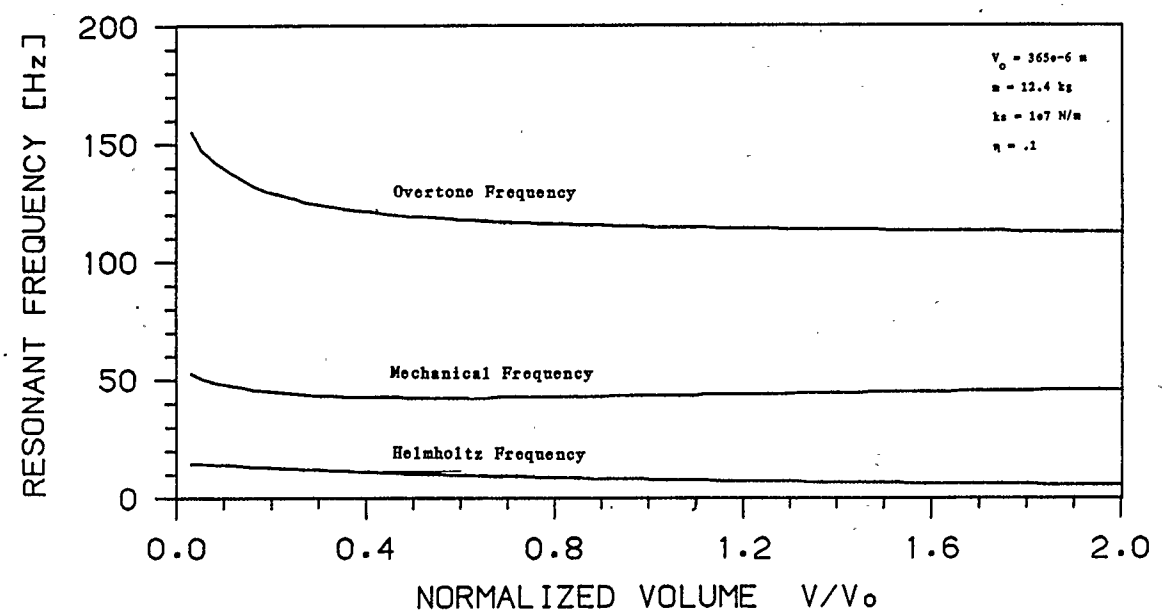

Figure 5.8 Effect of Transmitter Volume Space on Resonant Frequencies

5.3.4 Influence of the Lengths of the Conducting Tubes

Varying the lengths of the connecting tube has effects as shown in Figure 5.9. The higher the frequencies at which the peaks occur, the more they are shifted to the lower frequencies when the tubing length increases. For the Helmholtz frequency this shift is not significant.

Figure 5.10 shows the relationship between the length of transmission lines and the resonant frequencies of the secondary system. The reference length L_o was the length of the shortest possible lines used to connect the Barton transmitter. It can be observed that the resonant frequencies decrease as the transmitter lines lengthen. For shorter tubing (stiffer systems), the acoustic resonant frequencies grow, increasing also the mechanical resonant frequency. The most sensitive frequency for length changes is the highest acoustic frequency. In practical situations, this kind of plot can be used to determine the best length of transmission lines, avoiding system resonance with peaks in the differential pressure spectrum.

5.4 Experimental Evaluation of Secondary Device

5.4.1 Experimental Hardware and Testing Methods

The apparatus used for the simulation of the differential-pressure (Δp) in a run of the gas metering station is depicted in

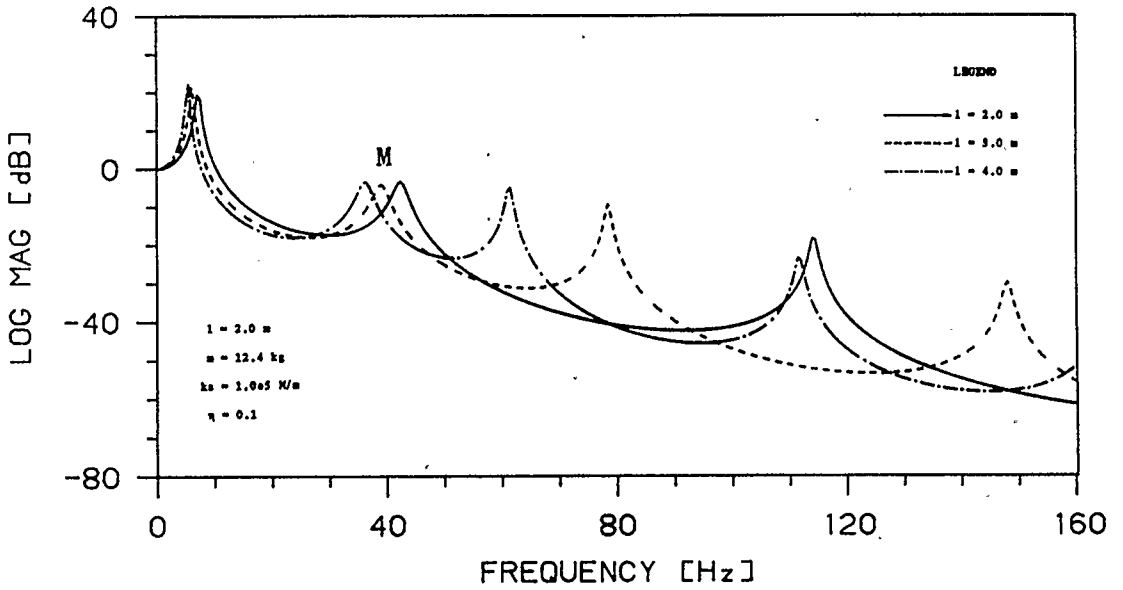

Figure 5.9 Effect of Tubing Length on Transmitter's Frequency Response

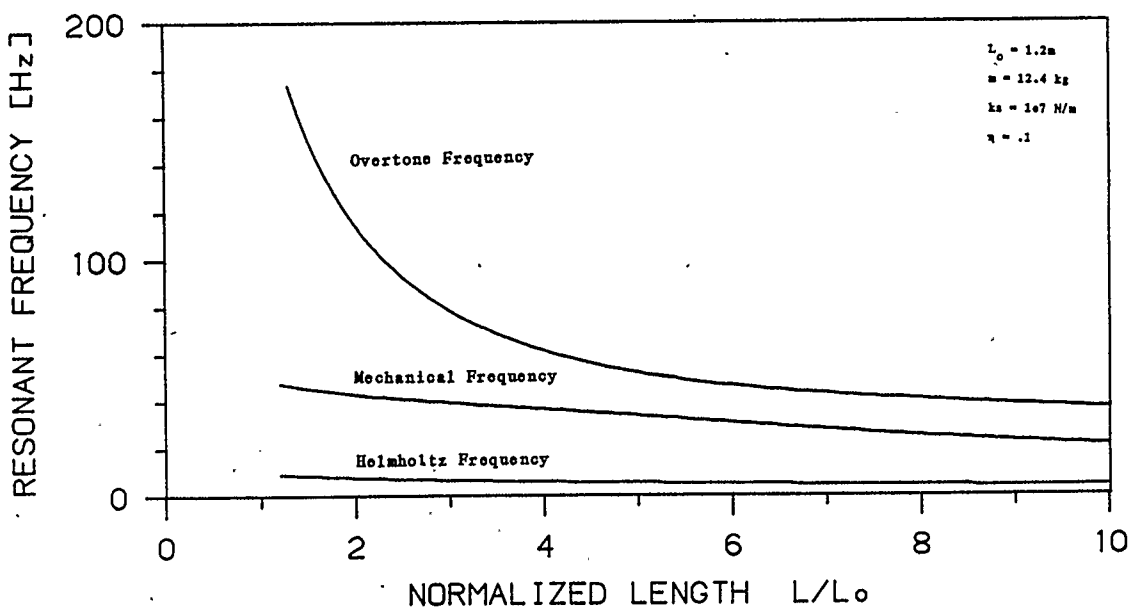

Figure 5.10 Effect of Tubing Length on Resonant Frequencies

Figure 5.11. A single-cylinder compressor (1), powered by a variable speed dynamometer motor, charged reservoir (3) through cooler (2). The static pressure was controlled by a bleed valve (4). After the desired static pressure in the tank was reached, the bleed valve was opened to allow flow. The amount of dynamic pressure variation transmitted from tank (3) to the differential-pressure gauge (8) through lines (7) was regulated by another set of valves (5). Two Kistler pressure-transducers (6) each, of which had flat frequency response from a fraction of 1 Hz to 30000 Hz, were connected to a differential amplifier (through charge amplifiers). The transducers constituted a reference differential-pressure transmitter. The reference transmitter was placed subsequently in two locations, i) in the mouth of a test transmitter chamber, ii) at the beginning of the tubing. The experimental transfer functions were obtained between the tested transmitters' signal and reference transmitter's signal for both locations. Signals from the reference and test transmitters were sent to the DSA (HP 5423A Digital Structural Analyzer) where they were digitized and stored on tape as time records or as transfer functions.

The transmitters were tested with different tubing lengths. The static pressure in the system was kept at one of four chosen levels: ambient, 50 psi (344.7 kPa), 100 psi (689.5 kPa), or 150 psi (1034.2 kPa). Gas temperature was held constant by the cooler at 23°C (296.15^{o}K) during the testing procedure. In this manner, the conditions for each transmitter tested were fully repeatable.

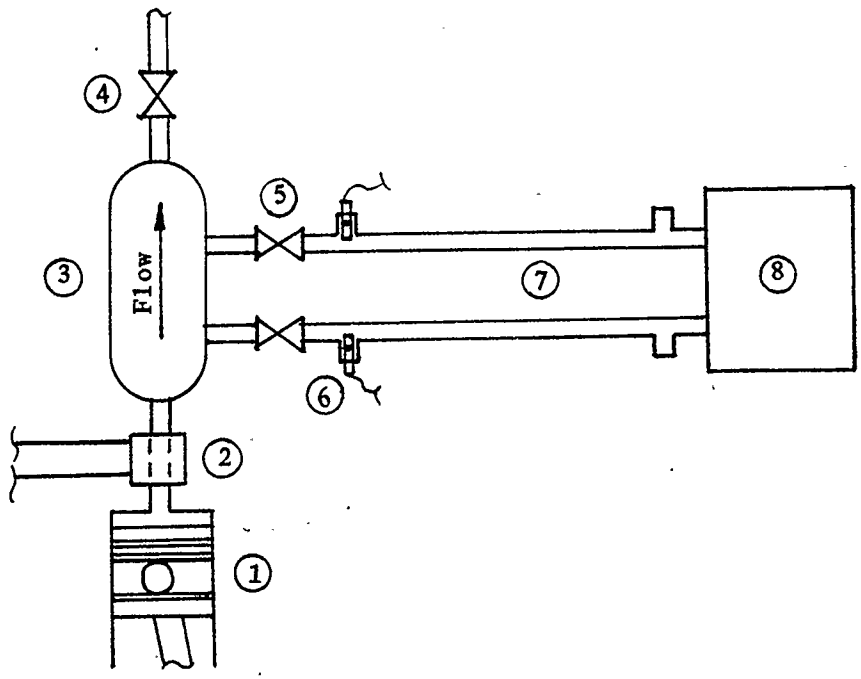

1) Compressor - Campbell Hansfeld (type A)
2) Cooler
3) Reservoir
4) Standard Valve (3/8'')
5) Bleeding Valve (3/8'')
6) Kistler's Transducer (no. 30439 and no. 43238)
7) Transmission Lines (tubing 3/8'')
8) Differential Pressure Gauge (Barton, Gould, Rosemount)

Figure 5.11 Apparatus Used in Secondary Device Evaluation

Before the experiments were carried out, the frequency response for the Kistler transducers were recorded. Those with the flattest characteristics were chosen for use in the experiment. The Barton transmitter was modified slightly to adapt to the experiment. The mechanical output, movement of its pen arm, was converted into an electrical signal by placing the Bently non-contacting displacement transducer close to the hinged point of the arm. The maximum displacement of the arm was sufficiently small, 0.004 m, and belonged to the linear part of the Bently's calibration curve. There was also the possibility of adjusting the Bently location for a different static pressure, so the movement of the arm could always be in the Bently's linear operational range.

The Barton, Gould and Rosemount transmitters examined were calibrated statically against another reference Rosemount transmitter whose maximum error of 0.2% was determined by an outside firm. The Kistler transducers were calibrated dynamically. Their errors were found to be smaller than 1% over the entire operating range 0-400 psi (2758 kPa), being the highest for upper limits. As the pressures in any of the experiments did not exceed 150 psi (1034.2 kPa), the error due to the Kistlers' nonlinearity was negligible.

5.4.2 Evaluation of the Barton Transmitter

The frequency characteristics of the secondary device, composed of the Barton differential-pressure transmitter and a 2.56 m

length of standard 3/8'' (9.5 mm) tubing were obtained. The frequency characteristics for the Barton transmitter itself were also determined. The predicted and experimental characteristics for the secondary device are shown in Figure 5.12 (a) and (b) respectively. A different scale is shown for these two plots because in the experiment, the signal was poor for frequencies higher than 50 Hz. The predicted and experimental resonant frequencies are the same; the magnitudes are different probably due to underestimation of the attenuation factor included in the program. The fundamental acoustic frequency is not visible in the plots because it is located in the region dominated by the mechanical element response. The curves included in Figure 5.12 (b) were obtained for different static pressures. They show no meaningful shift in frequency which means that the secondary device behaves as a linear system, at least for the tested conditions. The experimental characteristics for the Barton transmitter without transmission lines is shown in Figure 5.13. The same mechanical resonance frequency as before is present. Similarly as for the complete secondary device, the Barton transmitter alone was shown to behave linearly within the limitations of the test procedures.

Time histories for the Barton transmitter were recorded and compared to those of the reference transmitter (described in 5.4.1). The distorted dynamic pressure was in a form of a periodic wave having one of the following frequencies:

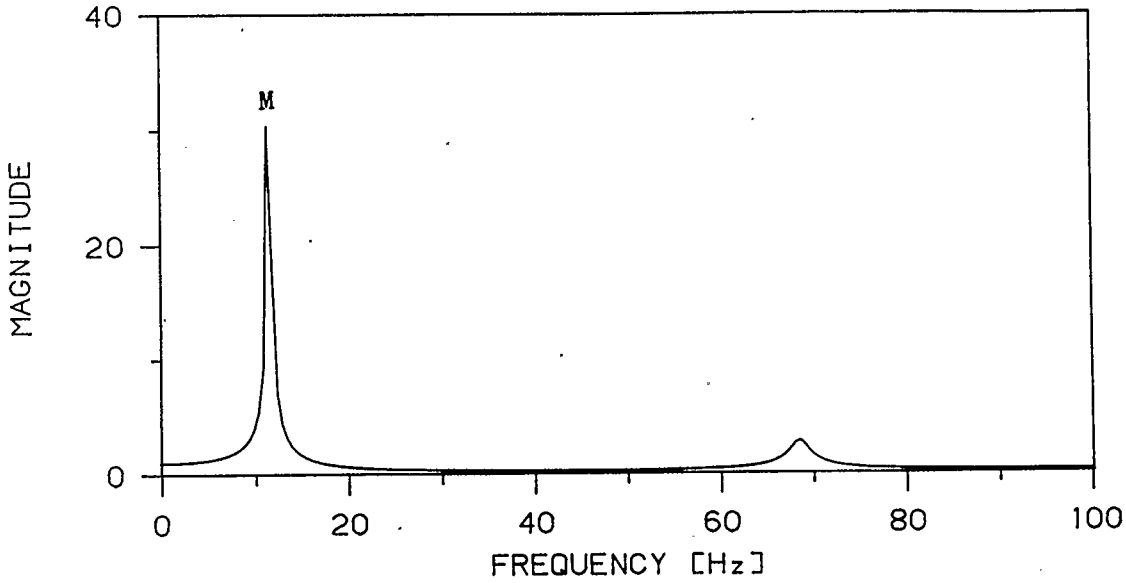

a) Predicted

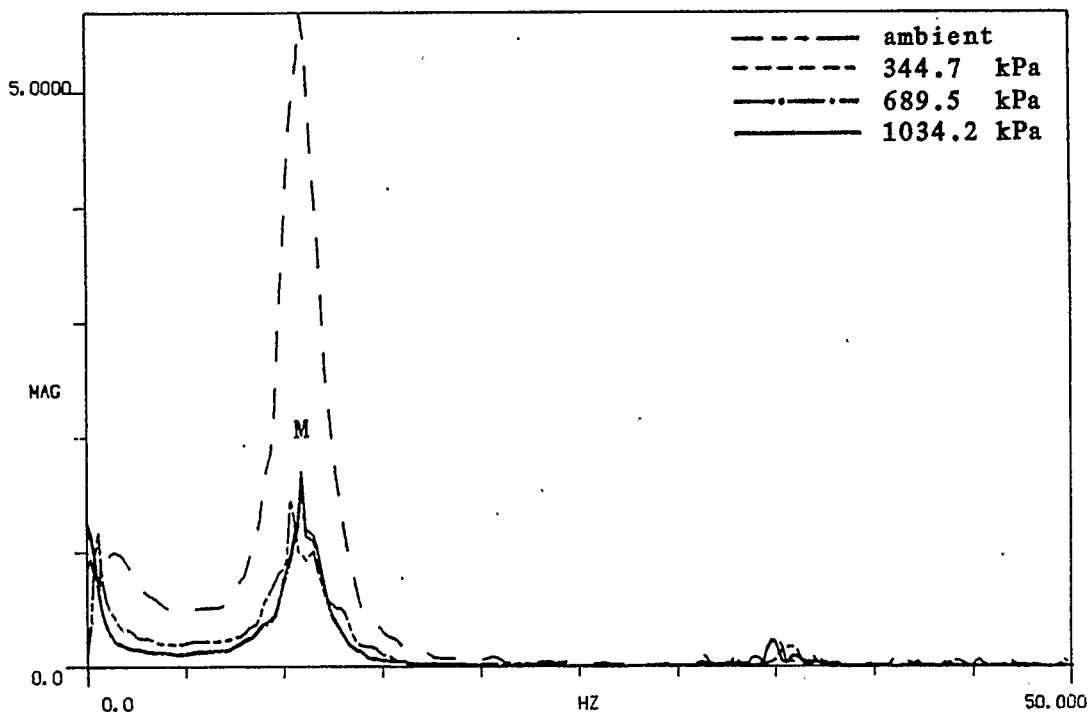

b) Experimental

Figure 5.12 Frequency Characteristics of Secondary Device Including Barton Transmitter

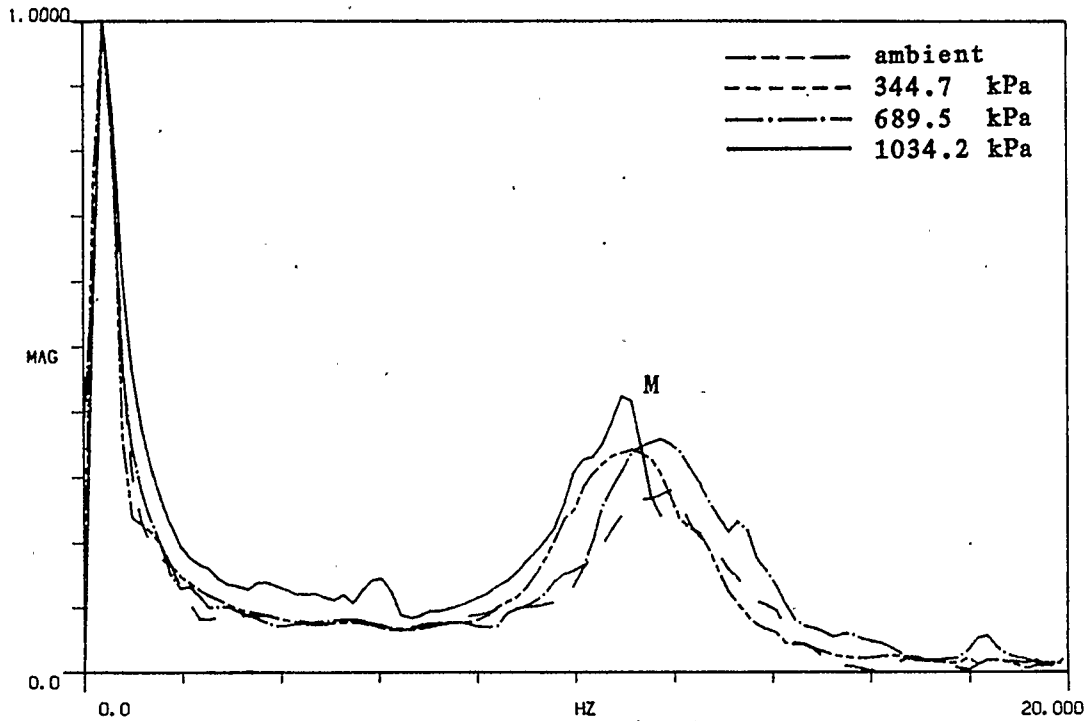

Figure 5.13 Frequency Characteristic of Barton Transmitter Alone

1) The same as the mechanical frequency of the secondary device including the Barton transmitter

2) The same as the acoustic resonant frequency of the secondary device including the Barton transmitter

3) Beyond the range of the above acoustic or mechanical resonant frequencies

The second case was impossible to realize with symmetric, 2.56 m-long connecting tubes of standard diameter 3/8'' (9.5 mm). As a result, only case 1) and 3) were examined as planned, and the corresponding plots are shown in Figure 5.14(a) and (b). To include also case 2), the length of one of the tubes was altered (to 6.62 m) making the system asymmetric. All three cases were examined for this configuration, and the corresponding plots are given in Figure 5.14(c), (d) and (e). From Figure 5.14 (a) and (b), it can be noticed that the Barton transmitter's signal lags behind that of the reference transmitter. The time lag is much larger when the mechanical resonance is present. The amplitudes for the Barton transmitter are significantly lower than amplitudes for the reference transmitter. The interesting point to note is that while the amplitudes measured by the reference transmitter remain basically the same for cases 1) and 2), the influence of mechanical resonance on the Barton transmitter is substantial. The measured amplitudes are almost two times higher when mechanical resonance is present. The behaviour of the asymmetrically arranged

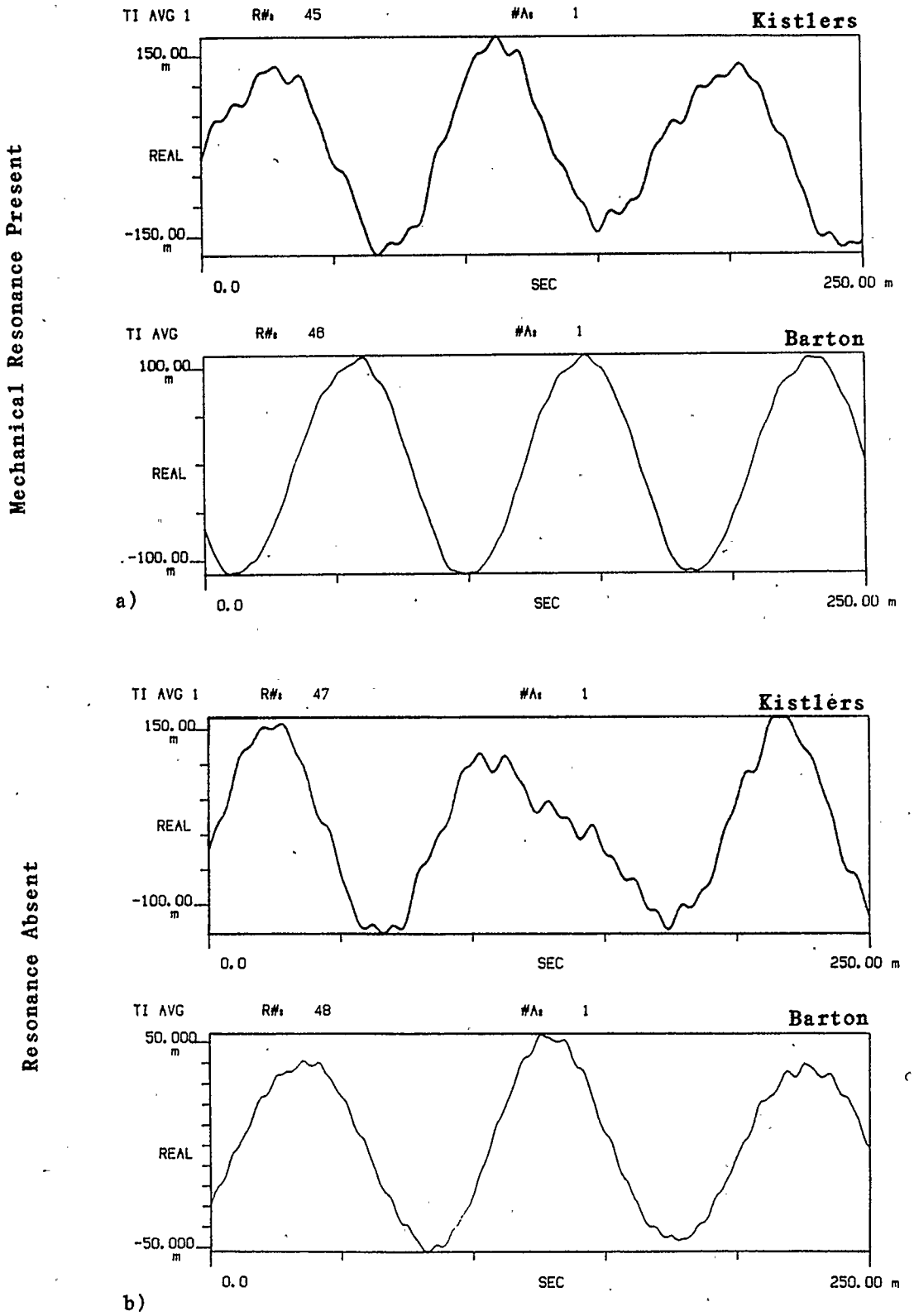

Figure 5.14 Time-Pressure Records for Barton and Reference Transmitters

Mechanical Resonance Present

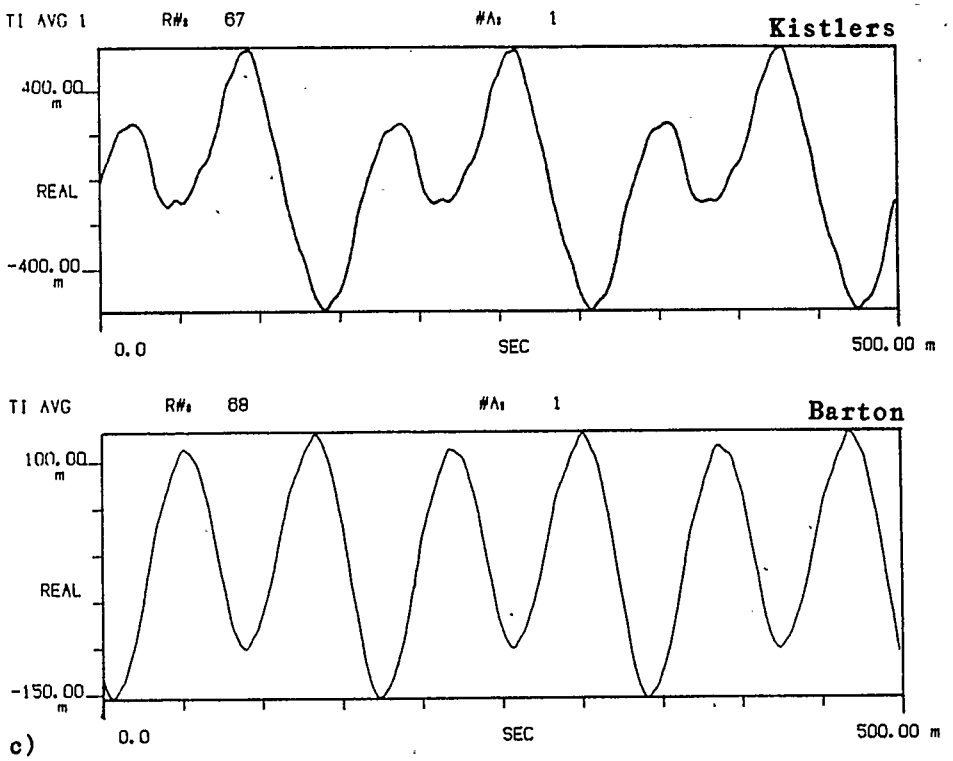

c)

Acoustic Resonance Present

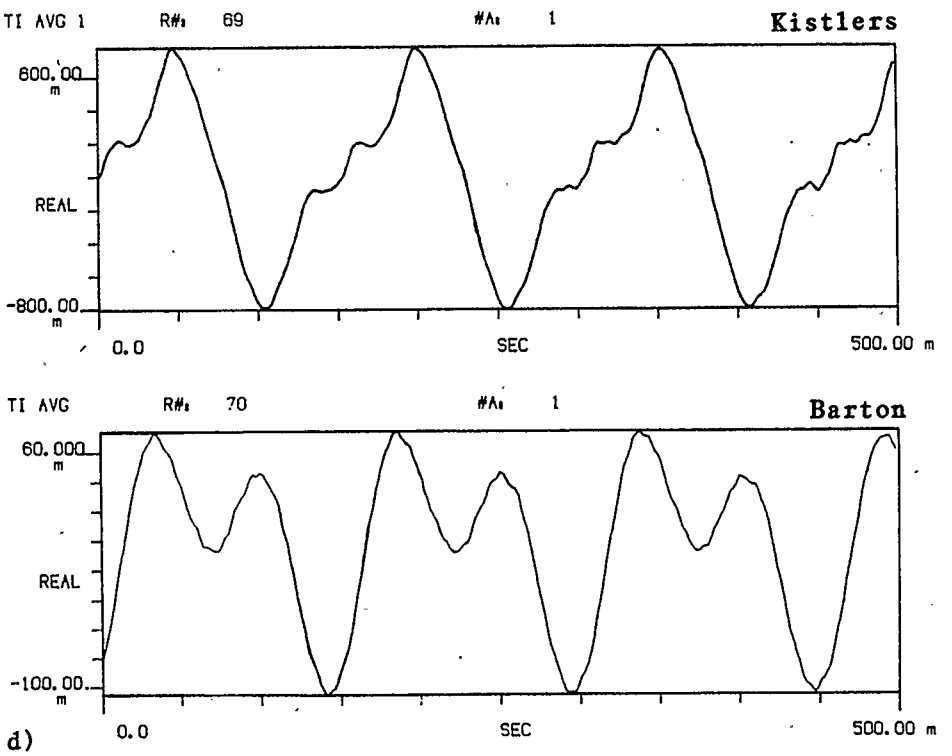

d)

Figure 5.14 (continued)

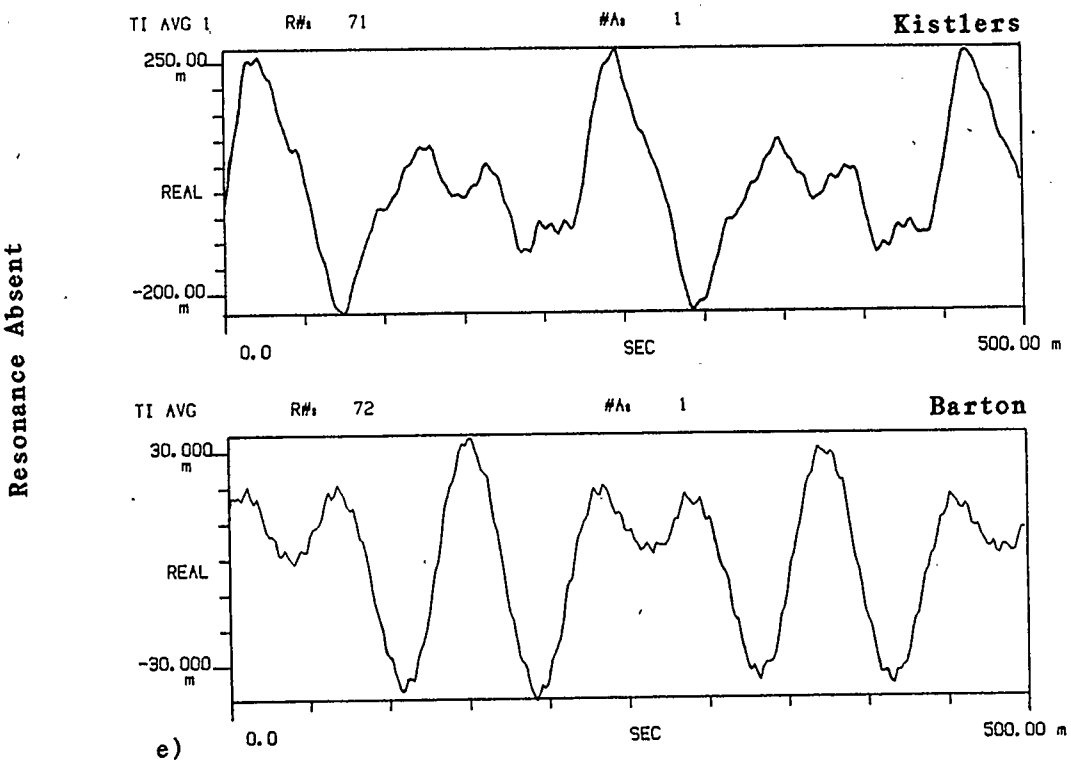

Figure 5.14 (continued)

secondary device is generally similar to the symmetrical case, but the effect of the resonances is exaggerated (higher magnitudes), as shown by the reference transmitter (see Figure 5.14 (c), (d) and (e)).

5.4.3 Evaluation of Gould Transmitter

Two frequency characteristics of the secondary device, including the Gould transmitter and 2.56 m length of standard 3/8'' (9.5 mm) diameter tubing, are shown in Figure 5.15. Part (a) of the figure presents the predicted characteristic, part (b) shows the experimental characteristics of the device. As for the Barton test, resonant frequencies coincide for both cases, but there is a difference in magnitudes. There are two acoustic peaks, the first of which represents, as usually, the Helmholtz resonant frequency. In Figure 5.16 the experimental characteristic of the Gould itself is given. The curve represents a typical second-order-device with very low frequency and high damping. There is no significant shift in characteristics for different static pressures both in the case of the complete secondary device and in the case of the Gould transmitter alone. This would suggest that the system and the transmitter itself are linear devices.

Time histories for the Gould and the reference transmitters were captured for two cases:

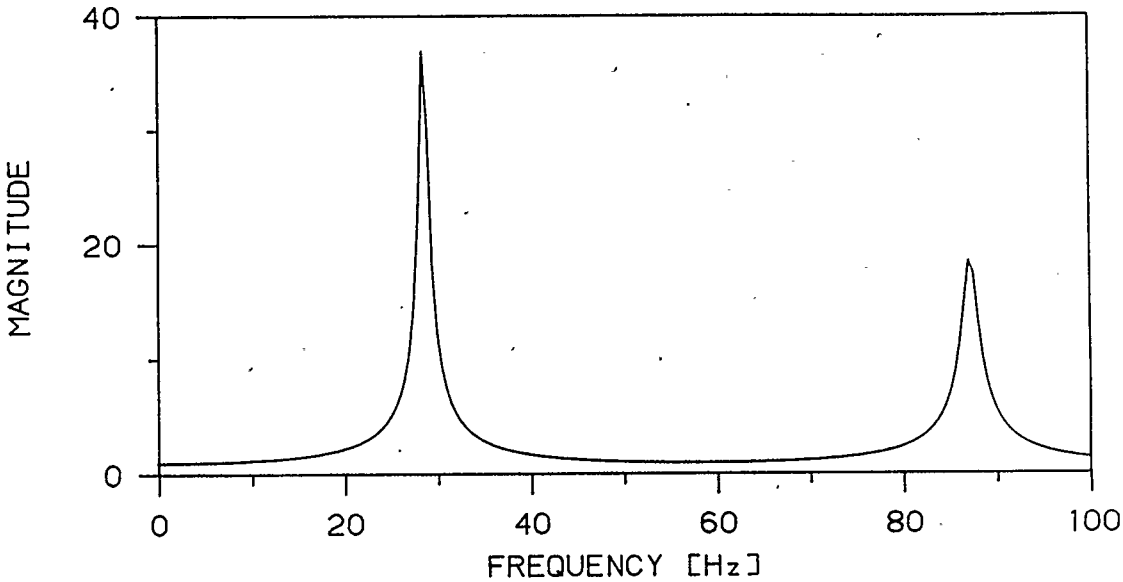

a) Predicted

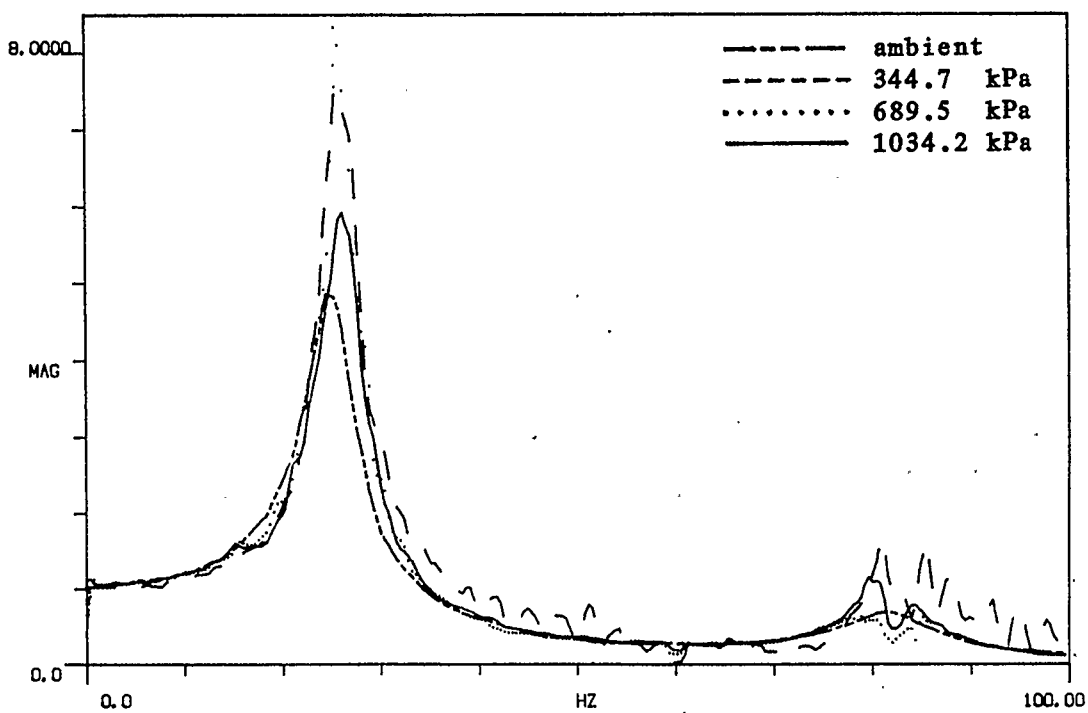

b) Experimental

Figure 5.15 Frequency Characteristics of Secondary Device Including Gould Transmitter

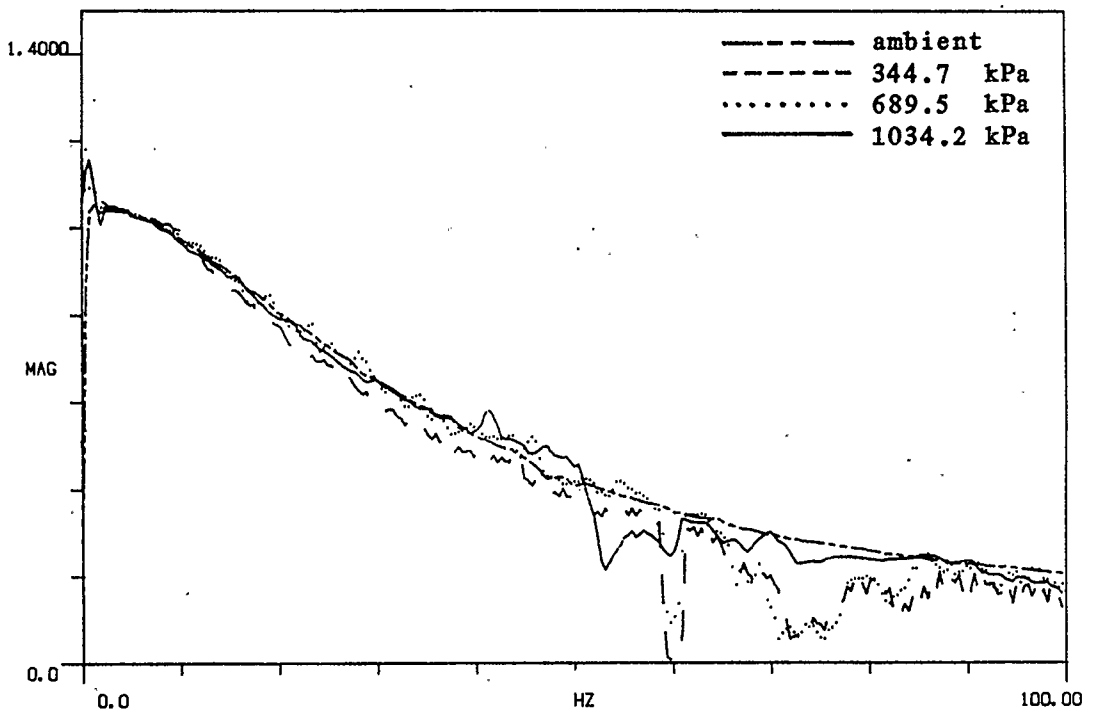

Figure 5.16 Frequency Characteristic of Gould Transmitter Alone

1) The repetition rate of the oscillatory dynamic pressure matched one of the acoustic resonant frequencies.

2) The repetition rate of the oscillatory dynamic pressure did not coincide with any resonant frequency in the system.

Both these cases were examined for the same dynamic input pressure as that used in the Barton test. Corresponding curves are depicted in Figure 5.17 (a) and (b). There was a similarity between time records for the Gould transmitter and the reference transmitter, although some details in the Gould's curve were partially lost because of the sensing element's inertia. The time lag was insignificant, and the magnitudes measured by the Gould transmitter were only slightly lower than those for the reference transmitter. However, one undesirable feature of the Gould transmitter was revealed in this test. This was its nonlinear behaviour shown in the cut-off minima especially when the acoustic resonance was present. The nonlinearity was speculated to be caused by high differential dynamic signals which pushed the sensing beam to the position where its motion was restricted. To verify this speculation the same test was performed for a lower dynamic input pressure. The plots are given in Figure 5.17 (c) and (d). As was expected, the nonlinearities disappeared, and the values of time lags were smaller.

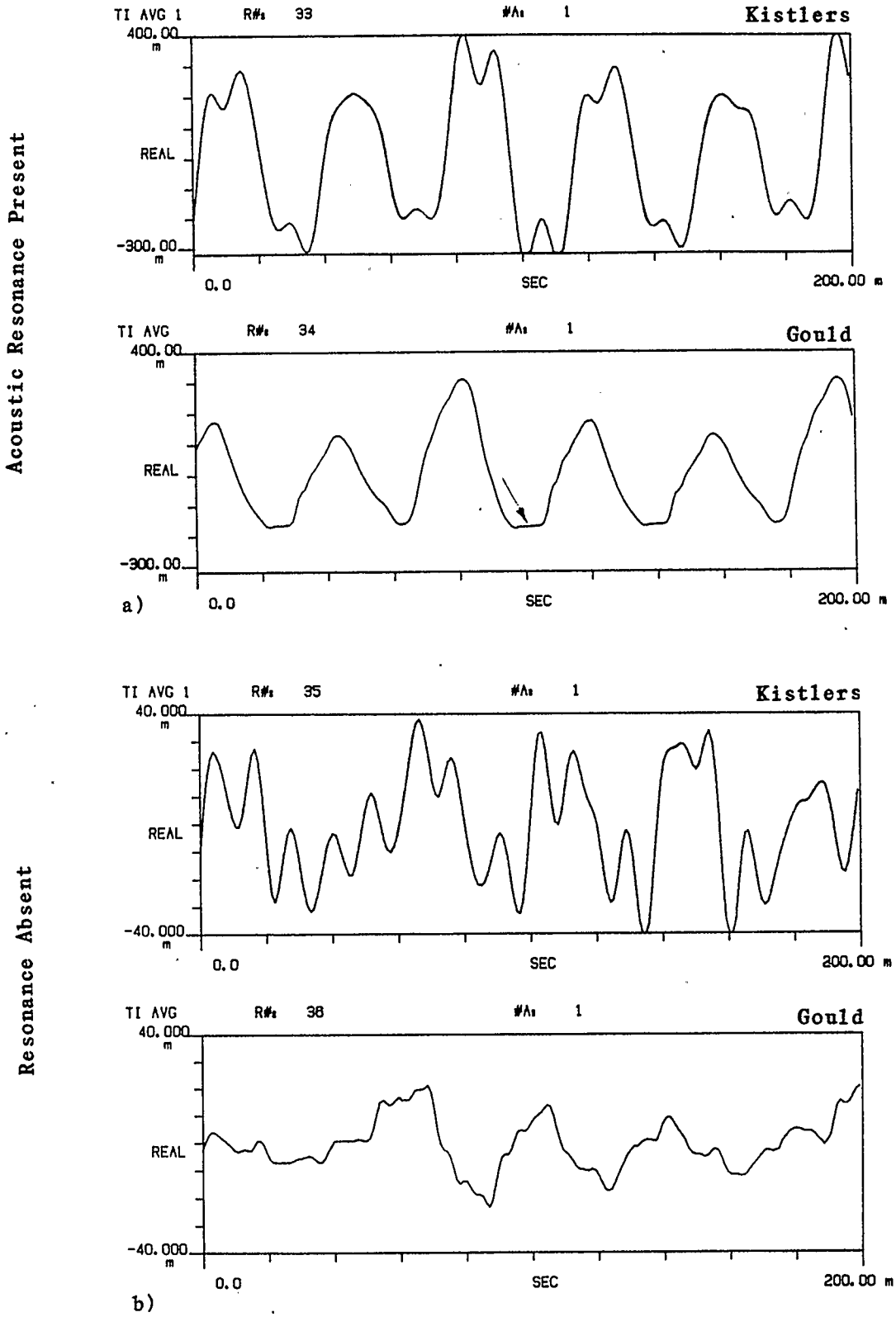

Figure 5.17 Time-Pressure Records for Gould and Reference Transmitters. Case 1 (a, b), Case 2 (c, d)

Acoustic Resonance Present

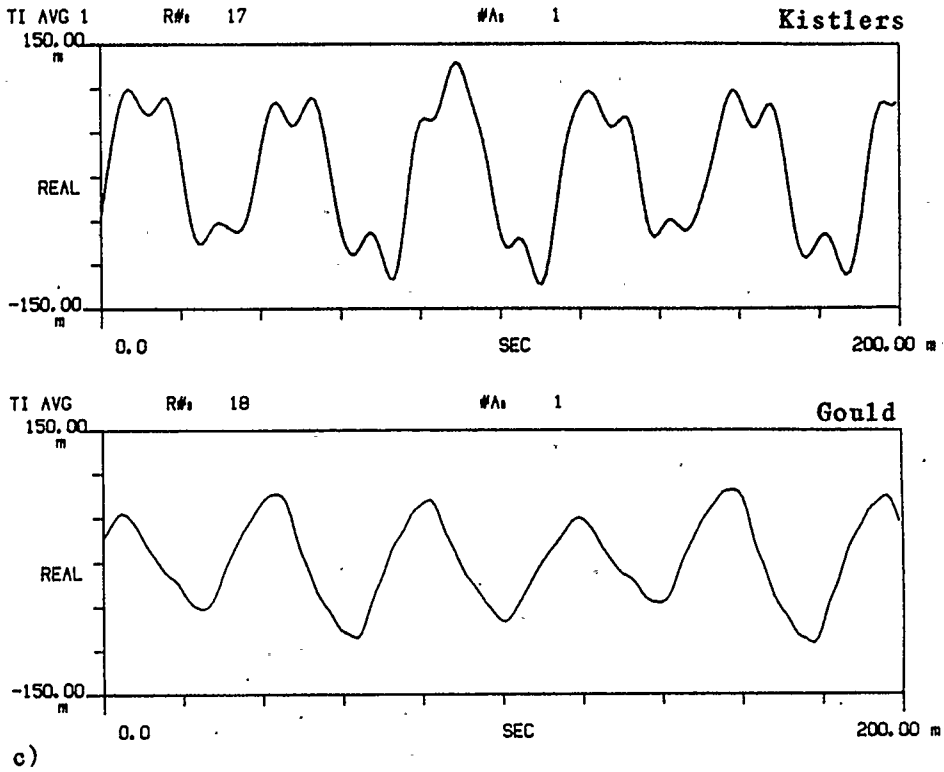

c)

Resonance Absent

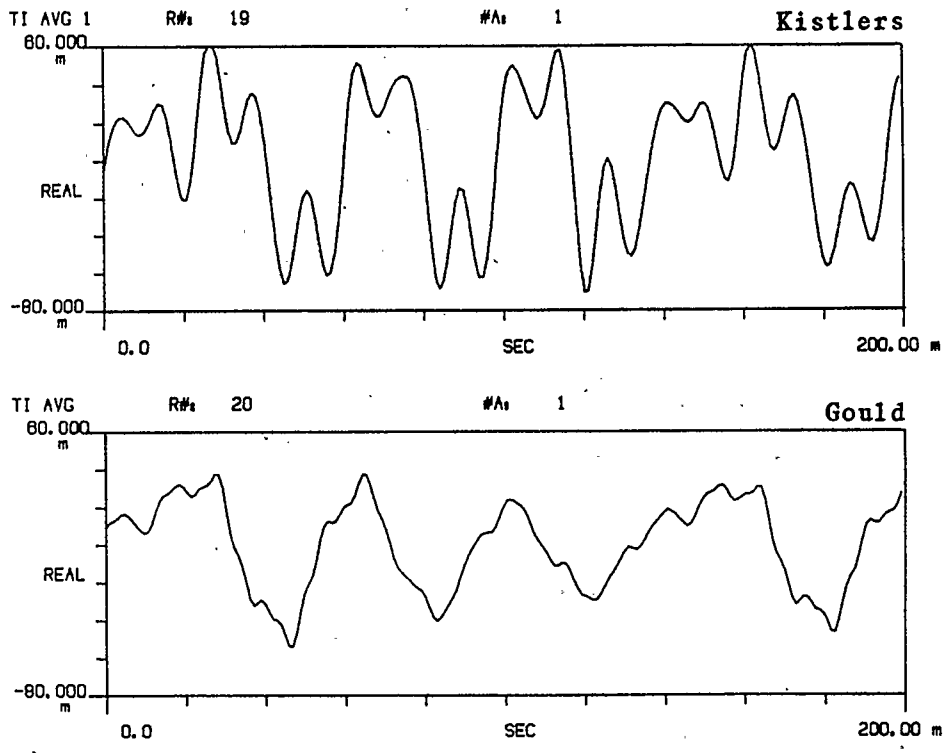

d)

Figure 5.17 (continued)

5.4.3 Evaluation of Rosemount Transmitter

The transfer functions are depicted in Figure 5.18 (a) and (b). Part (a) of the figure shows the predicted characteristic of the tested secondary device, the Rosemount transmitter and two 2.56 m by 3/8'' (9.5 mm) standard tubes. Part (b) shows the experimental curves for the same system. The scale is different because the signal above 50 Hz for the experiments was very poor. There are two acoustic peaks in the theoretical plot (the experimental plot shows only one peak due to a smaller range). The first peak corresponds to the system's Helmholtz frequency which coincides for the theoretical and experimental results. The peak magnitudes are different which, as for previous tests, is probably due to underestimation of the attenuation factor included in the program. In Figure 5.19 the experimental characteristic of the Rosemount transmitter without transmission lines is given. When this plot is compared to that of Figure 5.18 (b) it can be noticed that the peak at about 30 Hz results from the presence of transmission lines. The curves are not different when the static pressure in the system changes; the secondary device and the transmitter behave linearly.

Time histories for the reference and Rosemount transmitters are depicted in Figure 5.20. Two cases were investigated:

1) The dynamic pressure fundamental frequency was the same as the acoustic resonant frequency for the tested system

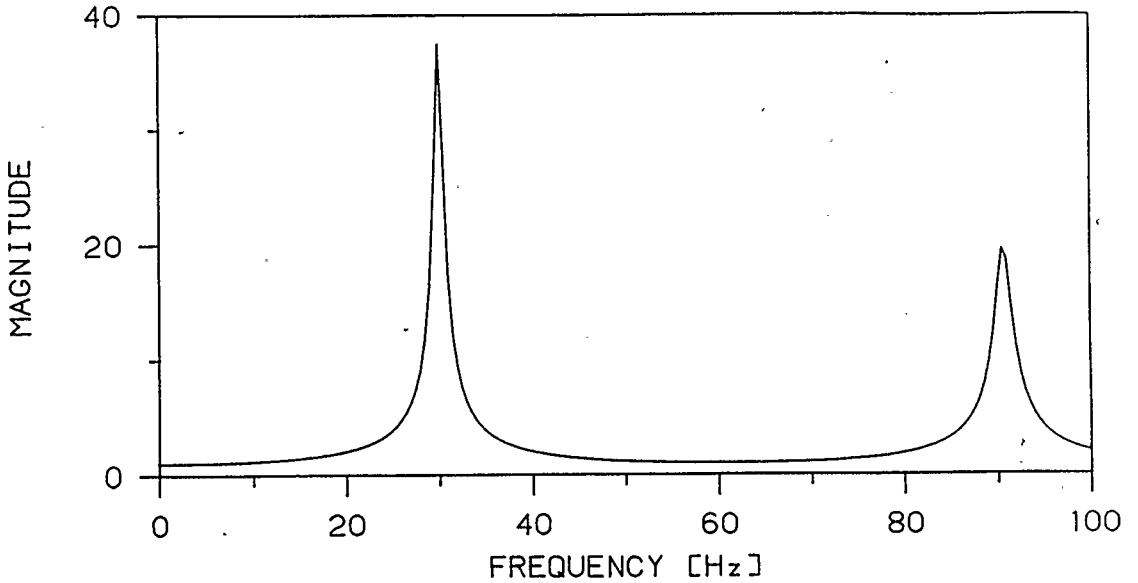

a) **Predicted**

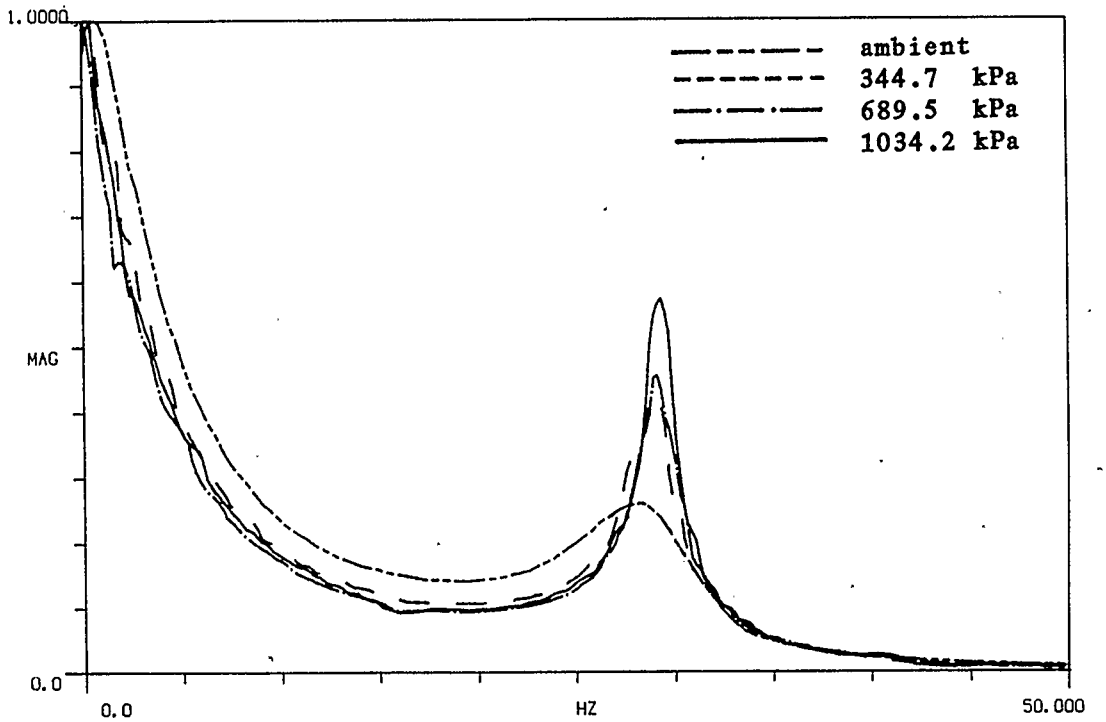

b) **Experimental**

Figure 5.18 Frequency Characteristics of Secondary Device Including Rosemount Transmitter

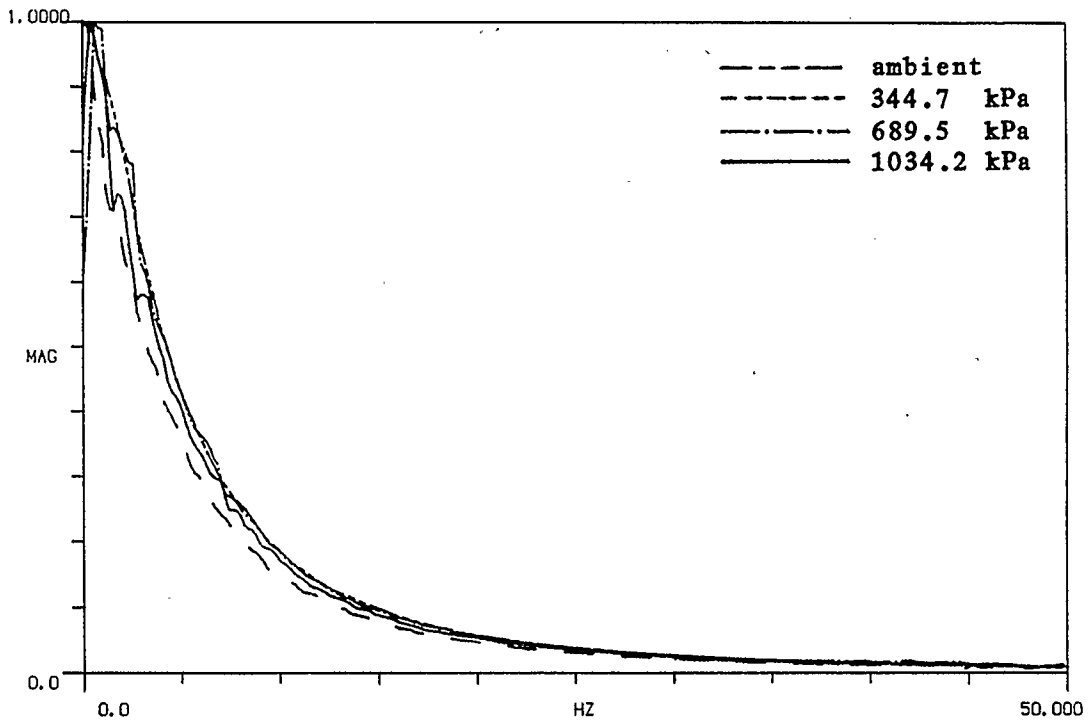

Figure 5.19 Frequency Characteristic of Rosemount Transmitter Alone

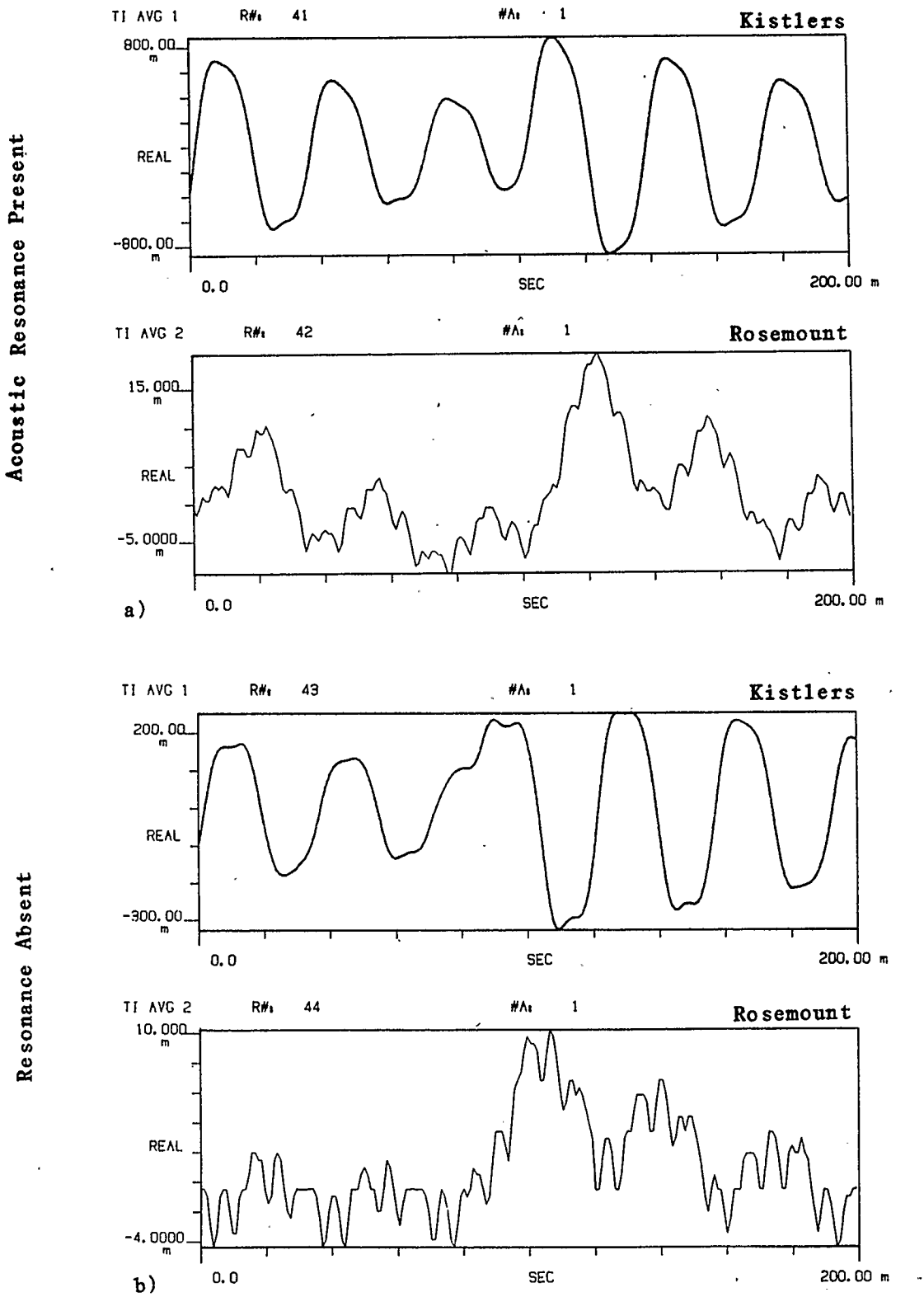

Figure 5.20 Time-Pressure Records for Rosemount and Reference Transmitters

2) The dynamic pressure fundamental frequency was not matched with any resonant frequency of the system

The time histories for both transmitters behave similarly, although the magnitudes are much smaller for the Rosemount. When there is a resonance, the Rosemount's time record is better matched to that of the reference transmitter than when there is no resonance in the system. The reason can be attributed to the Rosemount's wide working range 0 to 750'' H_2O and consequently to its inadequate sensitivity (poor data) for low dynamic loadings (the same dynamic level was used as for previous tests).

5.5 Conclusions

A secondary device which measures differential-pressure across an orifice plate was examined both theoretically, using a mathematical model, and practically, using three popular transmitters. Characteristics of the secondary device behaviour for different conditions were evaluated and found to be similar for the model and experiment. The results lead to the following conclusions:

1) Secondary devices can have resonant peaks in low frequency ranges (for the examined devices it is the range from 10 to 90 Hz). Such a system can be easily excited by pressure oscillations in the same frequency range.

2) The stiffness of the sensing element is a significant factor determining the natural frequencies of the secondary device.

Higher stiffnesses shift the natural frequencies towards higher values, which is desirable in many instances but is associated with loss of sensitivity.

3) Mechanical damping suppresses not only the mechanical resonant peaks but also the adjacent lower-frequency acoustic peaks. Consequently, the favourable effect is enhanced.

4) A lower volume space of the transmitter shifts the resonances towards higher values, but at the same time magnifies the amplitudes. It is then advisable to stay away from extrema.

5) Long connecting tubes are associated with the accumulation of more lower frequency resonances. Consequently, tubes should be as short as possible.

6) For the experimental conditions encountered, the secondary devices behaved similarly for different static pressures which shows that the systems are to a large extent linear.

7) Time-pressure records revealed large time lags for the Barton transmitter and a nonlinearity for the Gould transmitter (for high dynamic load).

CHAPTER 6

CONCLUSIONS AND RECOMMENDATIONS

6.1 Conclusions

In this work, a complete modelling process was implemented to evaluate a bridge-shaped gas metering station. The purpose of such an evaluation was two-fold:

1) to assess the behaviour of the bridge network and to find methods to reduce pulsations by altering various parameters

2) to investigate the performance of flow measuring devices and to find methods to make them best suited for a particular gas metering station.

The following models were developed and verified by experiment:

a) Model of an arbitrary bridge network

b) Model of a secondary flow measuring system

c) Model of a non-ideal gas used as a medium in the bridge network

To optimize pulsations the following should be considered while designing, altering and using a bridge-shaped gas metering station:

1) Varying the conditions of the flow, especially the temperature, can change the pattern of fluctuations and magnify them

to a high degree.

2) The fluctuations in the gas metering station strongly depend on the medium composition. Even seemingly insignificant mol fraction changes of the medium can have a significant effect on pulsations.

3) In general, rearranging the bridge network by increasing the number of runs results in lower fluctuations. The opposite effect is observed when the number of runs is decreased. The negative influence is more significant.

4) Closing of the valves results in more or less significant increase in fluctuations in the open runs, depending on the number and arrangement of the closed valves. Generally, closing a run downstream an orifice plate results in more significant increase in fluctuations at this orifice plate location.

5) The assessment of the bridge network input impedance allows one to estimate easily the effects of the network rearrangement by shutting down, adding or eliminating one (or more) run for given flow conditions, and medium composition. If the input impedance grows the fluctuations behave accordingly.

6) Modelling is useful for control of pulsations in any piping system because it can reveal pulsation characteristics of the system in advance. It enables one to decide how to change the system and avoid the consequences of pulsation.

The investigation of secondary device performance revealed that the Rosemount transmitter followed most closely the behaviour of the reference secondary system. The Barton and Gould transmitter's work was significantly impaired in resonant conditions. Moreover, the Barton's natural frequencies were very low (11 Hz) and its time characteristic showed a large lag. The Gould's time characteristic exhibited nonlinearities for high dynamic loading.

Apart from having desirable individual characteristic, the differential-pressure measuring device is expected to work properly when incorporated into the bridge network. The input to the secondary device is a differential pressure across the orifice plate. Therefore, it is necessary to consider the fluctuations of this differential pressure and compare their pattern to the characteristics of the secondary devices.

A procedure is proposed to predict the performance of the secondary device which is connected to a particular bridge network with specific geometry arrangement, flow conditions and medium:

1) Use the programs to calculate the magnitudes of differential-pressure fluctuations at a desired location

2) Obtain a frequency response of the secondary device

3) Compare both characteristics and check for coinciding resonant peaks

4) If a peak is present at the same frequency for both characteristics, change either characteristic altering one of the parameters which were described in Chapters 4 and 5.

Differential-pressure fluctuations for exemplary bridge network conditions are presented in Figure 6.1. When they are related to the Rosemount's characteristic (see Figure 6.2) it is noticed that the peaks near the frequency of 29 Hz coincide. Two sample methods are shown below to improve the measurement conditions:

1) Reducing the length of end pipes which results in vanishing of the peak around 29 Hz.

2) Adding one more run to the network which also causes the peak near 29 Hz to disappear.

6.2 Suggestions for Future Research

Apart from a special parallel network called a bridge network considered in this work, other networks are also used broadly. The analyses performed here could be repeated for them. The improvement of the orifice plate model, to make it useful also for higher flow conditions, would be very desirable.

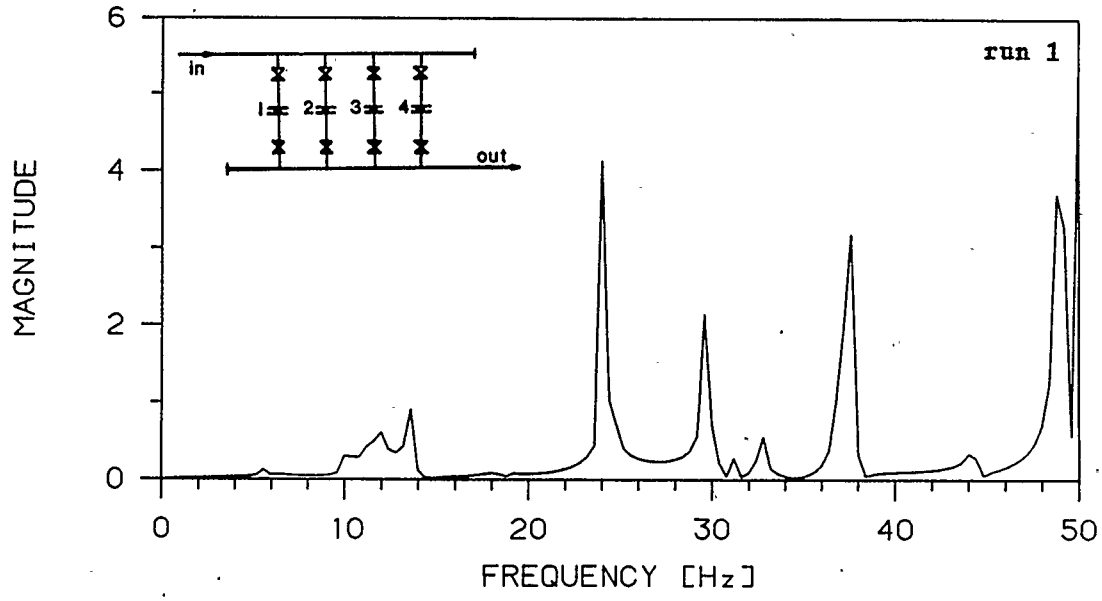

Figure 6.1 Differential-Pressure Fluctuation in the First Run for Reference Conditions

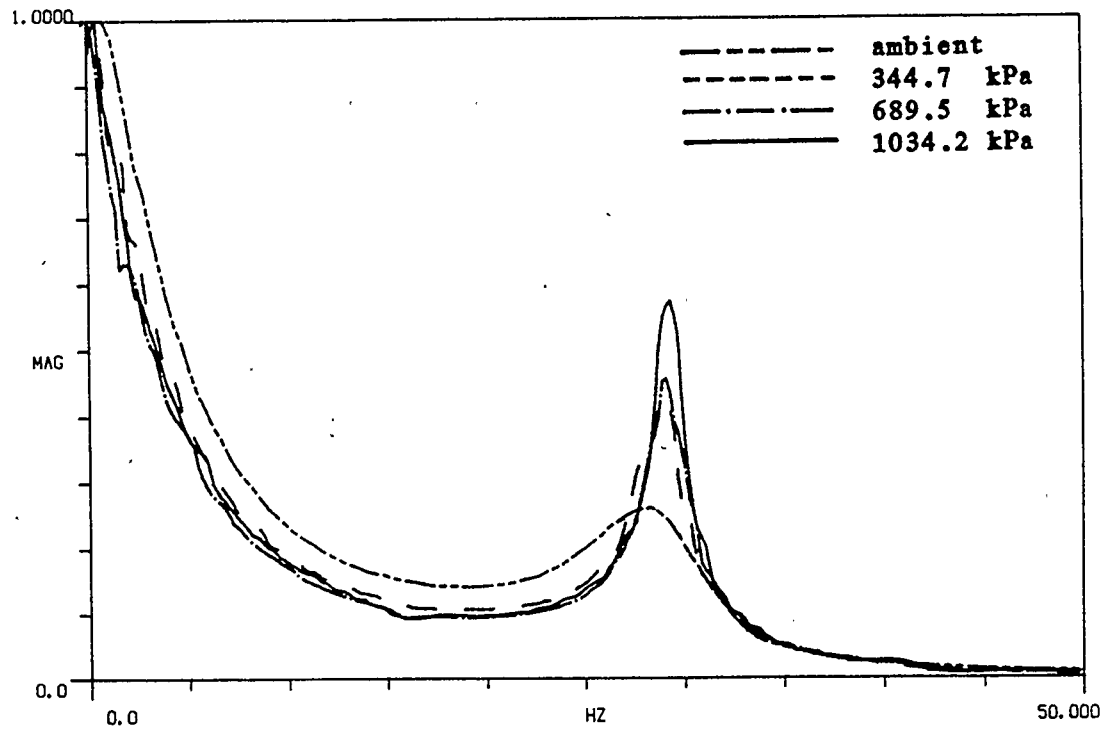

Figure 6.2 Secondary Device Characteristic

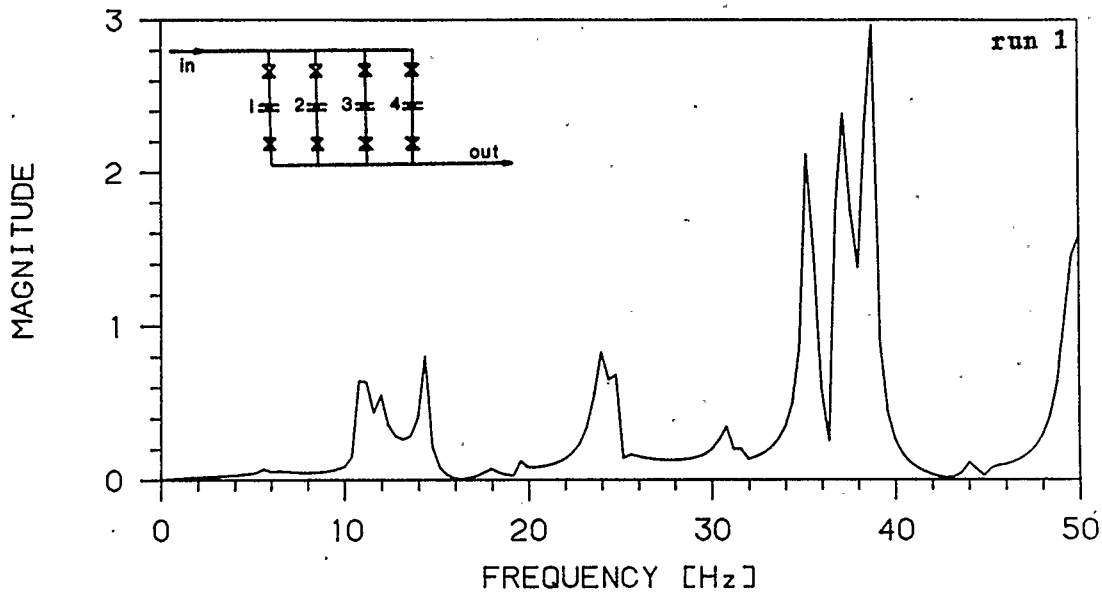

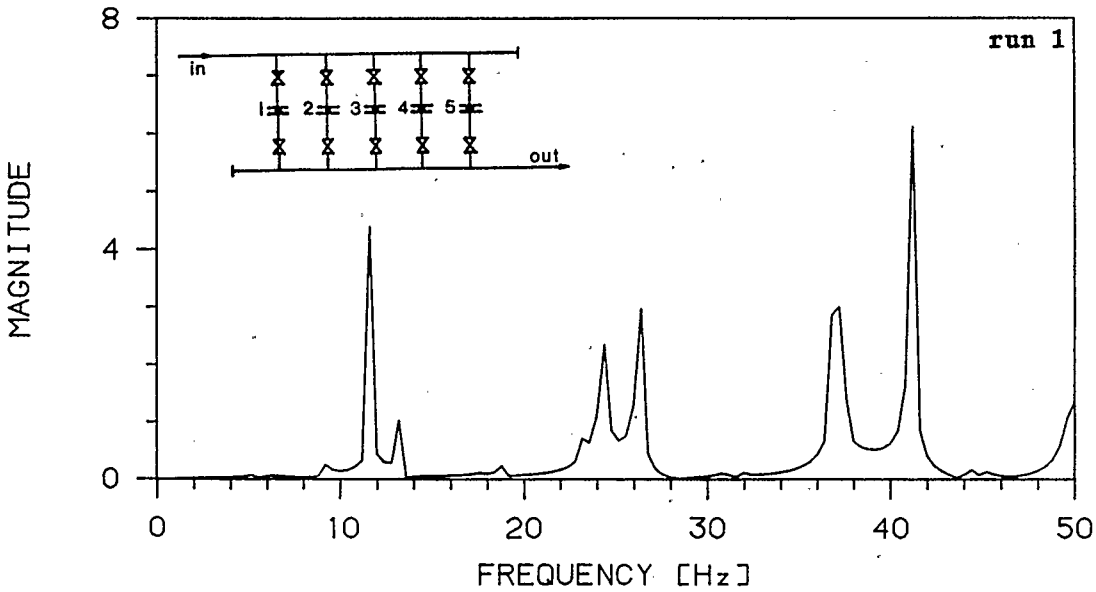

Figure 6.3 Differential-Pressure Fluctuations in the First Run for Varied Conditions

REFERENCES

1. Alfredson, R.J., and Davies, P.O.A.L., The Radiation of Sound from an Engine Exhaust, Journal of Sound and Vibration, 13, 389, 1970.

2. Alfredson, R.J., and Davies, P.O.A.L., Performance of Exhaust Silencer Components, Journal of Sound and Vibration, 15, 175, 1971.

3. Bell, C.J., et al., Experimental Study of Pneumatic Pulse Transmission in Circular Tubes, ISA Transactions, 11, 221, 1971.

4. Benedict, R.P., Response of Pressure-Sensing System, ASME Transactions, Journal of Basic Engineering, 82, 482, 1960.

5. Beranek, L.L., Noise and Vibration Control, McGraw-hill, N.Y., 1971.

6. Botros, K.K., et al., Attenuation of Pressure Pulsation in Pipeline Networks and Meter Station Proceedings of ASME, Fluids Engineering Conference, Boulder, Colorado, 1981.

7. Brown, F.T., The Transient Response of Fluid Lines, ASME Transactions, Journal of Basic Engineering, 84, 547, 1962.

8. Brown, F.T., A Quasi Method of Characteristics with Application to Fluid Lines with Frequency-Dependent Wall Shear and Heat Transfer, ASME Transactions, Journal of Basic Engineering, 91, 217, 1969.

9. Brown, F.T., et al., Small-Amplitude Frequency Behavior of Fluid Lines with Turbulent Flow, ASME Transactions, Journal of Basic Engineering, 91, 678, 1969.

10. Cederfeldt, L., On Use of the Finite Element Method on Some Acoustical Problems, ASME Transactions, Journal of Engineering for Industry, 104, 108, 1982.

11. Chung, J.Y., and Blaser, D.A., Transfer Function Method of Measuring In-Duct Acoustic Properties. I Theory, The Journal of the Acoustical Society of America, 68, 907, 1980.

12. Craggs, A., A Finite Element Method for Damped Acoustic Systems: An Application to Evaluate the Performance of Reactive Mufflers, Journal of Sound and Vibration, 48, 377, 1976.

13. Craggs, A., A Finite Element Method for Modelling Dissipative Mufflers with a Locally Reactive Lining, Journal of sound and Vibration, 54, 285, 1977.

14. Davies, P.O.A.L., et al., Reflection Coefficient for an Unflanged Pipe with Flow, Journal of Sound and Vibration, 72, 543, 1980.

15. Doebelin, E.O., Measurement Systems. Application and Design, McGraw-Hill, N.Y., 1983.

16. Doebelin, E.O., System Modeling Response. Theoretical and Experimental Approaches, John Wiley and Sons, N.Y., 1980.

17. D'Souza, A.F., and Oldenburger, R., Dynamic Response of Fluid Lines, ASME Transactions, Journal of Basic Engineering, 86, 589, 1964.

18. Fox, J.A., Pressure Transients in Pipe Netorks - A Computer Solution, Paper Presented at International Conference on Pressure Surges, University of Kent, Canterbury, England, 1972.

19. Franke, M.E., et al., Effects of Temperature, End-Conditions, Flow, and Branching on the Frequency Response of Pneumatic Lines, Journal of Dynamic Systems, Measurement, and Control, 15, 1972.

20. Gatley, .S., and Cohen, R., Methods for Evaluating the Performance of Small Acoustic Filters, The Journal of the Acoustical Society of America, 46, 6, 1969.

21. Goldschmidt, S., and Ury, J.F., The Influence of Transmission Line Geometry on the Measurement of Oscillatory Pressure, Paper Presented at Symposium on the Measurement of Pulsating Flow, University of Surrey, Guildford, England 1970.

22. Groves, T.K., The Adiabatic Expansion of Detonation Products and the Spherical Tylor Wave for TNT, PhD. D., Mc Gill University, Canada, 1967.

23. Hicks, E.J., Planning, Design Can Reduce Compressor Pulsation Effects, The Oil and Gas Journal, 39, July 24, 1978.

24. Hicks, E.J., Acoustic Filter Controls Recip Pump Pulsations, The Oil and Gas Journal, 67, Jan. 15, 1979.

25. Hirschfelder, J.O., et al., Molecular Theory of Gases and Liquids, John Wiley and Sons, N.Y., 1964.

26. Hord, J., Response of Pneumatic Pressure-Measurement Systems to a Step Input in the Free Molecule, Transition, and Continuum Flow Regimes, ISA Transactions, 6, 252, 1967.

27. Iberall, R.S., Attenuation of Oscillatory Pressure in Instrument Lines, Journal of Research of National Bureau of Standards, 45, 85, 1950.

28. Inaba, T., et al., Pulsating Laminar Flow in a Cylindrical Pipe with Through Flow, JSME Bulletin, 20, 442, 1977.

29. Ingard, U., and Singhal, V.K., Sound Attenuation in Turbulent Pipe Flow, The Journal of the Acoustical Society of America, 55, 535, 1974.

30. JANAF, Thermodynamical Data, The Dow Chemichal Co., Thermal Laboratory, Midland, Michigan, 1961.

31. Jones, A.D., and Brown, G.L., Determination of Two-Stroke Engine Exhaust Noise by the Method of Characteristics, Journal of Sound and Vibration, 82, 305, 1982.

32. Jones, A.D., Modelling the Exhaust Noise Radiated from Reciprocating Internal Combustion Engines - A Literature Review, Noise Control Engineering Journal, 23, 12, 1984.

33. Kagawa, Y., and Omote, T., Finite-Element Simulation of Acoustic Filters of Arbitrary Profile with Circular Cross Section, Journal of the Acoustical Society of America, 60, 1003, 1976.

34. Kantola, R., Transient Response of Fluid Lines Including Frequency Modulated Inputs, ASME Transactions, Journal of Basic Engineering, 93, 274, 1971.

35. Karal, F.C., The Analogous Acoustical Impedance for Discontinuities and Corrections of Circular Cross Sections, The Journal of the Acoustical Society of America, 25, 327, 1953.

36. Karam, J.T., and Franke, M.E., The Frequency Response of Pneumatic Lines, ASME Transactions, Journal of Basic Engineering, 89, 371, 1967.

37. Kathuriya, M.L., and Munjal, M.L., Measurement of the Acoustical Impedance of a Black Box at Low Frequencies Using a Shorter Impedance Tube, The Journal of the Acoustical Society of America, 62, 751, 1977.

38. Kathuriya, M.L., and Munjal, M.L., A Method for the Evaluation of the Acoustic Characteristics of an Engine Exhaust System in the Presence of Mean Flow, The Journal of the Acoustical Society of America, 60, 745, 1976.

39. Kathuriya, M.L., and Munjal, M.L., Method for Evaluation of the Acoustical Impedance o a Black Box with or without Mean Flow, Measuring Pressures at Fixed Positions, The Journal of the Acoustical Society of America, 62, 755, 1977.

40. Kathuriya, M.L., and Munjal, M.L., Experimental Evaluation of the Aeroacoustic Characteristics of a Source of Pulsating Gas Flow, The Journal of the Acoustical Society of America, 65, 240, 1979.

41. Kinsler, L.E., Fundamentals of Acoustics, John Wiley and Sons, N.Y., 1980.

42. Kulik, D.J., Gas Measurement Pulsation, Gas Measurement Institute, University of Kansas, Sept. 1982.

43. Lampton, M., Transmission Matrices in Electroacoustics, Acustica, 39, 239, 1978.

44. Lambert, R.F., and Steinbrueck, E.A., Acoustic Synthesis of a Flowduct Area Discontinuity, The Journal of the Acoustical Society of America, 67, 59, 1980.

45. Leland, T.W.Jr., and Mueller, W.H., Applying the Theory of Corresponding States to Multicomponent Systems, Industrial and Engineering Chemistry, 51, 597, 1959.

46. Levine, H., and Schwinger, J., On the Radiation of Sound from an Unflanged Circular Pipe, Physical Review, 73, 383, 1948.

47. Lung, T.Y., Acoustic Modelling and Testing of Piping Systems, M.Sc. Thesis, University of Calgary, Calgary, 1981.

48. Lung, T.Y., and Doige, A.G., Simulating the Performance of Pulsation Dampeners, International Journal of Modelling and Simulation, 3, 119, 1983.

49. Lung, T.Y., and Doige, A.G., A Time Averaging Transient Testing Method for Acoustic Properties of Piping Systems and Mufflers with Flow, The Journal of the Acoustical Society of America, 73, 867, 1983.

50. MacLaren, J.F.T., et al., A Comparison of Numerical Solutions of the Unsteady Flow Equations Applied to Reciprocating Compressor System, Journal of the Mechanical Engineering Society, 17, 271, 1975.

51. Martin, R.J., and Moseley, d.S., Analysis of the Effect of Pulsation on the Response of Mercurial-Type Differential-Pressure Recorders, ASME Transactions, Paper No. 57-A-82, 1957.

52. Miles, J., The Reflection of Sound Due to a Change in Cross Section of a Circular Tube, The Journal of the Acoustical Society of America, 16, 14, 1944.

53. Miles, J.H., Acoustic Transmission Matrix of a Variable Area Duct or Nozzle Carrying a Compressible Subsonic Flow, The Journal of the Acoustical Society of America, 69, 1577, 1981.

54. Munjal, M.L., et al., Velocity Ratio in the Analysis of Linear Dynamical Systems, Journal of Sound and Vibration, 26, 173, 1973.

55. Munjal, M.L., Velocity Ratio-Cum-Transfer Matrix Method for the Evaluation of a Muffler with Mean Flow, Journal of Sound and Vibration, 39, 105, 1975.

56. Munjal, M.L., Exhaust Noise and Its Control - A Review, Shock and Vibration Digest, 9, 21, 1977.

57. Munt, R.M., Acoustic Transmission Properties of a Jet Pipe with Subsonic Jet Flow, I: The Cold Jet Reflection Coefficient, Submitted to Journal of Sound and Vibration, 1980.

58. Nichols, N.B., The Linear Properties of Pneumatic Transmission Lines, ISA Transactions, 1, 5, 1962.

59. Ohmi, M., et al., Pressure Velocity Distributions in Pulsating Laminar Pipe Flow, JSME Bulletin, 19, 298, 1976.

60. Ohmi, M, and Usui, T., Pressure and Velocity Distributions in Pulsating Turbulent Pipe Flow: Part I. Theoretical Treatments, JSME Bulletin, 19, 307, 1976.

61. Othmer, D.F., and Chen, H.T., An Equation of State for Gas Mixtures, The American Institute of Chemical Engineers Journal, 12, 488, 1966.

62. Perry, R.H., et al., Perry's Chemical Engineers Handbook, McGraw-Hill, N.Y., 1963.

63. Pollack, M.L., The Acoustic Inertial End Correction, Journal of Sound and Vibration, 67, 558, 1979.

64. Prasad, M.G., and Crocker, M.J., Evaluation of Four-Pole Parameters for a Straight Pipe with a Mean Flow and a Linear Temperature Gradient, The Journal of the Acoustical Society of America, 69, 916, 1981.

65. Reamer, H.H., et al., Phase Equilibria in Hydrocarbon Systems, Industrial and Engineering Chemistry, 32, 206, 1940.

66. Reamer, H.H.,et al., Phase Equilibria in Hyrocarbon Systems, Industrial and Engineering Chemistry, 36, 88, 1944.

67. Reamer, H.H., et al., Phase Equilibria in Hydrocarbon Systems, Industrial and Engineering Chemistry, 37, 688, 1945.

68. Reamer, H.H. et al. Phase Equilibria in Hydrocarbon Systems, Industrial and Engineering Chemistry, 44, 198, 1952.

69. Reid, R.C., and Sherwood, T.K., The Properties of Gases and Liquids, McGraw-Hill, N.Y., 1966.

70. Rohman, C.P., and Grogan, E.C., On the Dynamics of Pneumatics Transmission Lines, ASME Transactions, Paper No. 56-SA-1, 1957.

71. Ronnenberger, D., Experimentelle Untersuxhuugen zum akustischen Reflexionsfaktor von unsteitigen Querschmittsanderungen in einem luftdurchstromten Rohr, Acustica 19, 222, 1967/68.

72. Sakai, T., and Saeki, S., Study on Pulsations of Reciprocating Compressor Piping Systems, JSME Bulletin, 16, 54, 1973.

73. Sakai, T., and Mitsuhashi, K., Study on Pulsations of Reciprocating Compressor Piping Systems, JSME Bulletin, 16, 63, 1973.

74. Sakai, T., and Mitsuhashi, K., Study on Pulsations of Reciprocating Compressor Piping Systems, JSME Bulletin, 16, 1675, 1973.

75. Santis, R., and Grande, B., An Equation for Predicting Third Virial Coefficients of Nonpolar Gases, The American Institute of Chemical Engineers Journal, 25, 931, 1971.

76. Scott, R.A., An Apparatus or Accurate Measurement of the Acoustic Impedance of Sound Absorbing Materials, Proceedings of the Physical Society, 58, 253, 1946.

77. Seimer, H.L., et al., A Methodology for the Estimation of Apparent Viscosity in Pulsatile Laminar/Turbulent Tube Flow, Paper, Mechanical Engineering Department, Lakehead University, Thunder Bay, Ontario, 1983.

78. Selected Values of Properties of Hydrocarbons, National Bureau of Standards, Prepared as Part of the Work of the APIR, Project 44, 1947.

79. Seybert, A.F. and Ross, D.F., Experimental Determination of Acoustic Properties Using a Two-Microphone Random Excitation Technique, The Journal of the Acoustical Society of America, 61, 1362, 1977.

80. Sharif, M.A., Determination of Speed of Sound from Decompression Wave Front Velocity in Moderately Dense Gases and Measurement of the Associated Isothermal Compressibility Coefficient and Compressibility Factor, University of Calgary, Calgary, 1984.

81. Sinclair, A.R., and Robins, A.W., A Method for the Determination of the Time Lag in Pressure Measuring Systems Incorporating Capillaries, NACA Technical Note, 1952.

82. Singh, R., and Katra, T., On the Dynamic Analysis and Evaluation of Compressor Mufflers, Proceedings of Perdue Compressor Technology Conference, July, 1976.

83. Snowdon, J.C., Mechanical Four-Pole Parameters and Their Application, Journal of Sound and Vibration, 15, 307, 1971.

84. Sparks, C.L., Pulsation Effects on Orifice Meters, ASME Transactions, Paper 82-T-40, 1982.

85. Sulivan, J.W., A Method for Modelling Perforated Tube Muffler Components. I Theory, The Journal of the Acoustical Society of America, 66, 772, 1979.

86. Sulivan, J.W., A Method for Modelling Perforated Tube Muffler Components. II Theory, The Journal of the Acoustical Society of America, 66,779, 1979.

87. Taback, I., The Response of Pressure Measuring Systems to Oscillating Pressures, NACA Technical Note, 1949.

88. To, C.W.S., and Doige, A.G., A Transient Testing Technique for the Determination of Matrix Parameters of Acoustic Systems, I: Theory and Principles, Journal of Sound and Vibration, 62,

207, 1978.

89. To, C.W.S., and Doige, A.G., The Application of a Transient Testing Method to the Determination of Acoustic Properties of Unknown Systems, Journal of Sound and Vibration, 71, 545, 1980.

90. To, C.W.S., and Doige, A.G., On Matrix Parameters of Acoustic Elements and Their Applications to the Acoustic Simulation of Piping Systems, Paper Presented at the World Congress on Systems Simulation and Scientific Computation, Concordia University, August 1982.

91. Young, C.I.J., and Crocker, M.J., Prediction of Transmission Loss in Mufflers by Finite-Element Method, Journal of the Acoustical Society of America, 57, 144, 1975.

92 Williams, T.J., et al., Pulsation Errors in Manometer Gages, ASME Transactions, Paper 55-A-92, 1955.

93. Williams, T.J., Behavior of the Secondary Devices in Pulsating Flow Measurement, Paper Presented at Symposium on the Measurement of Pulsating Flow, University of Surrey, Guildford, England.

94. Wylie, E.B., et al., Unsteady-State Natural-Gas Calculations in Complex Pipe Systems, Society of Petroleum Engineers Journal, 14, 35, 1974.

95. Wylie, E.B., and Streeter, V.L., Fluid Transients, McGraw-Hill N.Y.,1978.

96. Zielke, W., Frequency-Dependent Friction in Transient Pipe Flow, ASME Transactions, Journal of Basic Engineering, 90, 217, 1968.

97. Zucrow, M.J., and Hoffman, J.D., Gas Dynamics, John Wiley and Sons, N.Y., 1976.

APPENDIX A

Well-Known Thermodynamic Relationships Used in Calculation of Density and Speed of Sound

The equations in this appendix are given for better understanding and completeness of Chapter 2. These equations can be found in any textbook on thermodynamics.

$$\frac{1}{k} = \rho RT \left[Z + \rho \left(\frac{\partial Z}{\partial \rho}\right)_T\right] \tag{A.1}$$

where, k is isothermal compressibility

$$\left(\frac{\partial P}{\partial T}\right)_V = \frac{b\rho}{b} ZR + \frac{R}{b} [dB^*(b\rho)^2 + dC^*(b\rho)^3] \tag{A.2}$$

$$\beta = \left(\frac{\partial P}{\partial T}\right)_V k \tag{A.3}$$

where, β is volume expansivity

$$cv_M = - Rb\rho[(2\ dB^* + d^2B^*) + \frac{b\rho}{2}(2\ dC + d^2C^*)] \tag{A.4}$$

where, cv_M is specific heat constant at constant volume for a mixture

$$cv = cv_{id} + cv_{Re} \tag{A.5}$$

where, cv_{id} and cv_{Re} are specific heat constants at constant volume for perfect gas and non-perfect gas respectively

$$cp = cv + \frac{T\beta^2}{\rho k} \tag{A.6}$$

$$\gamma = cp/cv \tag{A.7}$$

where, γ is ratio of heat capacities

$$cp_{idM} = \sum_{i=1}^{i=n} y_i cp_{id} \tag{A.8}$$

where, cp_{idM} is specific heat constant at constant pressure for an ideal mixture, and y_i is mole concentration of i-th gas

$$cv = cp_{idM} - R \tag{A.9}$$

where, R is universal gas constant

$$c = \frac{\gamma}{\rho k} \tag{A.10}$$

where c is speed of sound

APPENDIX B

Four-Pole Equation for a Mechanical Element

In this appendix, the four-pole equation for a piston subjected to a differential pressure is derived. The piston is represented as a mass whose motion is restricted by a spring and damper.

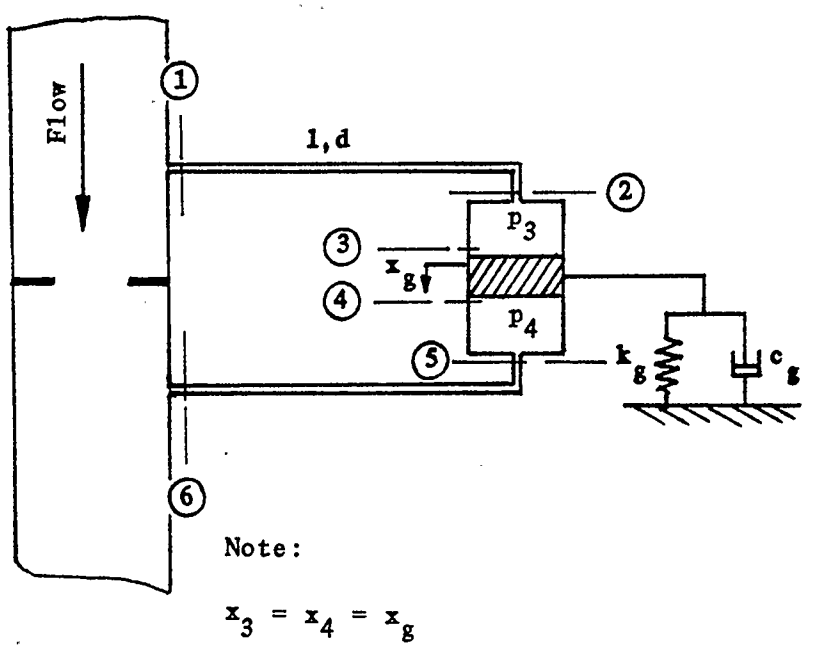

Figure B.1 Model of the Differential-Pressure Sensing Device

The differential equation of motion with a harmonic excitation is:

$$\ddot{x}_g + 2\eta\omega_n\dot{x}_g + \omega_n^2 x_g = (P_3 - P_4)\frac{S_g}{m}e^{i\omega t} \tag{B.1}$$

where P_3 and P_4 are complex amplitudes of pulsating pressures p_3

and p_4 respectively. The solution for equation (B.1) has the form

$$x_g = X_g \quad e^{i\omega t} \tag{B.2}$$

Substituting (B.2) into (B.1) gives:

$$\omega_n^2 = (1 + i2\eta r - r^2)X_g = (P_3 - P_4)\ \frac{S_g}{m} \tag{B.3}$$

where, $\omega_n^2 = k_g/m$, $r = \omega/\omega_n$, $\eta = c/c_c$.

Rearrangement of (B.3) results in:

$$P_3 = P_4 + (k_g/S_g)(1 + i2\eta r - r^2)X_g \tag{B.4}$$

The transfer matrix notation of (B.4) is:

$$\begin{bmatrix} P_3 \\ X_g \end{bmatrix} = \begin{bmatrix} 1 & (k_g/S_g)(1 + i2\eta r - r^2) \\ 0 & 1 \end{bmatrix} \tag{B.5}$$

APPENDIX C

Model of the Pressure Sensing Device - Simplification

If the mechanical stiffness of the sensing element is considered to be large compared to that of the acoustic system, the model introduced in section 5.2 can be reduced to a model presented in Figure C1.

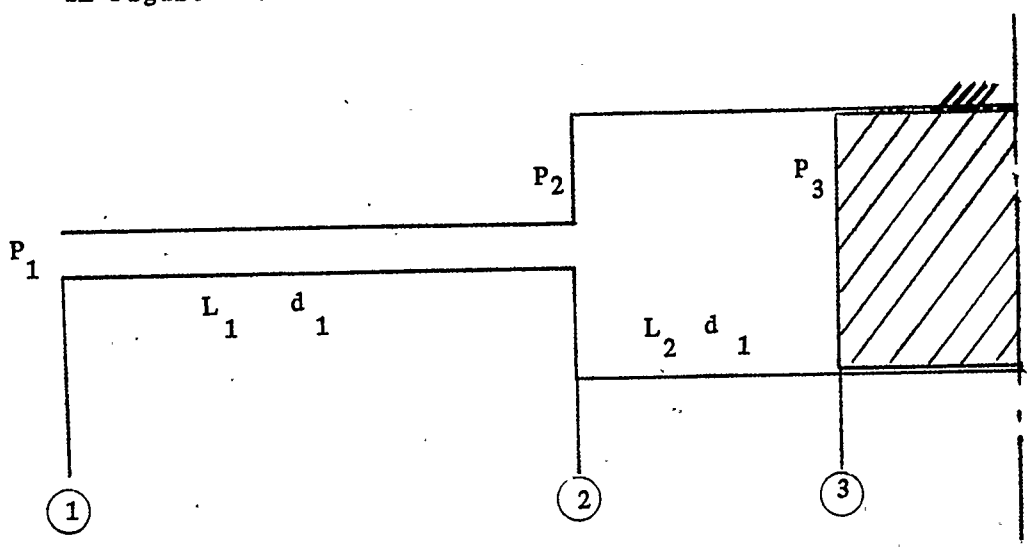

Figure C.1 Simplified Model of the Pressure Sensing Device

As a result, only one side of the secondary device is examined. To further simplify the model, the acoustic damping is excluded. The four-pole parameter equation for the system is given by:

$$\begin{bmatrix} P_1 \\ V_1 \end{bmatrix} = [T]_{12}\ [T]_{23} \begin{bmatrix} P_3 \\ V_3 \end{bmatrix} \tag{C.1}$$

where

$$T_{12} = \begin{bmatrix} \cos kL_1 & iZ_{01}\sin kL_1 \\ 1/Z_{01}\sin kL_1 & \cos kL_1 \end{bmatrix} \tag{C.2}$$

$$T_{23} = \begin{bmatrix} \cos kL_2 & iZ_{02}\sin kL_2 \\ 1/Z_{02}\sin kL_2 & \cos kL_2 \end{bmatrix} \tag{C.3}$$

Substituting $Z_{01} = 4\rho c/(\pi d_1^2)$, $Z_{02} = 4\rho c/(\pi d_2^2)$, and $U_3 = 0$ into equation (C1) results in:

$$\frac{P_1}{P_3} = \cos kL_1 \cos kL_2 - \left[\frac{d_2}{d_1}\right]^2 \sin kL_1 \sin kL_2 \tag{C.4}$$

For acoustic resonance condition P_3 is large compared to P_1, therefore the right hand side of equation (C.4) has to be zero. This gives:

$$\tan kL_1 \tan kL_2 = \left[\frac{d_1}{d_2}\right]^2 \tag{C.5}$$

Equation (C.5) can be solved for frequency f $(f = kc/(2\pi))$. Considering a situation where an approximation $\tan kL_1 = kL_1$ and $\tan kL_2 = kL_2$ can be used, equation (C.5) can be written as:

$$k^2 L_1 L_2 = \left[\frac{d_1}{d_2}\right]^2 \tag{C.6}$$

or

$$k = \left[\frac{d_1^2 \pi/4}{d_2^2 L_1 L_2 \pi/4}\right]^2 \tag{C.7}$$

Subsequently, after substituting $k = 2\pi f/c$, and solving for f, equation (C.7) becomes the well-known Helmholtz equation:

$$f = f_H = \frac{c}{2\pi}\left[\frac{S_1}{V_2 L_1}\right] \tag{C.8}$$

where $S_1 = \pi d_1^2/4$ and $V_2 = (\pi d_2^2/4)\ L_2$ The above equation holds when the wave length is long compared to the dimensions of the acoustic system.